

# **Electrophysiological and computational studies on the mechanisms and functional impact of cortical synchronization**

Dissertation  
zur Erlangung des Doktorgrades  
der Naturwissenschaften

Vorgelegt beim Fachbereich Physik  
der Johann Wolfgang Goethe-Universität  
in Frankfurt am Main

Von  
Michael Niessing  
aus Marburg

Frankfurt  
D

## Contents

<b>I</b>	<b>Introduction.....</b>	<b>1</b>
A	<i>Brain Science History.....</i>	<i>1</i>
B	<i>Structural Constraints of Cortical Operation.....</i>	<i>7</i>
1	The Retinogeniculocortical Path .....	7
2	The Primary Visual Cortex .....	8
3	Visual Pathways.....	10
C	<i>Concepts of Information Representation and Processing.....</i>	<i>11</i>
1	Information that Enters the System.....	11
2	Hierarchical Versus Distributed Processing .....	13
3	Binding by Synchrony.....	14
D	<i>The Aim of the Thesis.....</i>	<i>16</i>
<b>II</b>	<b>Materials and Methods .....</b>	<b>21</b>
A	<i>Animal Experiment.....</i>	<i>21</i>
1	Overview .....	21
2	A New Technique for Targeted Cell Recordings.....	22
2.1	The General Approach for Targeted Recordings According to Feature Maps.....	22
2.2	The Apparatus.....	23
2.3	The Software.....	30
2.4	Ex-Vivo Test of System Precision .....	34
2.5	Optical Imaging of Intrinsic Signals .....	35
2.6	Electrophysiology.....	35
2.7	Procedure for the Alignment of Electrodes with the Functional Maps.....	36
2.8	Animal Preparation.....	37
3	Stimuli and Postulations.....	37
3.1	The Foreground/Background Grating .....	38
3.2	The Gabor Patch .....	39
3.3	Experiments and Stimulus Application.....	40
4	Data Analysis.....	42
4.1	A New Method for the Removal of Correlated Noise .....	42
4.2	A New Software Design for Flexible Data Organization and Data Access .....	46
4.3	Spike Extraction.....	48
4.4	Spike Sorting.....	49
4.5	Cross-Correlation Analysis.....	52
B	<i>Computer Simulation.....</i>	<i>55</i>
1	The Simulation Environment.....	55
2	The Model Neurons.....	57
2.1	Morphology and Electrotonic Properties .....	57
2.2	Ion Currents and Channel Kinetics.....	58
2.3	Synapses.....	60
3	The Network Architecture .....	61
3.1	Intra-Columnar Architecture.....	61
3.2	Inter-Columnar Architecture.....	61
4	The Network Input .....	62
5	Data Analysis.....	62

<b>III</b>	<b>Results .....</b>	<b>65</b>
<i>A</i>	<i>Animal Experiment .....</i>	<i>65</i>
1	A New Technique for Targeted Cell Recordings .....	65
1.1	System Precision.....	65
1.2	Animal Experiment .....	66
2	Data Analysis.....	70
2.1	A New Method for Removal of Correlated Noise.....	70
2.2	A New Software Design for Flexible Data Organization and Data Access .....	73
2.3	Spike Sorting.....	73
2.4	Foreground/Background Gratings .....	74
2.5	Gabor Patches .....	75
<i>B</i>	<i>Computer Simulations.....</i>	<i>79</i>
<b>IV</b>	<b>Discussion.....</b>	<b>87</b>
<i>A</i>	<i>Animal Experiment .....</i>	<i>87</i>
1	A New Technique for Targeted Cell Recording .....	87
1.1	Summary.....	87
1.2	Fabrication of the Tube Grid .....	87
1.3	System Precision & Handling.....	88
1.4	Alternative Approaches .....	90
1.5	Conclusion.....	91
2	Data Analysis.....	92
2.1	Summary.....	92
2.2	A New Method for the Removal of Correlated Noise .....	93
2.3	Spike Extraction.....	94
2.4	Foreground/Background Gratings .....	96
2.5	Gabor Patches .....	96
<i>B</i>	<i>Computer Simulation.....</i>	<i>98</i>
<b>V</b>	<b>Reference List.....</b>	<b>101</b>
<b>VI</b>	<b>Summary .....</b>	<b>119</b>
<b>VII</b>	<b>Ausführliche Zusammenfassung .....</b>	<b>121</b>
<b>VIII</b>	<b>Lebenslauf.....</b>	<b>127</b>



# I Introduction

## A Brain Science History

The earliest signs of human interest in the brain can be derived from archaeological records of skulls as old as seven thousand years. Some of these skulls bear traces of so called trepanations, the removal of a disk-like piece of skull. The healed edges of the holes suggest that 70 % of the people lived on after the trepanation for a considerable period of time, excluding the possibility that the trepanations were due to accidents or sacrifices. However, there is no clear evidence that the trepanations served to gain knowledge about the brain, but a comparison to the habits and motivations of primitive populations in modern times suggests that diseases with head located symptoms were believed to be caused by demons which had to be exempt from the wrapping skull. This superstitious belief combined with cases in which trepanation led to relief, as can be envisaged, for instance, for pressure related migraine, may have led to a mutual manifestation of the practice of trepanations and the theory of demons causing the symptoms.

The oldest recorded mention of the brain is the Egyptian hieroglyph shown in Fig. 1. It has been dated back to the 17th century B.C. At this time the Brain was thought to be an organ merely in charge of supplying mucus to the nose. Since then, many famous philosophers and scientist have come to highly



**Fig. 1: Egypt hieroglyph of the word *ayis* (=brain) as found in the Edwin Smith "Surgical" Papyrus from about 1700 BC.**

diverging conclusions on the function of the brain. For instance, Pythagoras (570-496 B.C.), Hippocrates (460-377 B.C.) and Plato (427-347 B.C.) already considered the brain to be the most precious organ and Plato even ascribed intellectual abilities to it. By contrast, his famous student Aristotle (384-322 B.C.), thought of the brain as a finned heat exchanger for cooling the heart, which in turn, he posited to be the seat of mental processes. 450 years later, the renowned surgeon Galen (130-200 A.C.) assigned sensory processing and motor control to the brain and, based on his own observations, developed the theory of “animal spirit”, a volatile content of nerve tracks and brain ventricles which he thought to be the seat of the soul. His work appeared so conclusive and consistent that it influenced scientists for more than 1600 years. Galen’s theory of animal spirit became a manifest and was refined and

extended, especially during mediaeval times. Here, the first model of brain function arose: the animal spirit was believed to flow and transform between the ventricles like waters flow and transform into different forms in roman fountains. With this model in mind, scientists assigned different mental abilities such as memorizing or thinking to the basins of the fountain, such that the model was consistent with the anatomical knowledge about the brain ventricles. René Descartes (1596-1650) maintained the idea of animal spirit, but noticed that the model of the roman fountain had sever flaws. He invented a mechanistic model by comparing the brain with an organ, which at the end produces something abstract like music that he compared to humans' controlled and reasonable behavior. This model already included time as an important aspect under which all the complex interactions of air (animal spirit) and the mechanics (nerve interactions) of the organ must be appropriately organized in order to produce reasonable music (behavior). Descartes' organ model rendered the theory of animal spirit accessible to experimental inspection. During the following 200 years, experimental findings made it more and more complicated to maintain the ideas of the organ model and animal spirit. Giovanni Borelli (1608-1679), for instance, found that the animal spirit must be a fluid and not a gas and Alexander Monro primus (1697-1767) expected in vein nerve fibers to inflate if tied up strongly enough so that nothing could flow through them. Finally Isaac Newton (1643–1727) recognized that neither gas nor fluid could flow fast enough through nerve fibers and proposed a propagation principal carried by vibrations of the nerve filaments. Overall, experiment and theory conflicted ever more as time passed by, until in the middle of the 18<sup>th</sup> century perplexity laid upon brain science.

However, a major breakthrough was achieved when the physician Luigi Galvani (1737-1798) showed that muscles contracted when the nerves were stimulated with electrostatically charged metals. This finding could have led Galvani to conclude, that electricity is the quantity which “flows” through nerve fibers. However, in another experiment, he observed muscle contractions if the nerves were stimulated just by contacting two different uncharged metals. Galvani did not know that the two metals built up about one Volt in a moist environment and thus concluded that there must be some kind of bio-electricity which is irritable by different means. Once this particular kind of electricity is irritated, he thought, it would propagate through the nerves to the muscle which would be caused to contract. Allesandro Volta, physicist, inventor of the electrophorus and a friend Galvani's, gave a different explanation for Galvani's findings. He suggested that there was no other kind of electricity generated by the tissue, but instead that in both cases “normal” electricity was

generated by the experimental setup, i.e. the electrostatic charge and the two different metals in the moist environment. These two interpretations of the same findings led to the famous Galvani-Volta controversy, in which both scientists came to different conclusions, according to their scientific background. The controversy gave rise to a fruitful interdisciplinary dispute, which led Galvani to perform further important experiments and Volta to study the electrical flow between dissimilar metals and to invent the first battery in 1800. In honor of their work, André Ampère (1775-1836) named his invention for the measurement of electric currents *galvanometer* and the units for potential differences were named *Volt*. The Galvani -Volta controversy was finally solved by Du Bois-Reymond (1818-1896), who proved in 1843 that nerves electrotonically convey currents through their fibers. In 1849 he found that nerves are able to actively generate and propagate electrical current pulses. Thus, in the mid 19<sup>th</sup> century, the basic nature of neuronal communication was established, although the elements that interact, the neurons, and the interfaces between them, the synapses, were still unknown.

In the search for the structure of the cortical tissue, microscopy was the only available way to observe structures of microscopic dimensions. However, the microscopic techniques in the 19<sup>th</sup> century suffered from spherical and chromatic aberration. This caused a certain staining technique, the “black reaction”, invented by Camillo Golgi (1843-1926) in the seventies, to play an important role in the discovery of the composition of cortical tissue. This so called Golgi-Impregnation has the important and still unresolved quality of staining only a few neurons at a time, but these few neurons are stained entirely, even up into the most filigree structures of their dendritic trees. Using the Golgi-Impregnation, Ramón y Cajal (1852-1934) found strong evidence that the dendrites and axons as seen in the stained tissue are not parts of a continuous network, but belong to a confined and autonomous structure, a cell. Cajal’s findings raised the question on how neurons exchange information between each other. Departing from the work of Otto Loewi (1873-1961), this question was solved over the following decades. In 1897, the locations of signal exchange were named “synapses” by Sir Charles Sherrington (1857-1952) who showed that not only synaptic excitation exists, but also inhibition.

On the macroscopic level, Eduard Hitzig (1838-1907) und Theodor Fritsch (1838-1897) localized motor areas by electrically stimulating and removing cortical sites of a dog. The electrical stimulation of the motor areas produced certain movements by the dog, and after setting a lesion in the same area, the dog’s ability to move was impaired after waking up. Paul

Broca (1824-1880) localized an area for speech by observing that patients with aphasia usually had a brain lesion at the same cortical region in the left hemisphere. Finally, Korbinian Brodmann (1868-1918) was able to distinguish six layers and 47 areas of the human cortex due to cyto-architectonic features. Thus, physiological and histological evidence accumulated that the brain is functionally fragmented into areas of certain duties which communicate through bundles of nerve fibers.

As outlined above, brain science started into the 20<sup>th</sup> century with the knowledge that “animal spirit” is identical to electricity, that the basic computational units are confined cells with active electrical abilities “talking” to each other through chemical synapses, that the brain has a modular structure, and, finally, that the brain is the central organ for sensory, mental and motor processing. All this knowledge had severe consequences for the way scientists thought about the brain and its function. On the one hand, brain function seemed to require physical, i.e. deterministic, interactions of matter only. No mystical “animal spirit” was needed anymore. On the other hand, this mechanistic view led to the notion that the central quality of intelligence must reside in the logical operations on the information which is received, stored and processed by the brain. These operations could also be carried out by any non-biological system and would thus not be mechanistic at all. This setting was demanding enough to challenge scientific disciplines from psychology to meta-mathematics, to apply their knowledge and tools to the function of the Brain. The different disciplines remained separated from each other for at least three quarters of the 20<sup>th</sup> century, developing different formalisms of description. Towards the end of the 2<sup>nd</sup> millennium, the different disciplines increasingly profited from each other and started to merge, a process that is currently ongoing. It is beyond the scope of this historical introduction to give a comprehensive description of the rapidly accelerating progress made in the 20<sup>th</sup> century. Hence, a selection of representative or (for this work) especially interesting findings and developments is outlined in the following.

After developing the basic techniques to produce electricity using galvanic elements and to measure electric properties as current and voltage, time was ripe for the field of electrophysiology to ask and answer important questions. The previously mentioned finding of inter-neuronal inhibition by Sherrington was proven by electrophysiological studies in 1900. He shared the 1932 Nobel Prize with Lord Edgar Douglas Adrian, who suggested the all-or-none law of neuronal action potential generation in 1912 and found the intensity of sensory stimuli (1926) and the strength of muscle contraction to be coded in the discharge

frequencies of the respective sensory or motor neurons. In the late 20s, Hans Berger opened electrophysiological methods to medical application by presenting the first human electroencephalogram (EEG). Sir Alan Lloyd Hodgkin (1914-1998) and Andrew Fielding Huxley (\*1917) used a new electrophysiological technique, the voltage and current clamp, to study trans-membrane currents while blocking specific types of ion channels. In 1952 they published the differential equations for the dynamics of voltage sensitive ion channels which explained the generation of action potentials and established the foundation for the numerical simulation of neuronal processing. Another major step in the field of electrophysiology was the development of the patch clamp method by Erwin Neher (\*1944) and Bernd Sakmann (\*1942) at the end of the 70s. It reduced the noise level of the recordings drastically and allowed for the registration of currents, even of single ion channels. Overall, innumerable electrophysiological studies were performed in the 20<sup>th</sup> century, continuously reviving the discipline under a technological progress that improved the data quality, the number of electrodes simultaneously employable and the analysis capabilities.

Parallel to the developing electrophysiology, completely different techniques were also introduced. One is the Magnetoencephalography (MEG), which uses the fact that electrical currents are accompanied by magnetic fields. Thus, currents in the brain can be measured indirectly and non-invasively by highly sensitive magnetic field detectors (SQUIDS). The disadvantage of utilizing MEG is that it only measures tangential and not radial currents, thereby losing information in comparison to EEG. However, it is well suited to determine the position of the signal source and is therefore primarily used for pre-surgical determination of regions of interest. Positron emission tomography (PET) and functional magnetic resonance imaging (fMRI), both fairly new techniques, measure metabolic processes and are therefore well suited to detect regions of high activity in the brain. These techniques have the advantages of being non-invasive and capturing the entire brain or a large regions of interest. The main draw backs of PET and fMRI are the relatively low spatio-temporal resolution ( $\sim 1 \text{ mm}^3$  and 1 s, respectively). Optical imaging of intrinsic signals (OI) uses the fact that the activity dependent blood oxygenation level locally alters the optical properties of the cortical tissue. It is therefore possible to record from a macroscopic area (order of  $1 \text{ cm}^2$ ) of exposed cortical surface using a high-precision CCD camera. The temporal resolution of (OI) is comparable to that of the fMRI, since it detects the same kind of signal, but unlike fMRI the spatial resolution of OI is not limited by the recording device but by the attenuation of light in the tissue and lies at about  $80 \mu\text{m}$ . Subsequently to OI, a related technique was introduced, the

so called fast optical imaging (fOI). In principal, fOI works the same way OI does but it uses the optical properties of voltage sensitive dyes to measure electrical neuronal activity directly. By using a fast camera this technique yields a temporal resolution in the order of 1 ms and the same spatial resolution as OI. Draw backs of fOI are possible influences of the dye on the neuronal activity and many difficulties in its concrete application. Other technical progress was made by combining techniques like EEG and fMRI or extracellular recordings with fMRI. The main work of this dissertation lines up with these approaches and aims at developing a technique that combines massively parallel extracellular recordings in vivo with OI, such that OI serves as a cue for the placement of the recording electrodes into functionally pre-determined cortical sites.

*Literature:*

- D.R. Hofstadter, *Gödel, Escher, Bach: An Eternal Golden Braid*. Harvester Press Ltd, 1979, Great Britain.
- S. Finger, *Origins of Neurosciences*. Oxford, 1994.
- A. Villa, *Time and the Brain*, Oxford, 1999.
- R Illing, *Geschichte der Hirnforschung*, In Lexikon der Neurowissenschaft. Spektrum Verlag, Heidelberg.

## B Structural Constraints of Cortical Operation

### 1 The Retinogeniculocortical Path

Neuronal processing of visual information starts in the retina where a two dimensional image of the visual scene is focussed onto the photo receptors of the retina. The signals of the photo receptors are integrated by ganglion cells of at least three kinds, which for the cat visual system are termed  $\alpha$ ,  $\beta$  and  $\gamma$  ganglion cells. The  $\alpha$  cells contribute most to the retinal signals received by the cortical area under investigation here. Their large dendritic trees capture signals over a larger spatial region than the other cell types, thus yielding larger receptive fields (RFs) with highest contrast sensitivity at low spatial frequencies (Troy, 1987). Furthermore, the  $\alpha$  cells are the most sensitive cells for the detection of fast changes in light intensity and fast movements within the visual scene. For details about the signal contributions of the different ganglion cells, see Freeman, 1991; Shapley and Perry, 1986; Shapley and Victor, 1978; Shapley and Victor, 1981; Shapley and Victor, 1980; Shapley and Victor, 1979; Troy, 1987; Wässle and Boycott, 1991; Troy and Enroth-Cugell, 1993.

The retina transmits the information about the visual scene to the dorsal division of the lateral geniculate nucleus (LGN). The different ganglion cell types of the retina, the  $\alpha$ ,  $\beta$  and  $\gamma$  cells, build up distinct pathways to the LGN which are termed Y, X and W paths, respectively. The LGN mainly consists of cell layers which are specifically innervated by fibres of a certain ganglion cell type and of a certain eye. Within the layers, the signals of the two retinae and the different signal types are topologically reorganized such that within a column perpendicular to the layers all neurons code for the same area in the visual field (Bishop et al., 1962; Sanderson, 1971). These continuous columns then project the signals of both eyes to the cortical areas whilst maintaining separate paths for the signals X, Y and W. Area 17 receives stereoscopic afferents of the X and the Y signal, whereas area 18 receives the Y signal only. Several details about the LGN were left out for simplicity but its computational role is still a matter of debate. The LGN has commonly been viewed as a relay station simply in charge of reorganizing and further projecting pathways from the retinae. This view is clearly oversimplified but the fact that areas 17 and 18 are silent when the input of the LGN is removed (Lee et al., 1998; Malpeli, 1983; Malpeli et al., 1986; Mignard and Malpeli, 1991)

and that back projections to the LGN exist underlines that the LGN serves as the most important input to the primary visual cortex and would rather receive modulatory input (Singer, 1977) from other areas than to have computational duties itself.

## 2 The Primary Visual Cortex

As mentioned above, the first cortical areas to receive input directly from the LGN are areas 17 and 18 and are therefore recognized to establish together the primary visual cortex. Since they receive different signals from the LGN, these two areas process different kinds of information in parallel and are called the primary visual cortex (PVC). Area 18 primarily receives Y signals which originate from the a cells in the retina. Due to the RF properties of the a ganglion cells, area 18 receives mainly information about transient luminance changes and fast movements of the low spatial frequency components of the visual scene. The afferents enter the cortex by means of neuronal projections from the LGN terminating in layer 4A out of the six-fold laminated cortical tissue. From there, the signals spread through local circuits perpendicular through all layers establishing so called micro columns. The micro columns have an average spacing of 56  $\mu\text{m}$ , consist of about 200 neurons and are believed to be interconnected via large layer 5 pyramidal cells. This concept of micro columns is best known for area 17, but since the overall organization of area 18 resembles that of area 17 quite closely one can envisage that the concept of micro columns holds true for area 18 as well. In this work, one particular type of local circuit plays an important role for the computer model: it is the reciprocal coupling of excitatory pyramidal cells of layer 5 to basket cells of layer 2/3. This circuit is a candidate for the generation of gamma network oscillations (Silva et al., 1991).

Departing from the micro columns, the next larger structure is that of the functional columns. Columns are clusters of neurons with similar functional properties that extend perpendicular to the cortical surface through all cortical layers and exhibit a typical diameter of about 0.4 mm (cat visual cortex, Hubel and Wiesel, 1962; Hubel et al., 1977; Bonhoeffer and Grinvald, 1991). In contrast to the micro columns, the functional columns are not strictly confined regions or anatomical quantiles, instead, a functional column will shift its centre of mass, maintaining a large overlap with the former column, for small deposits of the stimulus in feature space. For the example of orientation columns, a turning of the stimulus orientation until its identity is reached would cause the activated population to travel on a circle around a

singularity point. The gross structure was identified by optical imaging (OI) techniques (Blasdel and Salama, 1986, Grinvald et al., 1986, Bonhoeffer and Grinvald, 1993, Bonhoeffer and Grinvald, 1991, Hübener et al., 1997, Bonhoeffer and Grinvald, 1996). Fig. 2 shows a colour coded feature map as determined by OI. The orientation columns were identified for a set of eight orientations and displayed by one colour for each orientation resulting in formations around the singularity points that look like toy propeller. That is why a singularity point together with the surrounding feature domains is called pinwheel. The figure also shows other structural details like ocular dominance columns and a so called hyper column (cut out layer), which is defined as the smallest piece of cortex that contains all processing units identified for the area, i.e. ocular dominance columns of both eyes each containing a complete set of feature representations. It is noteworthy that this organization principles have been shown to be an optimization of the feature space coverage (Swindale et al., 2000, Carreira-Perpinan and Goodhill, 2002).



**Fig. 2:** Sketch of the functional organization of a piece of primary visual cortex. The color coding of the orientation columns was adopted from the visualization schemes commonly used for OI data. The respective stimulus orientation for each color is displayed at the bottom right. The elongated columns marked with R and L represent the ocular dominance columns. The small piece of cortex at the top right depicts the area of a hyper column.

The columnar organization of the visual cortex is accompanied by a network between the columns that is structured with respect to the columnar specificity and cortical distance. (Kisvarday et al., 1997; Gilbert and Wiesel, 1989; Schmidt et al., 1997; Löwel and Singer, 1992). Two types of long range connections between columns of the same specificity have been described to emerge (Galuske and Singer, 1996) in the adult cortex, one as sparse pyramid-pyramid connections (Gilbert and Wiesel, 1989; Kisvarday and Eysel, 1992), the other as sparse pyramid-basket cell connections (Douglas and Martin, 1990; Douglas and Martin, 2004; White, 1989). The combined effect of these inter-columnar connections on the dynamics of cortical activity will be considered further by the computer simulations performed for this thesis.

Going back to the peculiarities of the PVC of the cat, the functional surround shall be outlined

briefly. The PVC of the cat is commonly viewed to consist of area 17 and 18 since both areas receive parallel input from the retinogeniculocortical pathway. Both areas are reciprocally connected and project transcortically to area 19, area 20 and the middle suprasylvian sulcal cortex (Rosenquist, 1985). They also have descending efferents to several subcortical structures including a back projection to the LGN (Updyke, 1977). Hence, although the cat PVC is commonly viewed as being the first cortical instance that detects features of a scene and transmits its computations to higher cortical areas, it is already embedded into a massively inter-connected network in which it can participate in setting off ongoing activity against the live transmission of visual scenes from the eyes.

For a deeper discussion of any aspect touched in this section see (Payne, 2003).

### **3 Visual Pathways**

The cat primary visual cortex is commonly accepted to consist of two areas, area 17 and area 18. Hence, there is more than one upwards stream building a strict hierarchical network for the processing of visual information. The same holds true for other mammals including humans, but in other species the stream usually diverges after the PVC. One stream, which processes the “what” aspect, i.e. the identification of objects, follows a ventral path and the other stream was identified to follow a dorsal path (Goodale et al., 1991; Goodale and Milner, 1992) and is concerned with the “where” of a visual scene (Goldman-Rakic, 1995; Bullier et al., 1996; Barbas, 1988). The two streams were correspondingly termed the “what” and the “where” paths. However, the two pathways can not be viewed as independent entities. Already areas 17 and 18 of the cat are reciprocally connected. Such reciprocal connections are maintained throughout the what and where path, including more visual areas as the “hierarchy” is traversed (Rosenquist, 1985). Furthermore, the parallel streams are not only interconnected at each level in the hierarchy, they also project back onto the next lower level. Overall, the organization of the visual pathways thus follows three principles, i) hierarchical bottom-up projections, ii) top-down projections iii) parallel pathways and iv) reciprocal connections between steps of the parallel pathways.

## C Concepts of Information Representation and Processing

### 1 Information that Enters the System

Our bodies are continuously bombarded by electromagnetic waves. The evolution has equipped mammals with sensors that can detect such waves within a small range of wavelengths. Waves of a length between 1.5 mm and 0.75  $\mu\text{m}$  can be sensed by the skin since it absorbs these wavelengths right at the surface, transforms the energy into heat and thereby stimulates the thermal receptors of the skin. The heat is perceived with little spatial resolution and without depth information. However, electromagnetic waves in the range of 0.8  $\mu\text{m}$  to 0.4  $\mu\text{m}$  departing from within a cone towards the eye converge through an adaptable lens onto the retina where photoreceptors translate the electromagnetic field energy into transmembrane deflections from electro-chemical equilibrium. The two dimensional images are sensed with high resolution, with stereoscopic depth information and with the knowledge of the spatial position, which is provided by the interplay between the visual scene and the motor system that positions the body, head and eyes.

The retinae of the two eyes contain at any moment all visual information about the visual scene as is, i.e. without contextual information. And since there are no efferents to the retinae, this information must be complete in the sense that all information necessary to perceive the visual scene as we do must have been transmitted by the retina before. Clearly, this amount of information is less than the amount of information that is physically contained in the scene, because that would reach infinity due to the continuous nature of time, space and colors. Thus, the retina has to perform some kind of data reduction and compression. Indeed, as outlined in the following, some perceptual phenomena could be related to retinal signal processing.

Several aspects of retinal processing can be illustrated by modern digital compression methods for movies. On the one hand, these methods mirror strategies of the retina and on the other hand, they remove information that would not be transmitted by the retina anyway and which's absence would therefore not be perceived anyway. At a first step the spatio-temporal continuum of, for simplicity, grey scale values is sampled spatially into pixels, temporally into frames and then grey scale values are stored with a certain bit depth by the camera. Unlike the retina, the spatial sampling resolution of a camera is isotropic and can be reduced

so far that its size remains below the angular resolution of the spectator. The retina also samples the scene spatially by virtue of its photoreceptors. But since the eyes, head, trunk *et cetera* can be moved by the spectator, the visual scene can be shifted on the retina. By virtue of this ability, the retina could develop a kind of data reduction by defining a region of high spatial resolution, the fovea, and reducing the resolution towards the periphery. Any region of interest can be inspected with high resolution by shifting that region onto the fovea<sup>1</sup>. Already the photoreceptors of the retina have been found to limit the temporal resolution of perception, because the peaks of their membrane potentials fuse for too fast luminance changes, thereby producing a potential and percept about equal to the temporal mean luminance (Miller et al 1961). Another psychophysical correspondence has been found between the perceived luminance and the logarithmic response function of photoreceptors to the light intensity. Hence, the frame rate of movies have been set to the temporal resolution of the photoreceptors and modern movie compression methods scale the grey scale resolution to the slope of the photoreceptor response function. Ganglion cells integrate excitatory and inhibitory signals from the photoreceptors, producing RFs that are rather sensitive to fast temporal and small local changes in the luminance than to slow or global changes (KUFFLER, 1953). Thus, these cells rather transmit changes per se but an image pixel by pixel. Picking up the analogy to the movie compression methods, great progress was made, when recently an algorithm was introduced that stores a whole frame from time to time, but in between, it detects and stores only changes of the scene. It is sensible to suggest that the retinogeniculocortical pathway uses analogous computations, but with lower compression rates since it adheres to pure analogue live computation, redundancy and evolutionary constraints such as fastest operation possible whenever cues of danger emerge in the scene. The brain may be a system that optimized the ratios between data compression and operational necessities under the limitations of the computational resources it can draw from. However, the common view of the retinal RF structure associates it with various functional operations ranging from static image processing like gradient detection to the detection of temporal changes in luminance (e.g.: Shapley and Perry, 1986).

---

<sup>1</sup> For the production of movies, this strategy is not an option, since no one knows the location of the scene the spectator will shift onto his foveae.

## 2 Hierarchical Versus Distributed Processing

The increasing complexity of the RFs along the retinogeniculocortical pathway (Hubel and Wiesel, 1959) pointed towards a concept of hierarchical feed forward connections that converge from hierarchically lower RFs onto higher cells in a way that more complex RFs emerge. For instance, it was proposed that the orientation selectivity of cells in the primary visual cortex (PVC) is a result of collinearly arranged thalamic cells converging onto the same cortical cell. Indeed, the RFs were found to increase in size, complexity, abstraction and specialization along the cortical hierarchy (Zeki, 1974; Desimone et al., 1985; Maunsell and Newsome, 1987; Livingstone and Hubel, 1984; von der Heydt et al., 1984; von der Heydt and Peterhans, 1989; Peterhans and von der, 1989; von der Heydt and Peterhans, 1989; Adelson and Movshon, 1982; Gallant et al., 1993; Tanaka, 1992; Tanaka, 1993; Rolls, 1992; Yamane et al., 1988; Miyashita, 1993; Wachsmuth et al., 1994). Consequently, it was proposed that at the end of the hierarchy single neurons of extremely high specificity should exist that form the neuronal correlate of perception. This concept was termed the single unit doctrine of perception and found its most excessive interpretation in the suggestion of pontific cells (Sherrington, 1941). Each of these cells would code for one percept. The existence of pontific cells was denied (BARLOW, 1972), because the combinatorial variety of possible percepts would clearly exceed the number of neurons in the brain. Thus, theoretical considerations rendered it reasonable to expect “cardinal” cells instead of pontific cells. Thereafter, a group of cardinal cells with lower selectivity than the pontific cells would represent the percept (BARLOW, 1972). The existence of cardinal cells seems to be confirmed in so far, as highly specific cells were found (e.g.: Cooke et al., 2003; Graziano et al., 2004) and these were shown not to be activated alone (Wang et al., 1996), but other organization principles render it difficult to maintain this concept as will be discussed further below.

However, it seems reasonable to accept the concept of the feed forward convergence to ever higher cortical areas and ever more complex RFs. But it is equally clear, that this processing strategy is at least modulated, if not intermingled with other processes, because back-projections from higher to lower areas are known from anatomy to exist (Hupe et al., 1998; Kohn and Worgotter, 1996; Murphy and Sillito, 1996) and higher cognitive functions that are attributed to higher cortical areas, such as attention, have been shown to modulate the response of neurons even as far down in the hierarchy as in the LGN (Singer, 1977) and primary visual cortex (Luck et al., 1997; Buchel and Friston, 1997; Steinmetz et al., 2000;

Fries et al., 2001; Treue, 2001). Furthermore, the overall connectivity and response variability suggests that the incoming information meets a network that matches the new information with the ongoing activity (Tsodyks et al., 1999; Kenet et al., 2003), perhaps expectancy, and dynamically conducts the processing depending on intermediate results, network states or other variables.

To summarize, the visual system follows several functional principles. The first is that of hierarchically ordered feed forward streams, the second is the top-down influence of higher areas onto the previous one (which bends the notion of the “hierarchy” towards a “loop” when ongoing activity is considered), and the third principle is that of distributed processing in highly interacting areas. The distributed processing of visual information leads to highly specific, invariant and therefore abstract RFs. For instance, a neuron may detect a cup despite of color and position, but for the whole percept all this information is required. We are able to perceive and distinguish a blue cup right hand side to a red cup. And this information must be available for further processes, as required in visuo-motor tasks, since we are able to reach for the blue/red or left/right cup. Thus, the massive interconnectivity of the areas suggests, that the neuronal representation of visual objects resides in the distributed activity of groups of neurons throughout the visual pathways and up to the association areas.

### **3 Binding by Synchrony**

The distributed processing of the cerebral cortex raises the question on how the relatedness of the distributed representation is maintained. For the visual system this problem is most obvious for several objects of, say, different colours. The information about which colour belongs to which object is not clear when the representation of the objects and the colours reside in different cortical sites. At least in higher cortical areas with large or location invariant RFs, such relational information could not be maintained by a “labelled line code” that could be imagined from the retinotopic organization of the PVC. And even for area 17 with its high spatial resolution stimuli have been designed, that question the membership of neurons in the representation of one object if several objects are present (von Grunau and Dube, 1993; Gail et al., 2004). Several concepts were suggested to solve this problem of binding together distributed representations to an ensemble. From attentional spotlights to areas, that establish dynamic arrays of pointers to ensemble members, a variety of solutions to the binding problem were proposed (for in depth discussions, see: Neuron, Issue (10), 1999).

However, the most economical way to bind neurons together to ensembles is, to deposit the membership information within the neuron's signal itself. In order for this membership information not to interfere with the primary representational duty of the cell, a second, orthogonal coding dimension is required. Such a coding dimension has been proposed to reside in the relational temporal fine structure of the neurons participating in an ensemble (von der Malsburg, 1981; von der Malsburg and Schneider, 1986; Singer, 1990; Singer and Gray, 1995, Milner, 1974). Such a relational code would not interfere with the rate information as claimed above, because the relative timing of action potentials can be altered without changing the rate (Riehle et al., 1997; Samonds et al., 2004). Furthermore, since some APs could be synchronized with one ensemble and other APs with another, a neuron could participate in several ensembles, still without interfering with the rate code. Neurons have been shown to be able to act as integrators, being sensitive to input rates, and as coincidence detectors, either by virtue of their intrinsic cell properties (Abeles, 1982; Softky, 1994; König et al., 1996; Gerstner et al., 1996; Agmon-Snir et al., 1998; Koch et al., 1996), modulatory effects (Munk et al., 1996; Whittington et al., 1998; Herculano-Houzel et al., 1999) or by virtue of the network input itself (Douglas and Martin, 1991; Softky, 1995; Tiesinga and Sejnowski, 2004). Therefore, it seems reasonable that receiving rate sensitive neurons can detect representations and coincidence sensitive neurons can detect ensemble membership information. Thus, the relation that has been proposed to bind neurons together to ensembles is the synchronicity of their discharges.

There are four basic mechanisms that can influence the degree of synchronization between neurons. The first one, although trivial on first sight, is to change the chance level of coinciding spikes to occur by changing the inter spike interval (ISI) distributions of the neurons. Depending on the propagation properties of ISI distributions, which is subject to current research, this rather passive appearing mechanism could possibly propagate from an area where grouping criteria were found, to other distributed areas where different features are represented but still bound together through that "coincidence by chance". The second mechanism synchronizes and desynchronizes neuronal populations by means of network oscillations. Two or more groups of neurons can thereby be synchronized by oscillating coherently or by contributing their spikes to the same cycles, whereas the groups can be desynchronized by shifting the relative oscillation phase or by skipping the cycles during which the other ensemble is active. Although one could argue that the oscillations alter the rate and are therefore no orthogonal information stream, it appears that the rate can still be

represented in the oscillation amplitude but at the expense of some resolution or quantization in time. The third mechanism produces synchrony above the chance level of any underlying ISI distribution and results from the convergence of synchronous APs onto a neuron with coincidence detection capabilities. If the neurons that provide this input also converge onto other neurons, then the two receiving neurons are likely to exceed the spiking threshold at the same time and will exhibit synchronous APs. This concept of converging and diverging connections has been pushed to its extreme by Moshe Abeles, who proposed chains of neuronal groups that propagate volleys of synchronous activity. This was successively modelled by connecting the groups in an excitatory all-to-all fashion.

Experimental evidence for the synchronization of cell populations was derived from oscillations in the local field potential (LFP) recorded from the primary visual cortex of the cat (Gray and Singer, 1987; Gray and Singer, 1989; Gray et al., 1989; Eckhorn et al., 1988). Since the low pass filter of the LFP signal would average out any asynchronous contributions, these oscillations provided evidence that a large group of neurons had synchronized their activity. Oscillatory activity was subsequently also shown for small groups of nearby cells (Gray and Singer, 1989; Gray et al., 1989). The synchronization of more distant cells was found in cat between areas (Eckhorn et al., 1988, Engel et al., 1991, Nelson et al., 1992) and hemispheres (Engel et al., 1991, Nowak et al., 1995) and the same findings could be reproduced for the monkey cortex (Ts'o and Gilbert, 1988, Kreiter and Singer, 1996, Fries et al., 1994, Salin and Bullier, 1995, Kreiter and Singer, 1992, Eckhorn et al., 1993). The stimulus dependent synchronization and desynchronization according to the hypothesis of binding by synchrony could be confirmed (Gray and Singer, 1989, Engel et al., 1991, Engel et al., 1991, Kreiter and Singer, 1996). Furthermore, evidence for the synchronization as predicted by the synfire chain model was found (Toyama et al., 1981; Abeles, 1982, Abeles et al., 1993; Ikegaya et al., 2004), manifesting in precisely repeating inter-coincidence intervals.

## **D The Aim of the Thesis**

Summarizing the previous sections, the function of the brain is based on the coordinated interaction of the activity of millions of neurons. In the cerebral cortex these neurons are embedded into a well defined architecture, which is characterized by a high degree of functional and structural organization. Sensory areas usually contain a topologically ordered map of sensory surfaces and feature domains. Examples are the retinotopic (Tusa et al., 1978;

Tusa et al., 1979), somatotopic (Jones et al., 1978) and the tonotopic maps (Merzenich et al., 1975) in low level sensory areas. Allowing for some variability in details, these topological organizations are remarkably similar among animals of the same species (Tusa et al., 1979) and even across species including humans (Reppas et al., 1997; Gelnar et al., 1998; Ruben et al., 2001). Another architectonic feature of the neocortex is its functional columnar organization. The columns are interconnected selectively according to their functional properties and cortical distance (Gilbert and Wiesel, 1983; Gilbert and Wiesel, 1989; Kisvarday et al., 1997; Schmidt and Löwel, 2001). Unlike the general topographic organization, the patterns of these functional sub-networks exhibit considerable inter-individual variability, even between animals of the same species (e.g. Horton and Hocking, 1996) and, therefore, these patterns have to be determined individually.

Current concepts and strategies in neuroscience research are based on these microstructural and connectivistic facts. Theoretical considerations and recent experimental results (Salinas and Sejnowski, 2001; for reviews see Engel et al., 2001) on the representation and processing of sensory information stress the need to search for distributed population codes by assessing temporal relations among distributed responses in order to explain how essential computations such as scene segmentation, feature binding or the flow of information are performed. To achieve these tasks, parallel electrophysiological recordings from multiple functionally defined neurons have to be accomplished. Ideally, the different recording sites should be targetable with sufficient precision to obtain responses from preselected members of the different functional micronetworks described above. This requires a priori knowledge about the potential recording sites and methods for the precise placement of electrodes.

As the topographic organization of functional sub-networks varies from individual to individual, the respective feature maps have to be determined prior to electrode placement and then targeting methods are required that permit precise placement of multiple electrodes according to the topology of the functional maps.

The main problem that this dissertation aimed to solve was the development of a targeting method meeting the requirements outlined above. Three approaches were pursued from which two disqualified for various reasons (IIA1). The experiences with the first two approaches, the spatial acuity of at least 200  $\mu\text{m}$  and the applicability to many electrodes in parallel made it obvious, that a high precision device was required that could not be produced by classical

techniques like drilling or etching. Therefore, a matrix of extremely precise guide tubes (IIA2.2) was developed in cooperation with a company providing RMPD<sup>®</sup> (Rapid Micro Product Development) production techniques. In order to be able to relate the guide tube positions to the OI maps, several devices (IIA2.2) and software packages (IIA2.3) were developed. Subsequently, the new method was tested to meet the criteria for an application to animal experiments (IIA2.4, IIIA1.1).

Since the method turned out to be of sufficient precision, experiments were performed under its application. The questions addressed by these experiments targeted the formation of assemblies via stimulus dependent synchronization and desynchronization. Before, the dynamic emergence of such assemblies has primarily been shown to exist by virtue of pairs of multi unit responses. Therefore, the experiments performed here aimed to follow the need to manifest the dynamics of assemblies by means of large pools of simultaneously recorded activity and to investigate the participation of single neurons in assemblies by separating neuronal action potential waveforms before further analyzing their synchronization behavior. These experiments test a central prediction of the hypothesis of binding by synchrony and investigate the underlying mechanisms of ensemble participation.

In order to obtain well separable AP waveforms, undisturbed signals are required. Although multiple sources of noise were identified and removed during and in between experiments, some disturbances remained. Therefore, a method for the removal of correlated noise was developed and implemented (IIA4.1). Furthermore, the continuous recording of 16 channels did not allow to use high sampling frequencies, for the amount of data could have not been stored on commonly available storage media. Thus, a method for the reconstruction and subsequent up-sampling of AP waveforms was developed (IIA4.4) in order to render the waveforms comparable. Finally, the prospect of analyzing 16 recording sites which are further divided into, say three, single units per channel resulting in about 50 time series and 1176 pairwise cross-correlations, made it necessary to develop an analysis concept that requires little manual intervention. Hence, an analysis framework was developed that allows for the automated processing of large numbers of simultaneous time series (IIA4.2).

The experimental approach described above can only test the underlying hypotheses on the functional role of neuronal synchronization, but it can not access the “hidden variables” of the system that led to the network behavior. The type of synchronization investigated in this work

is the synchronization of intra-areal but distant columns. Such long range synchronizations were found to be usually of oscillatory nature, and the mechanisms that lead to the synchronization of distant columnar oscillation are still a matter of debate. Hence, a network simulation was performed in parallel to the experimental approach, addressing the question, to what extent the current knowledge about the intrinsic connectivity of the cortex can account for the synchronization of distant columns.



## II Materials and Methods

### A Animal Experiment

#### 1 Overview

The need for targeted parallel recordings, as outlined in the previous chapter, led the course of this thesis work through several experimental approaches. Three different techniques were invented in order to optimize the crop of electrode combinations that are appropriate for testing the hypotheses that sensory interrelations are coded by temporal relations of neuronal activity.

The first approach was to use a commercial electrode manipulator (32 Electrode Matrix, ThomasRecording, Germany) with a fixed electrode arrangement which was then positioned by visual control according to the previously recorded feature maps.

The second approach used a custom-made piece of acrylic glass with drilled holes in as guide tubes for the electrodes (Fig. 3). It was mounted onto a slide which was movable unidirectional across the cortex and able to be fixated by means of two grub screws. The holder of the slide could be mounted above the cortex in one out of eight rotational positions. The movability of the slide together with the possibility of rotating the holder yielded a vast variety of possibilities for the holes to be positioned above the cortex. This option was then used to optimize the hole positions with respect to a map of cortical activity, as can be obtained by e.g. optical imaging of intrinsic signals. This is, to optimize the yield of recording sites of a specific feature selectivity. However, this approach had to be discarded due to several reasons: i) the available techniques for drilling limited the aspect ratio of the holes to about 2.0:0.4 mm. Since this aspect ratio determines the angular play an electrode can exploit, the holes did not allow for precise guidance of the electrodes to a specific cortical site. Furthermore, the precision turned out to be degraded by ii) the elasticity of the acrylic glass and iii) the variance of electrode thickness. These issues further led to problems such as electrodes getting stuck in the holes, rendering them immobile. Since the holes had a diameter of 0.3 mm the electrodes had to be rather thick, which always results in dimpling problems (i.e. the electrodes push the cortical tissue down) when using multiple electrodes. Following these drawbacks, neither the technique nor the actual data obtained using this technique were further used in the course of this work.

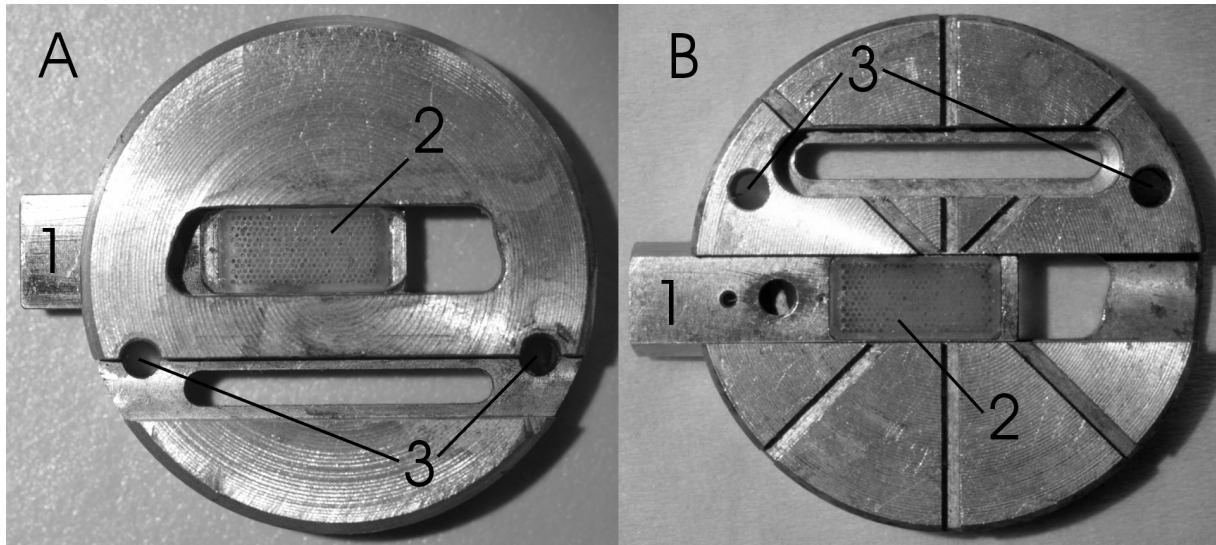


**Fig. 3:** The device of the second approach to perform targeted electrophysiological recordings. A) Birds eye view. B) View of the bottom side. Numbers mark 1) the slit, 2) the acrylic glass inset with guiding holes and 3) the holes for fastening the whole device above the cortex with screws.

Based on the experiences with the second approach, a new technique for the targeted recording from multiple cortical sites in parallel was developed. This third approach maintained the idea of having an array of holes through which to guide the electrodes to certain positions on the cortex. In order to do better than in the second approach, we specially developed an array of holes with an extremely high aspect ratio. The details of this successfully applied technique are outlined in greater detail in the following chapter.

The general experimental procedure was the same for all three approaches, but there were some peculiarities in the third approach requiring special attention. Therefore, the experimental procedure is outlined in the following chapter for the third approach only. The procedure for the other cases can be deduced from this description by leaving out the steps unique to the third approach.

## **2 A New Technique for Targeted Cell Recordings**

### **2.1 The General Approach for Targeted Recordings According to Feature Maps**

As a general approach for the parallel electrophysiological recording from multiple predefined sites of a feature map, feature maps were obtained by optical imaging of intrinsic signals (OI) and subsequently electrodes were placed by using an array of densely packed guide tubes. This array is positioned above the cortex providing a lattice of possible electrode insertion

sites. In order to relate the positions of the guide tubes to positions on the feature map, a fixed reference frame is required. In this approach, the reference to cortical coordinates is established by a metal ring, the *base ring*, which is cemented onto the skull. This ring serves as a base for both, the optical imaging chamber and the array of guide tubes. As the positions of the guide tubes with respect to the base ring are fixed, the only variable in this procedure to be determined is the exact position of the feature map. This part of the alignment procedure is achieved by projecting a coordinate system grid onto the cortical surface by means of a slide projector. The coordinate system is set into a defined position and rotation with respect to the base ring by adjusting the projected grid to little marks at defined positions on the optical imaging chamber. An image of the projected coordinate system is taken with the optical imaging camera in exactly the same position as for the recording of the feature maps. Thus, the coordinate lines are visible in the image of the cortical surface and give all positional information about the feature map that is needed to align it with the guide tube positions. Finally, a set of guide tubes is selected for inserting the electrodes according to the desired feature constellation of the neurons to be recorded from. This procedure allows for the targeted recording of functionally specified neurons.

Before describing the procedure of electrode targeting in greater detail, the parts of the targeting device are described more comprehensively below.

## 2.2 The Apparatus

**Head holder** (not shown): consists of a rippled bolt that is cemented to the skull and fastened to the stereotactic frame. The head holder has a flat design as it must not interfere with the beam of the coordinate projection device.

**Base ring** (Fig. 5A1, Fig. 5B1 and Fig. 6C): a titanium ring of 20 mm inner diameter, 30 mm outer diameter and 2 mm height. On the upper side, eight equidistantly arranged bridge-like protrusions 1 mm in height and 1 mm in width jut out of the surface, running radially from the inner to the outer ring diameter. Furthermore, the ring has a threaded hole in the middle between each protrusion at a radius of 25 mm.

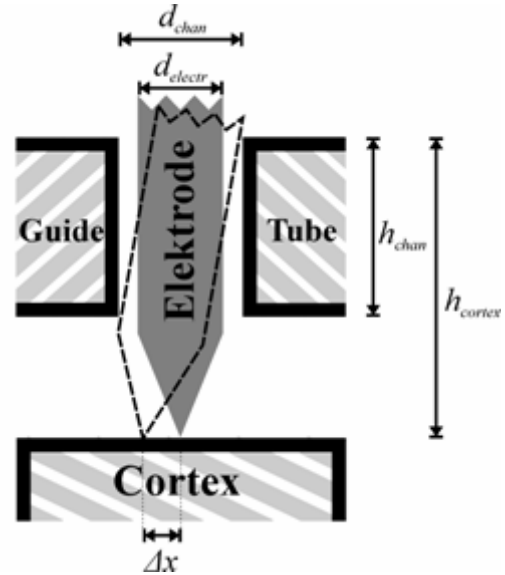
**Optical Imaging Chamber (OIC)** (Fig. 5A2-8, Fig. 5B2, Fig. 5D and Fig. 6): the basic concept of the OIC design has been adopted from Bonhoeffer and Grinvald, 1996. However, for the special purpose pursued here, the design had to be modified and new features had to be added. The resulting OIC is constructed as follows: a metal chamber (Fig. 5A2, Fig. 5B2 and

Fig. 6A), 9 mm in height, manufactured to fit on the base ring by having the same inner and outer diameter and at its bottom face (Fig. 5B2) the inverse geometry of the base ring's top surface (Fig. 5B1). At 2.5 mm height the inner diameter increases from 20 mm to 25 mm, producing a plateau inside the chamber. A glass plate (Fig. 5A4 and Fig. 6C) is placed onto the plateau with a silicone gasket ring (Fig. 5A3 and Fig. 6B) in between. In order to close the chamber a threaded metal ring (Fig. 5A5 and Fig. 6D) is screwed into the OIC that presses the glass plate against the plateau and provides a tight seal. At a height of 1 mm, two filling plugs (Fig. 5D indicated by an asterisk, Fig. 6H) are mounted on opposing sides of the chamber in order to fill the chamber with silicone oil for the optical recording. A metal plate with coordinate marks (Fig. 5A7 and Fig. 6E) can be mounted on top of the chamber above the glass plate. These coordinate marks provide a reference for adjusting the projected coordinate system. An additional aluminium ring (Fig. 5A6, Fig. 5B3 and Fig. 6F) with an inner diameter of 30 mm, an outer diameter of 38 mm and a height of 5 mm can be slid over the chamber and secured with screws at the sides. A trench in the ring allows a semi-translucent mirror (Fig. 5A8, Fig. 5D and Fig. 6G) to be adjusted at an angle of  $45^\circ$  to the glass and metal plate. The ring with the mirror makes it possible to record with the vertically mounted OI camera whilst projecting the coordinate grid horizontally through the semi-translucent mirror into the OIC.

**Tube grid** (Fig. 5A9-10, Fig. 5E and Fig. 5F): a custom made plastic cylinder (Fig. 5A10 and Fig. 5E), 15 mm in height and 17 mm in diameter. It is inserted into a hollow metal cylinder (Fig. 5A9 and Fig. 5B4) which fits onto the base ring in the same way as the OIC. The metal cylinder has an opening with a fitted cover (Fig. 5A9b) at the lower front side through which the area below the plastic cylinder is accessible after insertion. A marginal notch, indicated in figure 1F, prevents the plastic cylinder from longitudinal or rotational movement within the metal cylinder. Parallel to its roll axis, the plastic cylinder contains about 3000 channels of  $150\ \mu\text{m}$  core diameter and a centre to centre distance of  $220\ \mu\text{m}$ . The geometry, especially the aspect ratio of the channels, is designed to lead electrodes to their target points, i.e. the point at which the rotational axis of the channel crosses the cortex, with extreme precision and the highest resolution possible. This precision can be calculated by using the dependence of the maximum electrode displacement on the channel aspect ratio and the electrode diameter (Fig. 4):

$$\Delta x = (d_{chan} - d_{electr}) \left( \frac{h_{cortex}}{h_{chan}} - \frac{1}{2} \right) = (0.15mm - 0.12mm) \left( \frac{20mm}{15mm} - \frac{1}{2} \right) = 0.025mm \quad (1)$$

where  $\Delta x$  is the maximum distance of the electrode tip to the rotational axis of the channel,  $d_{chan}$  the channel diameter,  $d_{electr}$  the electrode diameter,  $h_{cortex}$  the height of the upper end of the channel relative to the cortical surface and  $h_{chan}$  the height (length) of the channel. The values inserted are typical for the setup used here and yield a maximum error of  $25 \mu m$  in electrode position. Together with the uncertainty due to the resolution of the functional maps of  $25 \mu m$  the accuracy which can theoretically be reached with this approach is about  $50 \mu m$  (1).



**Fig. 4: Angular play of an electrode in a channel.**

The tube grid was developed in cooperation with microTEC GmbH (microTEC, Gesellschaft für Mikrotechnologie, Bismarckstrasse 142b, 47057 Duisburg, Germany) using RMPD<sup>®</sup> (Rapid Micro Product Development) technology.

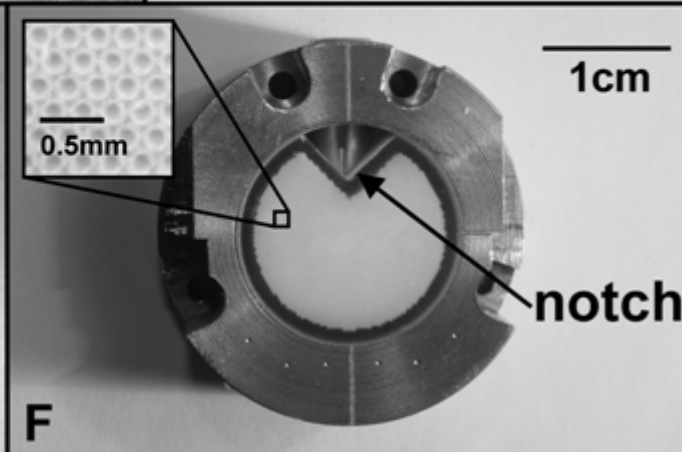
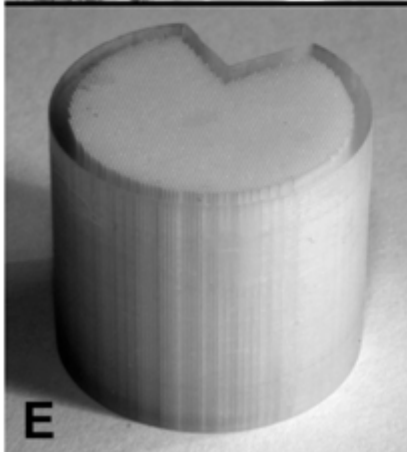
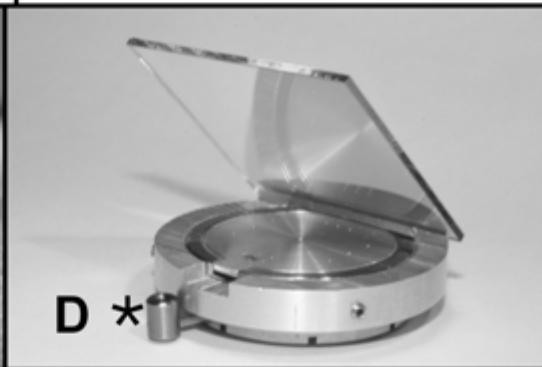
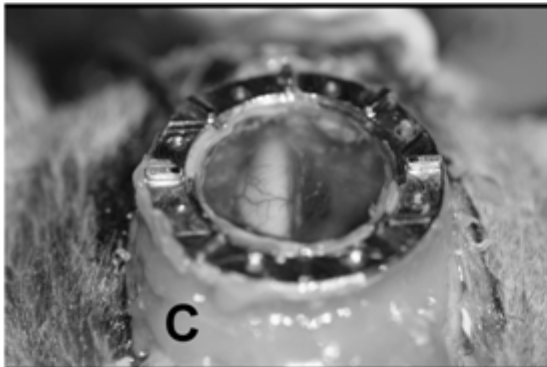
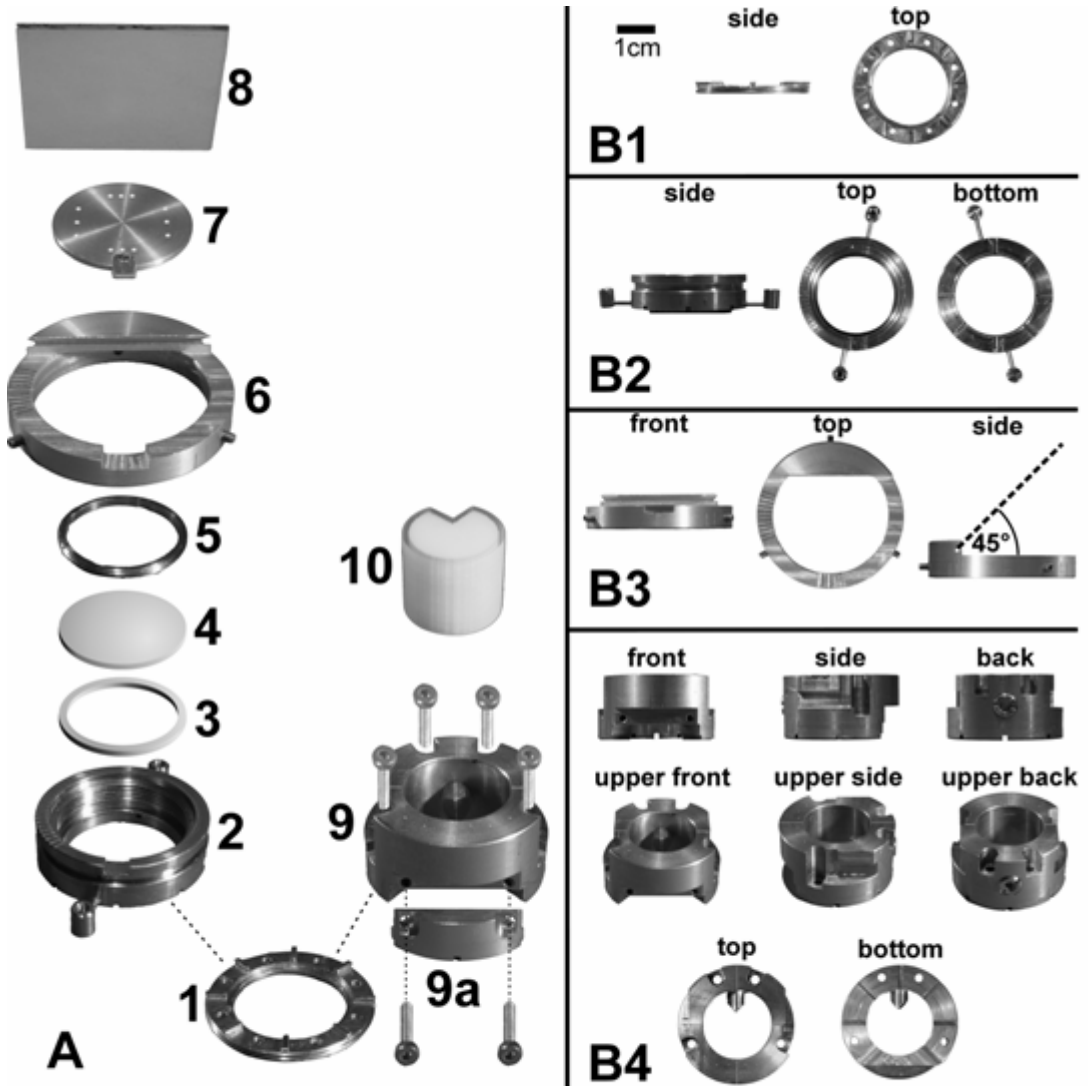


**Fig. 5:** Hardware items for placing electrodes according to a feature map. (A) Schematic illustration of how the OIC and the metal cylinder are pieced together from their components for mounting on the base ring (1). On the left side from the bottom to the top are shown: the basic optical imaging chamber (2), silicon gasket (3), glass plate (4), threaded metal ring (5), mirror holder (6), metal plate with coordinate marks (7) and the semi-translucent mirror (8). On the right side: metal cylinder with screws (9), cover for the opening of the metal cylinder (9a) and tube grid (10). Both devices, the OIC and the tube grid holder, can be mounted onto the base ring shown at the bottom centre. (B) Close-ups of the more complex components in (A). (B1) the base ring from side and above; (B2) the OIC from the side, above and from beneath; (B3) Mirror holder as seen from front, above and the left side (left to right, the dashed line indicates the mirror position); (B4) images of the metal cylinder (tube grid holder), the first row shows front, side and rear view; the images of the second row are taken from elevated front, side and rear positions. The images in the bottom row show the cylinder from above and beneath. (C) The base ring cemented onto the skull. (D) The optical imaging chamber with the coordinate metal plate and the semi-translucent mirror mounted onto it. The asterisk indicates one of the two filling plugs. (E) Close-up of the tube grid. (F) The tube grid mounted into the tube grid holder and fixated by a bolt. The inset shows an enlarged area of the tube grid, thus showing the geometry of the guide tube arrangement.

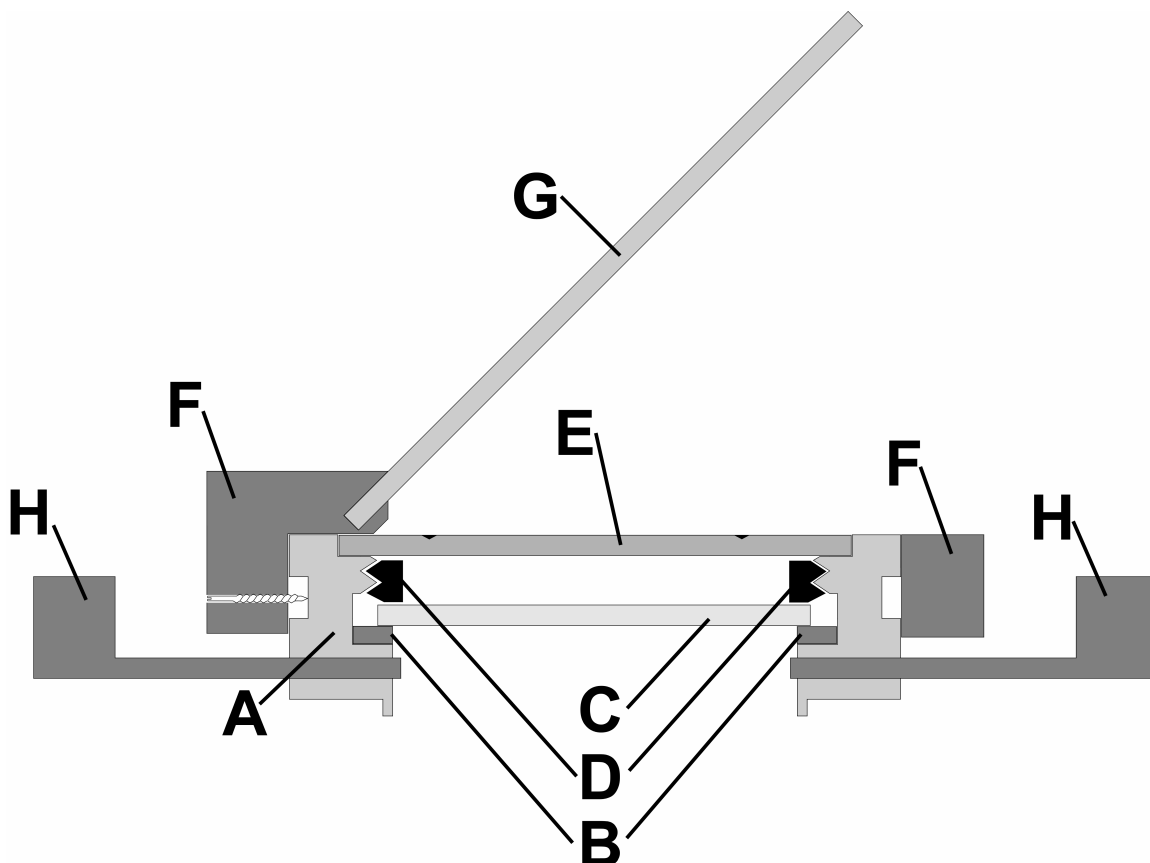


**Fig. 6:** True-to-scale cross-section sketch of the multi purpose optical imaging chamber for recording optical data and projection of a coordinate grid onto the cortical surface. (A) The chamber. (B) Silicon gasket ring. (C) Glass plate. (D) A threaded metal ring. (E) Metal plate with coordinate marks. (F) Outer ring serving as holder for the mirror. (G) Semi-translucent mirror. (H) Filling plugs.

**Projector** (Fig. 7): in order to determine the cortical coordinates of the optical imaging map, a coordinate system has to be projected onto the cortical surface. The projection device is mounted onto an optical bench (Fig. 7A) and consists of a modified slide projector (Fig. 7B), which allows for precise translational movement in all (x, y, z) axes by use of micro-drives (Fig. 7C) and an optical lens (f = 2 m) (Fig. 7D). Moving the slide in an x- or y-direction alters the position of the projected image, whereas a movement in the z-direction (that is parallel to the optical axis) will adjust the size to the reference size given on the metal plate (Fig. 5A7). The optical bench is movable (Fig. 6E) along the optical axis of the projector for adjusting the focus. It is mounted on a knuckle joint (Fig. 6F) to adjust the angle of the

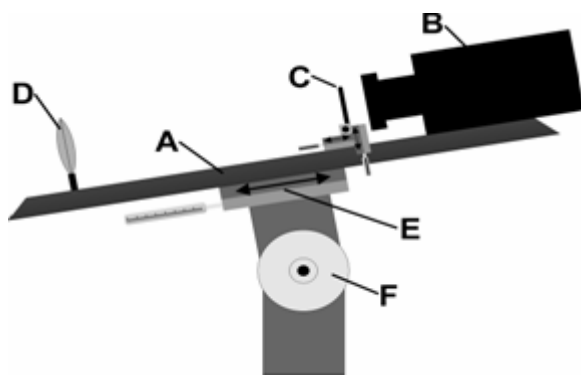


**Fig. 7: The projection device. (A) Slide projector without any slide inserted. (B) The slide of the coordinate grid mounted onto a xyz-axis stage. (C) Optical lens with a focal distance of 2 m. (D) Optical bench. (E) Linear micro-drive stage which moves the whole optical bench. (F) Knuckle joint.**

projector in the plane of the optical axis and the optical bench, i.e. vertically.

**Manipulator** (Fig. 8): a custom-made device, designed to move the electrodes back and forth. It consists of 16 linear micro-drives (Fig. 8 inset A), which can individually be moved at high precision. In order to minimize the spacing, the micro-drive movements are transmitted through Bowden cables, which converge onto a suspension (Fig. 8 inset B1), thereby confining them to an area of 14 x 6 mm. Electrodes are attached to the endings of the inner Bowden cables. These connections are established by insulating the

end parts of the inner Bowden cables with Teflon sockets (Fig. 8 inset B2), plugging small metal tubes (Fig. 8 inset B3) into the Teflon sockets and sticking the bent end parts of the electrodes into the metal tubes. The tension of the bent electrode end parts presses the electrode wires against the inner walls of the metal tubes, thus connecting them mechanically to the Bowden cable movements and electrically to the metal tubes. The metal tubes, in turn, are connected by thin wires (Fig. 8 inset B4) to the pre-amplifiers. To further reduce the spacing between the electrodes they are funneled through guide tubes (Fig. 8 inset B6) which depart from an area of 14 x 6 mm (Fig. 8 inset B5) onto an area of 8 x 4 mm (Fig. 8 inset B7). A few centimeters below, the metal cylinder (Fig. 8 inset B9) containing the tube grid (Fig. 8

inset B8) is attached to the manipulator to guarantee a fixed distance between the tube grid and the Bowden cable suspension.

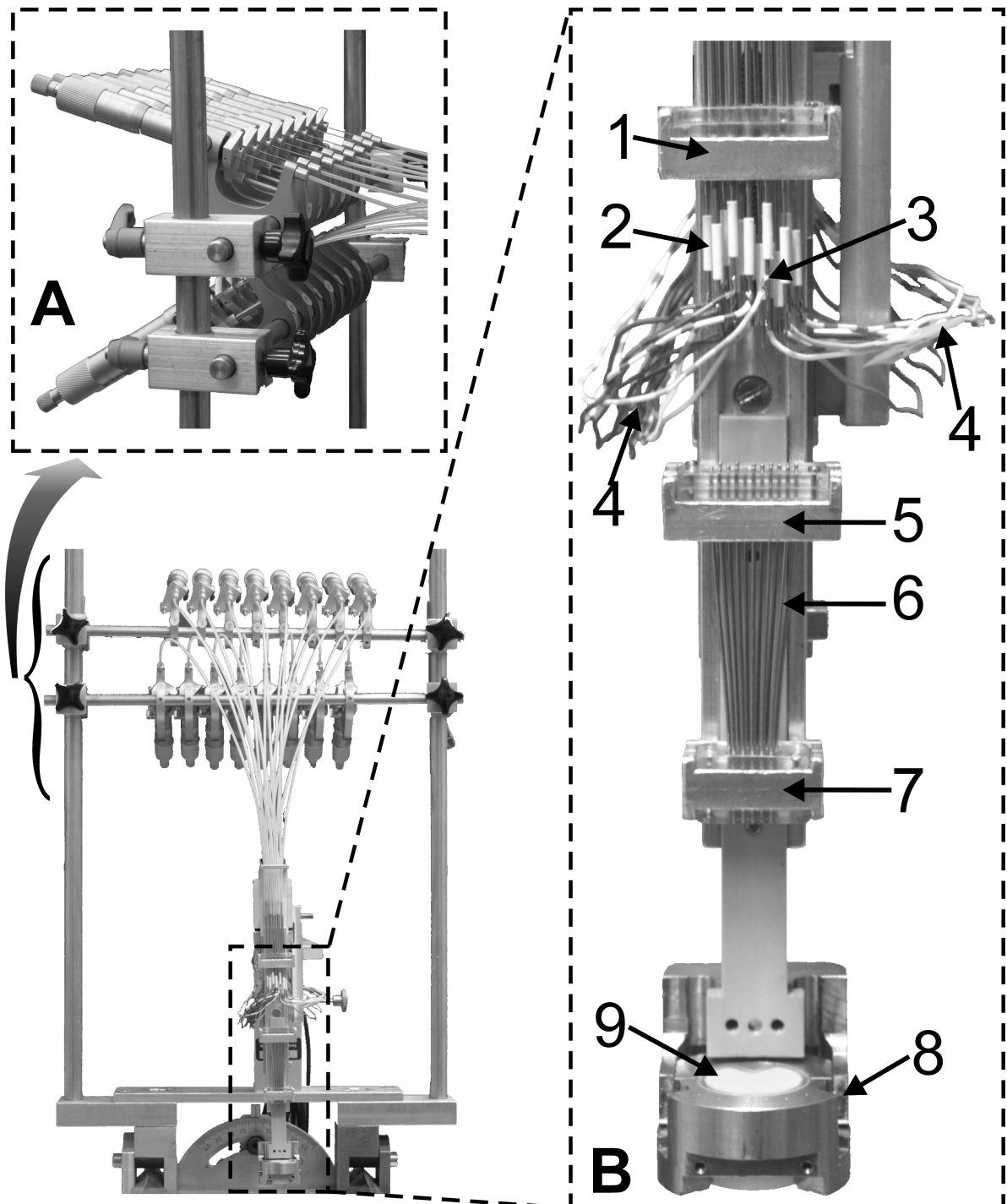


**Fig. 8:** The electrode manipulator. At the top, sixteen micro-drives are arranged in two rows (enlarged side view in inset A). The micro-drive movements are conveyed by Bowden cables which converge to a set geometry with closer spacing (B1). The inner wires of the Bowden cables are plugged into the upper side of insulating Teflon sockets (B2), whereas metal tubes are plugged in from the lower side (B3). Cables (B4) are soldered to the metal tubes, connecting them electrically to the amplification system. Converging tubes (B6) are drawn together 20 mm beneath the soldered metal tubes. Further below, the metal cylinder (B8) holding the tube grid (B9) can be mounted onto the manipulator system.

### 2.3 The Software

The mapping of the 4036 channels of the tube grid onto the cortical surface and onto the feature maps has to be accomplished during the experiment though experimental and medical circumstances not only restrict the time span of an experiment, but also degrade the data quality with time due to, for instance, degradation of the animal's general condition or degradation of the optics of the eyes. Thus, a mapping technique is required which is able to map all the channels comfortably, quickly, but yet reliably onto the cortical coordinates. Since most of the information is at hand digitally the mapping procedure is best implemented in a computer-aided fashion. The corresponding software was implemented under IDL 5.2, Research Soft Inc. and is described in the following.

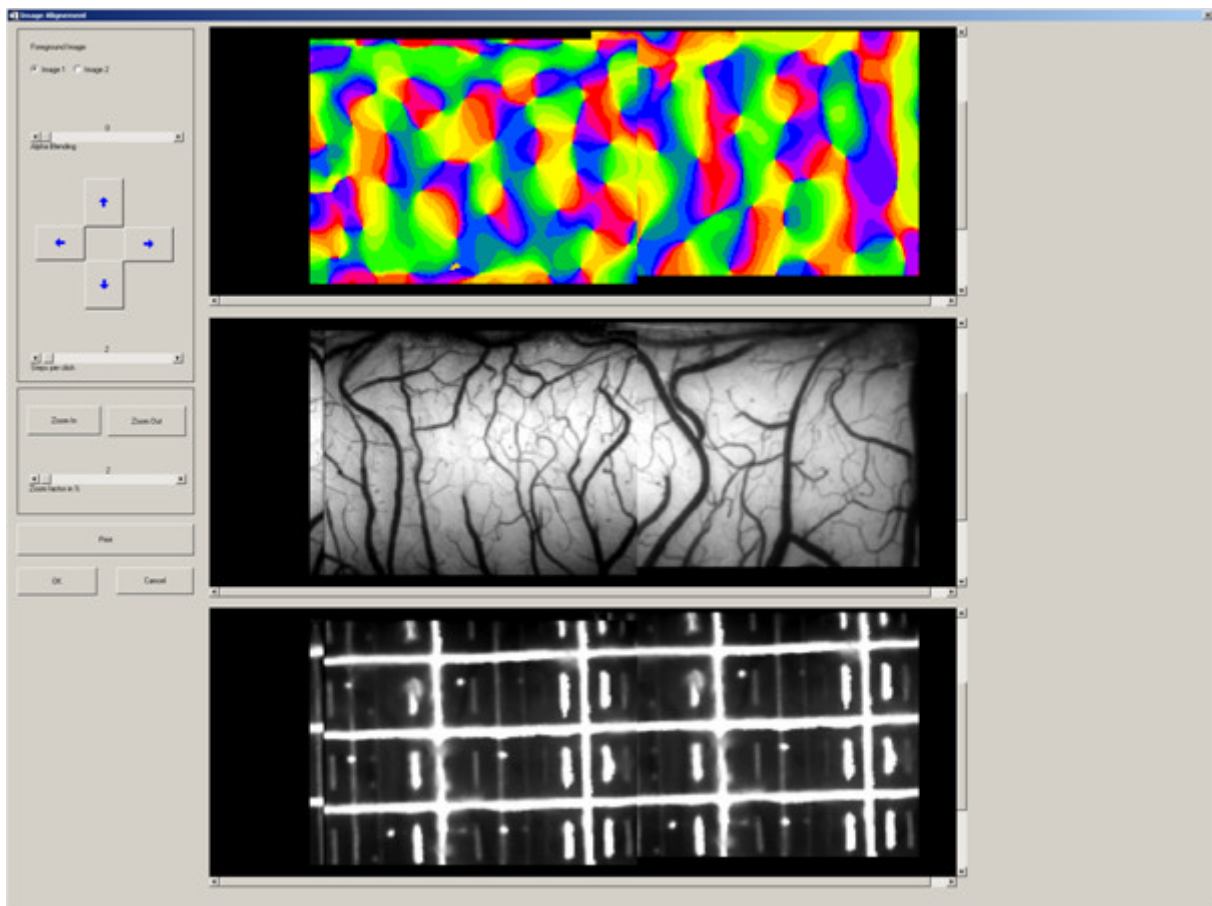


**Fig. 9:** User interface for the alignment of the partially overlapping images. The upper graphics display shows the two color coded functional maps, the centre display shows the image of the cortical surface and the lower display shows the images taken while the coordinate grid was projected onto the cortical surface. By means of the radio buttons, one of the two images can be chosen to be the foreground image which automatically is the one which can be moved by clicking the arrow buttons on the left. The user can zoom the displays in and out in order to achieve an optimal alignment by getting a closer view.

The size of one optical imaging map is about four by five millimeters. In order to cover a larger region the program allows for the use of two partially overlapping maps, which can be superimposed by virtue of the software as to in one large functional map. Since the feature maps, the video images from the cortical surface and the images of the projected coordinate grid are all taken from exactly the same positions, they can all serve as cues for the alignment of the images. For example, a branch of a blood vessel visible within the overlapping part of both feature maps is a well defined point which must be in register if the two images are well aligned. Therefore, the software displays all pairs of images and allows the user to align them in parallel by means of cursor buttons. Several helpful tools have been implemented such as the flipping of the foreground image or zooming in and out (Fig. 9).

After bringing the image pairs into register, the program needs information about the coordinate systems of the images and the cortex. Let  $\mathcal{P}$  be the coordinate system of the images, each element  $\mathbf{p}_i$  of which is a two dimensional vector uniquely specifying a point (or pixel) on the composite images. The second system  $\mathcal{O}$  has two dimensional elements  $\mathbf{o}_i$  as well and uniquely identifies cortical sites.  $\mathcal{O}$  is defined and visualized by the projected coordinate system (Fig. 10) which has a fixed position relative to the base ring. The transformation from  $\mathcal{P}$  to  $\mathcal{O}$  can be confined to consist of a translation  $\mathbf{o}_0$ , a rotation  $\mathbf{R}$  by an angle  $f$  and a linear scaling factor  $a$  and  $\beta$  for each dimension:

$$\mathbf{p}_i = \begin{pmatrix} p_i^x \\ p_i^y \end{pmatrix} = \begin{pmatrix} a \cos j & -b \sin j \\ a \sin j & b \cos j \end{pmatrix} \mathbf{o}_i + \mathbf{o}_0 = \mathbf{R}_i \mathbf{o}_i + \mathbf{o}_0 \quad (2)$$

It is known that  $a$  equals  $\beta$ , since the camera has quadratic pixels. Thus, this system of equations has four unknown parameters. In order to solve this, two pairs of  $\mathbf{p}_i$  and  $\mathbf{o}_i$  are required. Let the two vector pairs establish the equations  $\mathbf{p}_1 = \mathbf{R}_1 \mathbf{o}_1 + \mathbf{o}_0$  and  $\mathbf{p}_2 = \mathbf{R}_2 \mathbf{o}_2 + \mathbf{o}_0$ , it

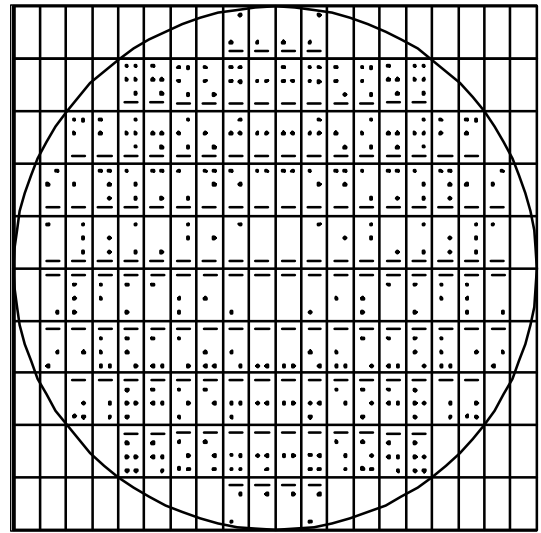


**Fig. 10: The coordinate grid projected onto the cortex in order to define a coordinate system of reference. The rectangles built by the coordinate grid bear codes in order to uniquely identify each rectangle. The bars code for whether the rectangle belongs to the posterior or the anterior half of the grid and the dots identify each rectangle within a hemisphere.**

then follows that

$$\mathbf{a} = \mathbf{b} = \frac{\sqrt{(\mathbf{p}_2 - \mathbf{p}_1)^2}}{\sqrt{(\mathbf{o}_2 - \mathbf{o}_1)^2}}$$

$$\mathbf{o}_0 = \frac{1}{2}[\mathbf{p}_1 + \mathbf{p}_2 - \mathbf{R}(\mathbf{o}_1 + \mathbf{o}_2)] \quad (3)$$

$$\mathbf{j} = \arccos\left(\frac{\langle \mathbf{p}_2 - \mathbf{p}_1 | \mathbf{o}_2 - \mathbf{o}_1 \rangle}{|\mathbf{p}_2 - \mathbf{p}_1| \cdot |\mathbf{o}_2 - \mathbf{o}_1|}\right)$$

Thus, in the next step, the program presents the composite image of the coordinate grid (Fig. 11). The user then selects two sites by mouse-click, thereby specifying  $\mathbf{o}_1$  and  $\mathbf{o}_2$ . The dot and bar coding between the coordinate lines (Fig. 10) enables the user to determine and to specify the corresponding  $\mathbf{p}_1$  and  $\mathbf{p}_2$  coordinate values in the given text fields (Fig. 11), whereby the coordinate transformation from  $\mathbf{?}$ , the feature map, to  $\mathbf{O}$ , the reference coordinate system, is established.

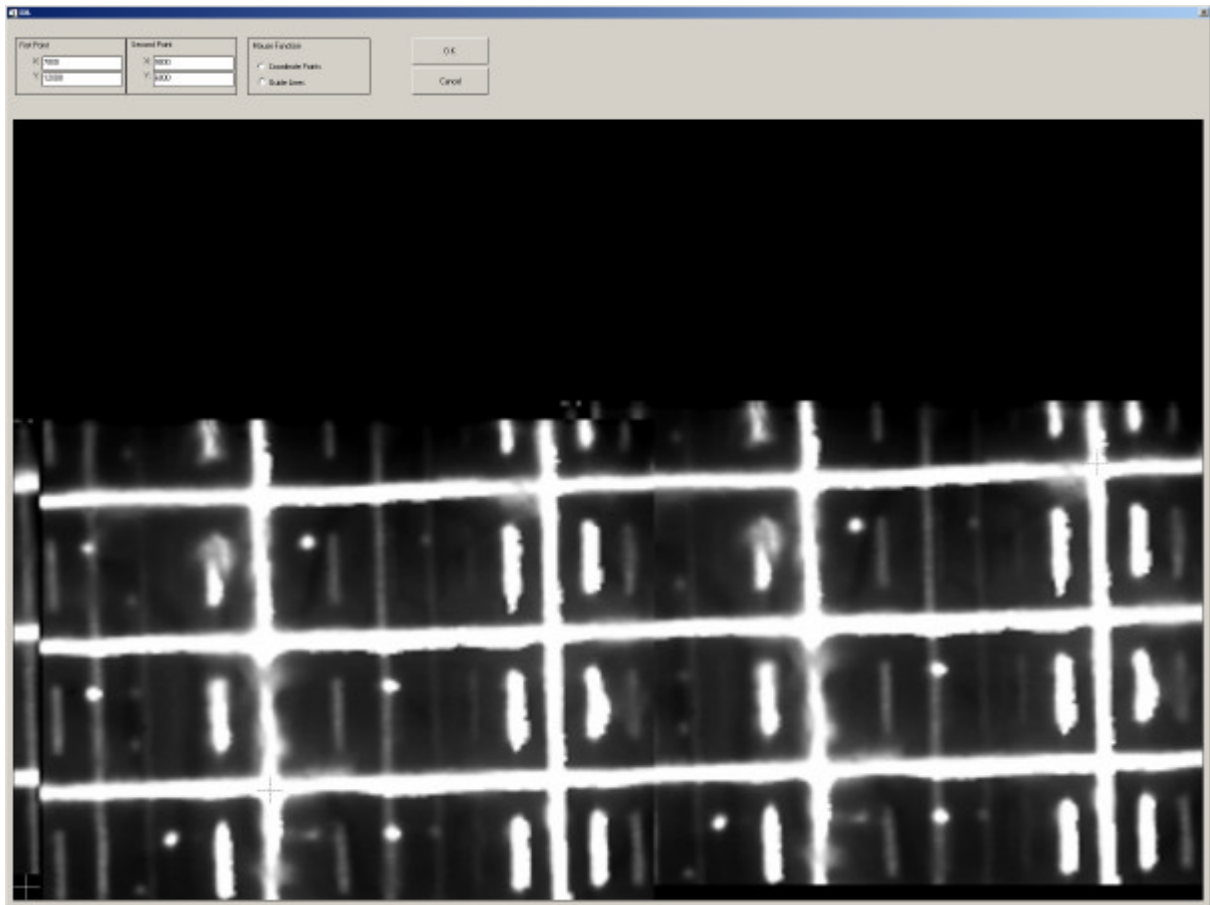


**Fig. 11:** User interface for assigning coordinates of two sites  $\mathbf{o}_1$  and  $\mathbf{o}_2$  within the image of the projected coordinate grid. The corresponding values for  $\mathbf{p}_1$  and  $\mathbf{p}_2$  are then determined by the dot and bar codes visible in the projected image and specified by entering the coordinates into the text field at the top.

Furthermore, data are required about the positions of the tube grid channels. Since the tube grid is manufactured by precision in the order of  $1\ \mu\text{m}$ , the channel positions only had to be determined once. However, the exact position of the tube grid relative to the tube grid holder has to be re-determined after each mounting. This is achieved by determining the position of the first channel of the tube grid relative to landmarks on the grid holder (Fig. 12). As the position of the landmarks on the holder is fixed with respect to the base ring, now the position of the tube grid is determined in relation to the coordinate system of the recorded activity maps. To this end, the user graphically determines the position of the first channel and the angle of the rows and enters these data into the software. The software in turn uses this information to calculate the positions of all the other channels as coordinates in the reference system O.

Now, the software has all the information required to calculate the channel positions on the feature map. This is done for all channels and the respective positions are indicated on the feature map, as shown in Fig. 13. The software enables the user to select the channels corresponding to the desired recording sites. The software offers further features, which help select the recording sites, such as switching the display to polar maps, switching the display to surface images (in order to avoid penetration of blood vessels) and displaying distances between the cursor and the last

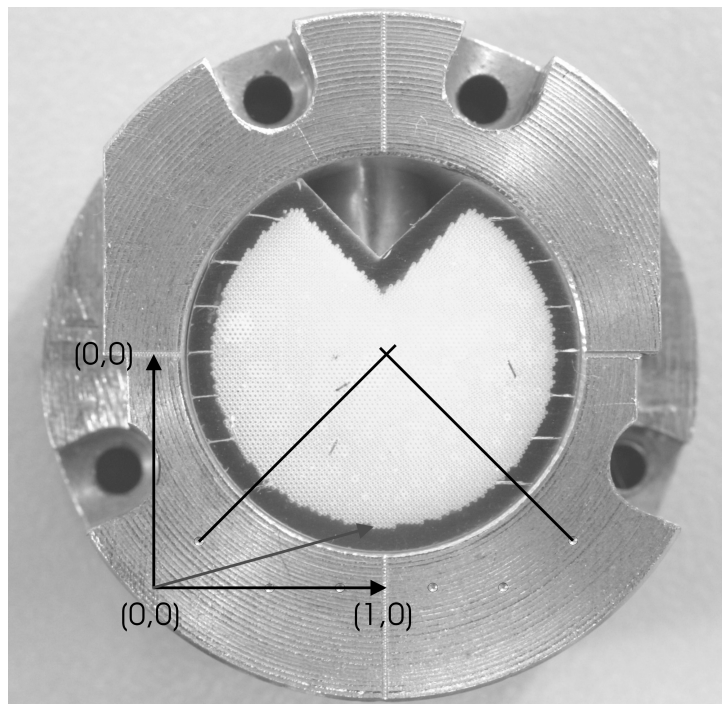


**Fig. 12:** Picture of the tube grid within its holder. The coordinate system was established by means of a commercial image processing software (Corel Draw 9.0). The scale and absolute position of the reference coordinate system is given by small indentations on the holder, from which the absolute position of the first channel (gray arrow) and the rotation of the tube grid within the holder were determined.

selected channel. After selecting the recording sites, a list of the channel rows and columns is obtained which guides the insertion of the electrodes into the appropriate places.

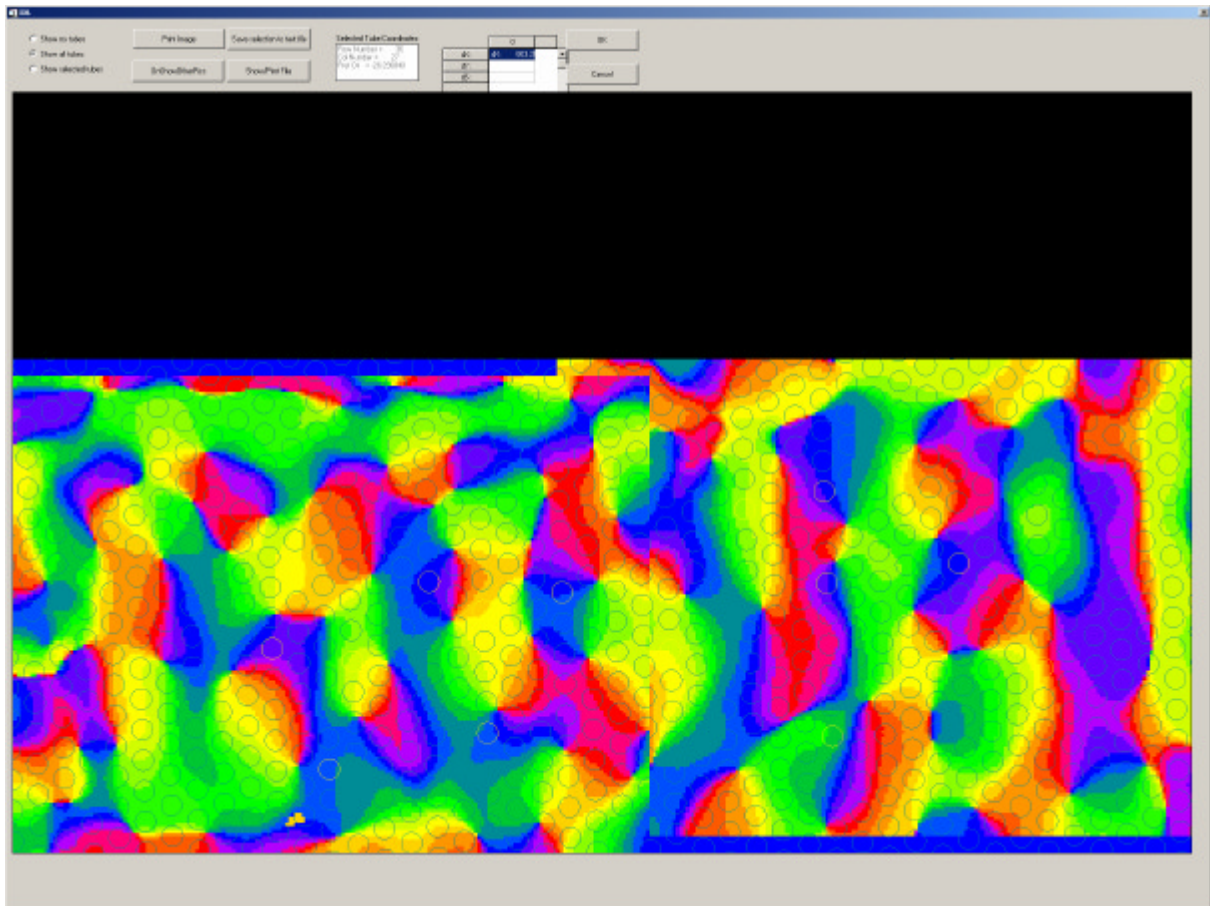


**Fig. 13:** User interface for the selection of tube grid channels. The circles on the feature map indicate the position an electrode would be led to if that specific channel were to be used to guide it. Channels can be selected by a mouse-click in the corresponding circle. The display can be set to display the feature maps, the corresponding polar plots, the vessel images or the coordinate images.

#### 2.4 Ex-Vivo Test of System Precision

Prior to its application in animal experiments, the method was thoroughly tested for its spatial precision. The examined variable was the system's ability to guide electrodes to the desired locations as defined by the channel positions of the tube grid. This was done by carrying out the whole procedure using a thin disc of plasticine in place of a live brain and a blunt electrode wire instead of an electrode with a tip. In lieu of recording activity maps, pictures were taken from the plasticine surface and landmarks on the plasticine surface served to realign the camera position. After the blunt electrode wires had been inserted into the selected guide tubes of the tube grid, they were advanced into the plasticine, leaving holes in the surface. The centre to centre distance of the electrode marks relative to the intended target points was measured from an additional image of the plasticine surface taken after removal of the electrodes.

## 2.5 Optical Imaging of Intrinsic Signals

Optical imaging was performed using standard techniques as described previously (Bonhoeffer and Grinvald, 1993). After fixation of the base ring, the OIC (Fig. 1A2, 1B2 and Fig. 2A) was mounted onto the base ring and sealed with wax. Subsequently, the dura mater was removed over the targeted hemisphere. The chamber was filled with silicone oil and closed with a transparent glass plate. Changes in the optical properties of the neuronal tissue were recorded with a commercial optical imaging system (ora2001, Optical Imaging Europe, Munich, Germany) under illumination by light with a wavelength of 620 nm. The optical imaging camera was fitted with a lens system consisting of two 50 mm Nikon objectives and a 2x extender providing a 3.6 x 4.8 mm field of view (Ratzlaff and Grinvald, 1991) at a resolution of 192 x 144 pixels. Visual stimuli were presented by means of either a 21" CRT computer screen (Hitachi, CM815ET Plus, refresh rate 100 Hz) or a projection on the reverse side of a silver screen using a CCD projector (Sony, VPL-PX30, refresh rate 60 Hz) at a distance of 570 mm. Two partially overlapping maps of orientation preference were obtained by optical imaging of intrinsic signals evoked by whole-field, high contrast square wave gratings with a spatial frequency of 0.15 cycles/degree moving in eight directions (0°, 45°, 90°, et cetera) orthogonally to the grating orientation at a velocity of 16 degrees/s. The stimulus sequence was pseudorandomly interleaved and 2-4 blocks of 8 repetitions for each stimulus condition were usually averaged. Stimuli were shown for 3 s, with an inter-stimulus interval of 7 s. Data were processed as described previously (Bonhoeffer and Grinvald, 1993), using the "cocktail blank normalization".

## 2.6 Electrophysiology

Extracellular recording of multi unit activity (MUA) was performed using tungsten electrodes (average impedance  $\sim 0.8$  MO at 1 kHz, shaft diameter  $\sim 120$   $\mu$ m, insulated with Epoxylite 6001 S, Epoxylite International LTD, England), which could be advanced longitudinally by means of the manipulator. The signals were amplified and band pass filtered (Butterworth, band pass from 800 Hz to 5 kHz). In order to calculate the orientation and selectivity of the MUAs during the experiment, action potentials were detected by a voltage threshold and stored as time stamps. All signals which showed clear single or multi unit activity were included in the analysis. The data for the direction tuning curves were obtained under visual stimulation with a sinusoidal grating drifting in 12 directions with a velocity of 10 degrees/s, a spatial frequency of 0.1 cycles/degree and averaged from 20 repetitions.

## 2.7 Procedure for the Alignment of Electrodes with the Functional Maps

After OI of two spatially slightly overlapping orientation maps, the semi-translucent mirror was mounted onto the OIC (Fig. 5A, Fig. 5D and Fig. 6). This could be done without moving the OI camera due to the flat design of the OIC. A coordinate grid was then projected through the semi-translucent mirror onto the metal plate fitted into the OIC. The projected coordinate grid was then adjusted to the coordinate marks in the metal plate and thus brought into a defined position and scale with respect to the base ring. After removing the metal plate, the whole optical bench with the projection device was advanced until the coordinate grid was focused on the cortical surface. Subsequently, an image of the coordinate grid was taken by the OI camera, in exactly the same position as used for the recording of functional maps. This enabled us to determine the precise position of each pixel relative to the base ring. In addition video images from the cortical surface were taken under illumination with green light to document the local blood vessel patterns. Therefore, three pairs of overlapping images existed at the end of this procedure: one pair of orientation maps, one pair of the projected coordinates and one pair of the images with the blood vessel patterns. All pairs of images covered the same cortical region, measuring approximately 4x8 mm.

The second device to be placed on the base ring was the tube grid fixated in the metal cylinder (Fig. 5A, Fig. 5B1 and Fig. 5F). The functional maps, the images of the projected coordinates, the images of the cortical surface and the exact position of the tube grid relative to the base ring were fed into a custom made computer program. This program, as described above, aligned all three pairs of images and calculated the positions of the guide tubes relative to the functional map. The guide tube positions were visualized as circles on the functional map as shown in figure Fig. 13. Subsequently, the desired recording sites were selected from the available guide tube positions by mouse-click on the respective positions on the functional map. After the computer program had returned the row and column numbers of the corresponding guide tubes the micro-electrodes were inserted manually under a microscope, backwards into the respective channels of the tube grid. The metal cylinder containing the tube grid was then attached to the manipulator chassis, so as to ensure a set distance between the tube grid and the Bowden cables' initial positions. The electrodes were funneled through the converging tubes of the manipulator (Fig. 7 inset B6), clamped to the Bowden cables by removing the insulation at the end parts with a piece of sandpaper, bending the upper ends and sticking them into the narrow metal tubes at the end parts of the Bowden cables (Fig. 7

inset B3). Finally, the manipulator, including the metal cylinder with the tube grid, was placed onto the stereotactic frame. The manipulator was moved until the metal cylinder came to rest on the base ring and was subsequently screwed tight onto the base ring. The electrodes were advanced under optical control (through the opening at the front of the tube grid holder) until their tips almost touched the cortical surface. The space between the cortex and the tube grid was then filled through this opening with Agar (3% in Saline) to minimize cortical movements and to protect the cortex. Subsequently, the micro-electrodes were advanced into the cortex.

## 2.8 Animal Preparation

Animal experiments were performed on cat visual cortical area 18. Anesthesia was initiated by intramuscular injection of ketamine hydrochlorid (10 mg/kg, Ketamin, CEVA Tiergesundheit GmbH, Düsseldorf, Germany) and xylazine hydrochlorid (2.5 mg/kg, Rompun, BayerVital, Leverkusen, Germany) and maintained after tracheotomy by artificial ventilation with a mixture of N<sub>2</sub>O (70%), O<sub>2</sub> (30%) and halothane (0.5-1.0%, Halotan, Eurim-Pharm Arzneimittel GmbH, Piding, Germany). The cat's head was fixed by mounting the head holder to the stereotactic frame and cementing the rippled bolt of the head holder to the cat's skull. Subsequently, a spherical craniotomy, 20 mm in diameter, was performed over occipital cortex centered on A2/L0, according to Reinoso-Suarez (, 1961). The base ring was placed concentrically over the craniotomy and cemented onto the skull (Fig. 1C). During this procedure the threaded holes in the base ring were temporarily closed with screws in order to prevent the cement from entering. After surgical procedures had been terminated, a systemic muscle relaxant (pancuronium, 0.3 mg/kg/h, Pancuronium, CuraMED Pharma GmbH, Karlsruhe, Germany) was administered intravenously to prevent eye movements during optical and electrophysiological recordings. All animal experiments were performed in accordance with the guidelines for the use of animals in research of the Society for Neuroscience and the German laws for the protection of animals.

## 3 Stimuli and Postulations

The visual stimuli for testing the binding hypothesis were designed during the experiments on the basis of intermediate results. The specificity and receptive field (RF) locations of the recorded neurons were determined using standard protocols (for direction tuning see 35, RF position: flashlight with a slit mask, stripes of different thickness and brightness and a custom

made computer program “MapRF” by Sergio Neuenschwander). Subsequently, stimuli were designed as outlined in the following sections.

### 3.1 The Foreground/Background Grating

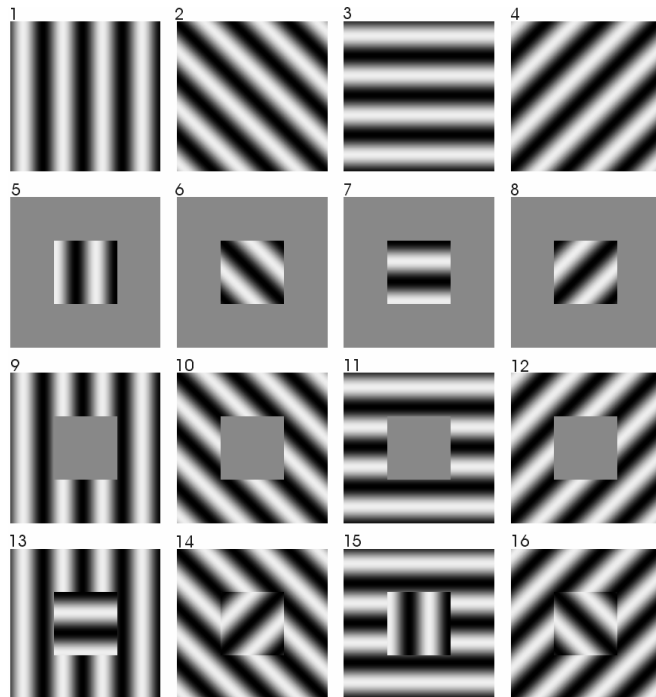


**Fig. 14: The conditions of the first set of stimuli. Conditions 1-4 have a background grating only. Conditions 5-8: plane background and gratings in the centre region. Condition 9-12: grating in the background being partially occluded by the centre region. Conditions 13-16: gratings in the background and orthogonal gratings in the centre region. The orientation of the gratings was shifted within each block of four conditions by 45° from condition to condition.**

The first stimulus set (Fig. 14) was constructed by setting the background of the display either to an iso-luminant blank screen or to a grating with an orientation of 0°, 45°, 90° or 135° and a spatial frequency of 0.1 cycles/degree. A rectangular region was selected within the background area, such that some RFs of equal orientation preference were entirely covered by that region. Depending on the stimulus condition, the selected region could be transparent, iso-luminant or display a grating. In order to avoid effects that are due to changes in the overall luminance, all iso-luminant surfaces were set to a grayscale level equal to the mean grayscale of the corresponding gratings. As shown in Fig.

14, the first four conditions consisted of the background grating in its different orientations only, whilst conditions 5-8 displayed the centre gratings on a plain iso-luminant background. Conditions 9-12 were composed of the background gratings partially occluded by the iso-luminant rectangle and, finally, conditions 13-16 consisted of orthogonal gratings for the background and the inner rectangle. Since the neurons in area 18 of cat visual cortex, from which the recordings were obtained, are motion sensitive, the gratings moved orthogonally to the grating orientation with a velocity of 10 degrees/s changing the direction of movement every second.

However, the set of sixteen stimulus configurations yielded several RFs within visually perceivable grating objects in various contexts. In conditions 1-4, all neurons had their

receptive fields within the same unique grating, whereas for the conditions 13-16 the neurons split into two groups, one having its RFs inside the inner rectangle and one having them within the visual (i.e. not occluded) part of the background. Conditions 5-12 served as a control that the RFs assigned to one of the two regions were not directly stimulated by the other region and thus could undoubtedly be assigned to represent one and only one visual object. According to the hypothesis of binding by synchrony, any two neurons not belonging to the same group should synchronize better for conditions 1-4 than for any other condition, because only for the first four conditions they represent the same visual object.

### 3.2 The Gabor Patch

The second stimulus was constructed by positioning Gabor patches onto the RFs into geometric constellations as to build up one visual object which can perceptual be broken apart into single objects by turning or removing a subset of Gabor patches.

The Gabor patches consisted of an iso-luminant background modulated by a sinusoidal grating, multiplied with a Gaussian:

$$I(x, y) = \frac{1}{A} e^{-\frac{\sqrt{(x-x_0)^2+(y-y_0)^2}}{s^2}} \cdot \frac{1}{2} \left\{ \cos \left( a \sqrt{(x-x_0)^2 - (y-y_0)^2} \cos \left[ \arctan \left( \frac{y-y_0}{x-x_0} \right) - \mathbf{j} \right] \right) + 1 \right\} \quad (4)$$

Where  $A$  is a scaling factor depending on the gray scale bit depth,  $x_0$  and  $y_0$  are the centre coordinates of the patch,  $s$  determines the width of the Gaussian,  $a$  regulates the spatial frequency of the sinusoidal grating and  $f$  defines the angle of the grating. Fig. 15 shows the display of one Gabor patch and its spatial luminance distribution.

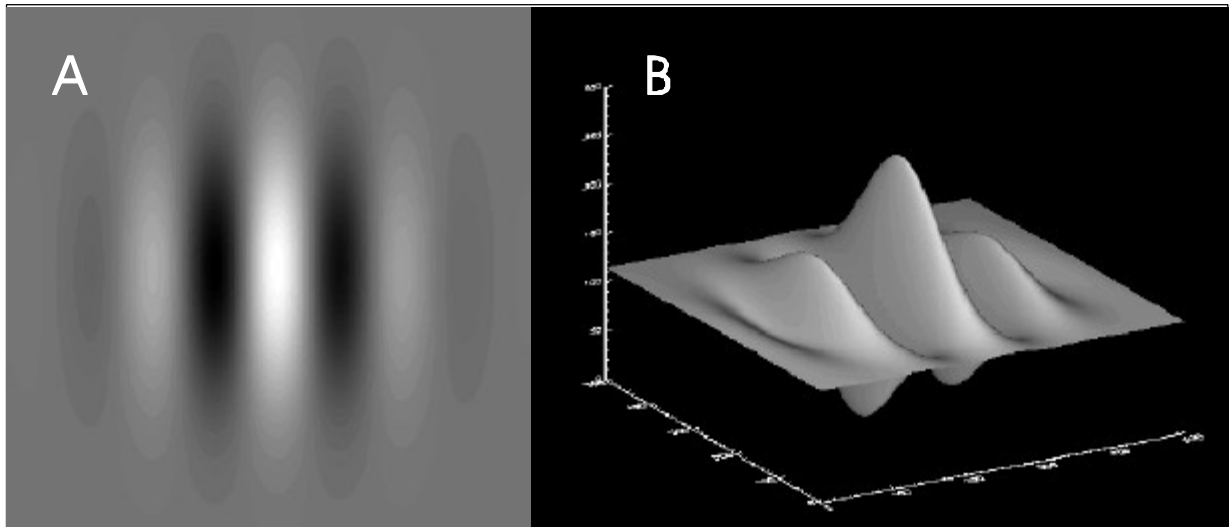


**Fig. 15: A single Gabor patch. A) as displayed on an isoluminant screen. B) The spatial distribution of gray scale values for the same Gabor patch.**

The Gabor patches were placed onto selected RFs and resized in order to optimally stimulate the neurons. The spatial frequency of the sinusoidal grid was 0.2 cycles/degree and moved with a velocity of 7 degree/s in one direction. As an simple example for the construction of visual objects out of Gabor patches assume two collinearly aligned RFs of the same direction specificity and a gap between their RFs. A visual object can then be created by placing one optimally stimulating Gabor patch onto each RF and one in between. This constellation would define a single line which can be split into distinct objects by either turning or leaving out the centre patch. Hence, two conditions would exist which stimulate the RF by means of exactly the same physical input, but with a change outside the RFs that alters the perception. By extending the line to at least five Gabor patches on five RFs, the middle one could be made to belong one time to the left and one time to the right segment and would thus render it possible to detect a switching of the centre neurons from participating in the ensemble of the left segment to the ensemble of the right segment.

### 3.3 Experiments and Stimulus Application

Overall, five experiments were performed in order to develop the targeting technique and to develop stimuli which are suited to investigate the dynamics of cell assemblies. Generally, the duration of an experiment as was performed here is restricted by the time the animal can be kept stable under anesthesia. This also restricts the yield of an experiment to recordings from two to seven sets of cells. Hence, the experiments yield recordings from 15 different sets of cells under stimulation with the foreground/background gratings. During the last three

experiments the Gabor patches were applied as well and eight different cell-stimulus configurations were obtained. In the following, those three Gabor patch stimuli are discussed in greater detail, which could successfully be analyzed. The reasons for rejecting the other stimuli will be outlined in chapter III, Results.

All subsequently described stimuli were presented in blocks of ten repetitions of each condition. The blocks were interleaved with other stimuli like gratings and foreground/background gratings in order to avoid neuronal adaptation. The presentation sequence of the different conditions was randomized within each block, such that no prediction was possible on the condition to appear next. In this fashion between 80 and 120 repetitions of each stimulus condition were collected.

a) Stimulus a) consisted of five Gabor patches arranged to build a cross. Fig. 16 shows the relative RF positions with the preferred grating orientations indicated by bars through the RFs and schematically displays the configuration of the Gabor patches for the different conditions.

Here, the constellation of the patches allowed two lines of coherently moving gratings to appear, depending on whether the inner patch was oriented horizontally or vertically. The hypothesis for this paradigm would be that the RFs 11, 7 and 9 synchronize for conditions 1, 3 and five and desynchronize for conditions 2 and 4 (in condition 6, the RFs 11 and 9 were stimulated orthogonally to their preferred orientation. Hence no prediction is possible for this combination). In conditions 2, 4 and 6 a vertical line appeared, therefore RFs 3 and 13 should synchronize under these conditions and desynchronize for all other conditions (this time, the centre RF was stimulated orthogonally, thus no prediction is made for the behavior in terms of synchronization).

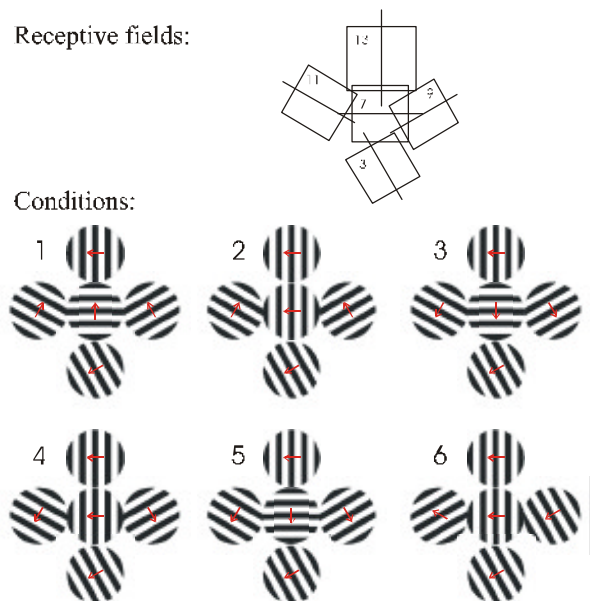
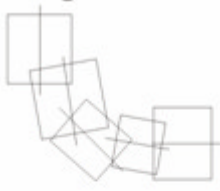


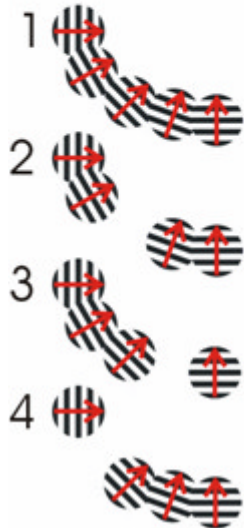
**Fig. 16: Receptive fields and stimulus configurations of stimulus a).** Top: Squares indicate the RF positions and sizes. The bars indicate the preferred grid orientation. Bottom: schematic drawings of the six stimulus configurations. The arrows indicate the direction of movement.

b) In the second experiment the same stimulus paradigm was used as in a).

**Receptive fields:**



**Conditions:**



c) Several Gabor patches were arranged to form a line. As shown in Fig. 17, the first condition displayed the entire line such that it represents one single visual object. For the other conditions, the line was split into two separate line fragments by removing a single Gabor patch instead of rotating them individually. In contrast to the stimuli a) and b), this paradigm excluded the possibility of incidentally stimulating a nearby RF of another Gabor patch by the rotated patch; a gap simply split the line into line fragments. The synchronization hypothesis predicts for this set of stimuli, that the synchronization of any two cells with receptive field on different line segments is less strong than in condition one, where all RFs belonged to the same object. Furthermore, by comparing conditions three and four, it would be possible to detect neurons of the centre patch switching the ensemble they participate in from the left line segment in condition three to the right line segment in condition four.

**Fig. 17: Stimulus c). Condition 1 shows a single line of Gabor patches. In the other conditions, the line was split at different locations by removing a Gabor patch.**

## 4 Data Analysis

### 4.1 A New Method for the Removal of Correlated Noise

The scientific need for collecting electrophysiological data synchronously from multiple cortical sites does not only complicate experimental work, but can also offer benefits not otherwise available for single electrode recordings. One of these virtues is the removal of noise and transient artifacts common to all recording channels.

The recording of electrical signals from cortical tissue demands highly sensitive probes since the signals of interest are in the order of some  $\mu\text{V}$ . High-tech impedance transducers and modern amplification devices certainly raise the data quality, but the sensing of electric or

magnetic fields e.g. from a monitor can sometimes not be avoided. Such interferences usually affect all electrodes in the same manner. Since the capacitive and inductive elements of the electrodes are very small, the time course of the disturbances will jitter far less among the channels than the sampling frequency could resolve. Only the amplitude will generally be different since electrode impedances typically vary between 0.8 to 1.5 M $\Omega$  at 1 kHz. A tool that is able to remove this type of noise thus needs to detect the common component of all channels, in spite of the differences in amplitude.

The approach taken here follows a suggestion made by Jeff Keating (personal communication) from the University of Pennsylvania to estimate the common noise by virtue of a principle component analysis (PCA). A comparison of this method with two other methods based on linear regression and signal to noise optimization respectively has been published in the meantime (Musial et al., 2002) and showed no significant differences in effectiveness. The underlying feature of the PCA being used provides estimates of the waveform that best represents all the original channels. Several principal components can be calculated and sorted with respect to their standard deviations. The component with the highest standard deviation is termed the first principal component and accounts per definition for a greater amount of signal variability in the original signals than the principal components of higher order (i.e. those with a smaller standard deviation). For N channels, the PCs can be estimated for channel m by calculating the PCs from the N-1 other channels, projecting them onto channel m to obtain a weight estimate and finally subtracting the weighted PCs from the original data of channel m. When successively applied to all channels, this procedure will remove a fair amount of common noise. The quality of this procedure depends on the number of channels used to estimate the common noise and on how well the assumptions about the similarity of the noise across the channels are met.

The cleaning procedure used here was implemented in IDL 5.2 (Research Soft Inc.<sup>®</sup>) and proceeds as outlined in the following steps:

- 1) For the reason of computational speed, data blocks of 1 s length are cut out of the data, leaving a two dimensional matrix **A** with n (=number of channels) times m (number of samples) elements.
- 2) In order to process channel m, a sub-matrix **B** is used containing all elements of **A** but the elements of channel m. The covariance matrix, its matrix of Eigen-vectors **P** and the vector of corresponding Eigen-values **v** are computed by IDL's 'PCOMP'

function. The channels are summed up weighted with the elements of the two Eigenvectors with the largest Eigen-values, thus yielding the PCs  $\mathbf{p}_1$  and  $\mathbf{p}_2$ .

- 3) The first two PCs  $\mathbf{p}_1$  and  $\mathbf{p}_2$  are projected onto the time series of channel  $m$  yielding the corresponding weights  $w_{i,m}$  (i.e. the ‘amplitude’ of the respective PC in the data):  $w_{i,m} = \mathbf{A}_m^T \mathbf{p}_i / (\mathbf{p}_i^T \mathbf{p}_i)$ .
- 4) The weighted PC vectors are subtracted from the original data:  $\mathbf{A}_{\text{clean},m} = \mathbf{A}_m - w_{1,m} \mathbf{P}_1 - w_{2,m} \mathbf{P}_2$ .
- 5) After repeating steps 2 to 4 for each channel,  $\mathbf{A}_{\text{Clean}}$  contains the first estimate of the cleaned data.
- 6) The noise estimates are clearly contaminated by action potentials, because each action potential contributes an amplitude of an order of its original amplitude divided by the number of channels. Thus, after having a first order estimate, the spikes can be reliably detected and removed to give way to an even better noise estimate. The detection of action potentials is accomplished by a threshold set to four times the standard deviation of the signal. Wherever the signal exceeds the threshold, a piece of data about this bin is substituted by the noise estimate given by  $w_{1,m} \mathbf{P}_1 + w_{2,m} \mathbf{P}_2$  for each channel. This is the best estimate possible on the appearance of the signal if no spike had occurred. Repeating steps two to five once again, this time calculating the noise estimates from the “spike-free” data, leaves us with a second order cleaned  $\mathbf{A}_{\text{Clean}}$ .

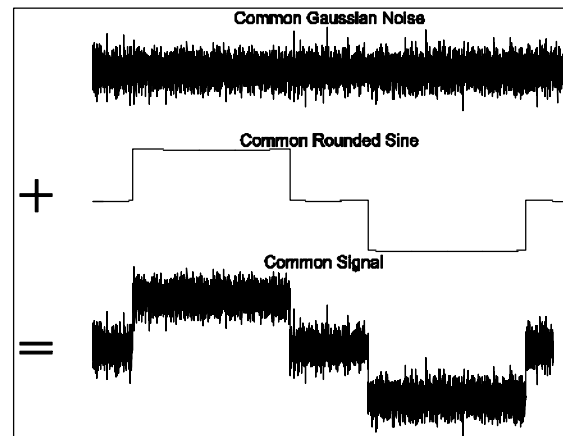
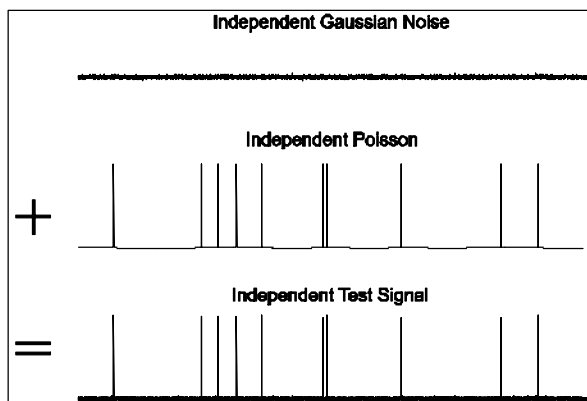
In order to assess the quality of the PCA cleaning operation, simulated data are required (Fig. 18) because the content of common and independent signals cannot be known for real neuronal data. To this end, random Gaussian noise was generated and superposed with a Poisson spike train. A similar noisy spike train was generated for each channel separately, using a different seed of the random number generator each time to make the signals independent. A further time series was generated by Gaussian noise and was added to a rounded sine wave (see Fig. 18). This unique time series was added to all the independent channels and represents the common disturbance inherent to all channels.

In order to evaluate the functionality of the implementation and the quality of the cleaning method, the simulated data sets were processed as described above. The method clearly

depends on several parameters such as noise amplitude, number of channels, etc. However, for practical purposes the dependency on the signal to noise ratio, on the common noise variability among the channels and on the number of channels is of particular interest in order to determine the boundary conditions of its applicability. Hence, these parameters were varied while the quality of the result was evaluated by the dimension free vector

$$q = \frac{1}{N_{bins}} \frac{\sum_i (A_i - A_{clean,i})^2}{\left(\sum_i A_i\right)^2} \quad (5)$$

where  $N_{bins}$  is the number of bins per time series,  $i$  indexes the bins of the time series from 1 to  $N$ . Each vector element of  $q$  thus represents a power and recording length independent measure of the cleaning quality of one channel. A scalar measure of the overall quality  $Q$  was obtained from  $q$  as  $Q = |q|/N_{chans}$ . Note that the smaller the value of  $Q$  is, the better the cleaning quality.



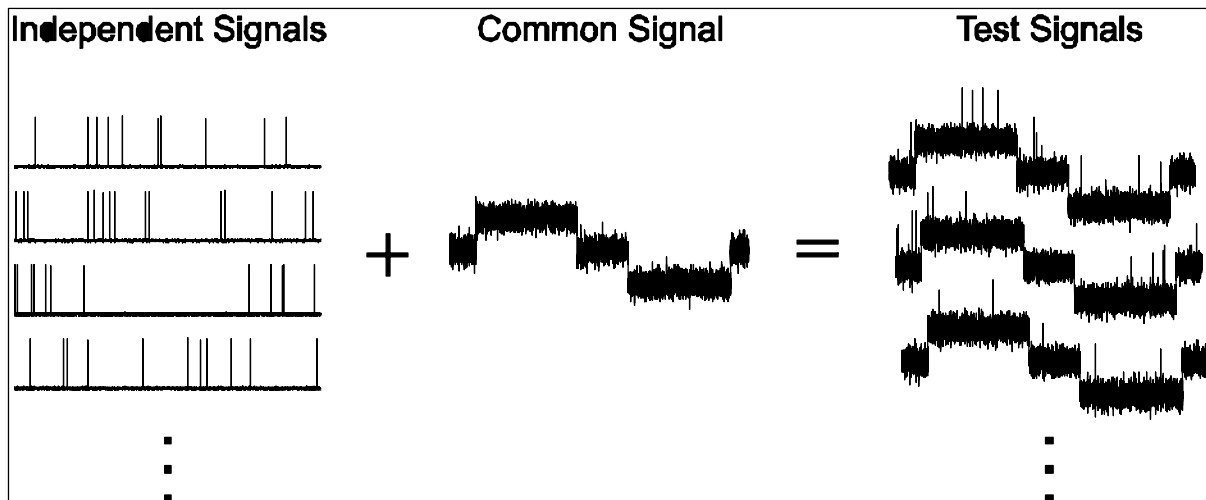


**Fig. 18:** Steps for creating the test signal for the PCA cleaning technique. Top left: for each simulated channel Gaussian white noise and a Poisson point process were superimposed. Top right: Gaussian white noise and a rounded sine wave were superimposed to simulate a disturbance to all channels. Bottom: The signals of the previous steps were superimposed to finally form the test signal.

#### 4.2 A New Software Design for Flexible Data Organization and Data Access

Current research on the representational and computational strategies of the brain requires multiple isochronous recordings. Since the field is developing continuously, new devices for recording, stimulating or generally for experimental controls are being introduced, either commercially or custom-made. New techniques and devices bring about new data formats. This diversity has already led to a lack of interchangeability of data between scientists. Since the diversity of data formats cannot be reduced easily, a tool is desirable to make as easy as possible to include new data formats into any existing analytical framework. Furthermore, the increase in the number of recording channels leads to an ‘explosion’ of the parameter space to be included into the analysis:

- 1) For each electrode, up to three or four cells may be isolated by spike sorting techniques (i.e. the attempt to isolate the activity of different neurons by their waveform).
- 2) For each cell, the receptive field (RF) properties must be determined.
- 3) For each receptive field, the relation of the RF properties to the different stimulus conditions (2 to 16) is important.

Hence, having 16 electrodes will usually result in thousands of combinatorial possibilities, which the analysis should be able to handle. And as science advances, ever more intermediate results, for instance the cortical or circadian state (i.e. sleep-wake-cycles), will be included into the analysis.

Modern concepts of computer science, such as object orientation and databases, are well suited to serving this situation. Thus, a framework for data analysis has been implemented using the high level language IDL, as this provides all essential concepts such as classes, inheritance, polymorphism and a SQL database interface. In the following, a draft of the architectural principles is given.

In order to ease the adaptation to new data formats, the inheritable class concept was utilized by defining a superclass which implements all methods that are not specific to any particular data format. It further defines virtual methods for those functions that are specific to the data format, in order to force an implementation after inheritance. In this way, all methods of the superclass are instantly usable after deriving the class for a particular data format, thereby reducing the need for new code to a minimum. The non-specific methods generally implement the handling of meta information about the data, whereas the specific (virtual) methods implement the concrete reading of data from storage media.

In order to be able to treat very different kinds of data uniformly, some abstraction is required to enable the framework to manage optical imaging data, for instance, by virtue of the same methods used for electrophysiological recordings. Therefore, all data are thought to be categorizable into 'lines' and 'data sets'. For example, in electrophysiology the electrodes are usually assigned to channels, that would correspond to 'lines' and the successively recorded trials would make up the 'data sets'. Similarly, a digitalized picture could be adjusted either by abstracting the pixel rows to 'lines' and each single pixel to a 'data set', or by having only one 'line' containing one 'data set', which consists of the image as a whole. As for the data

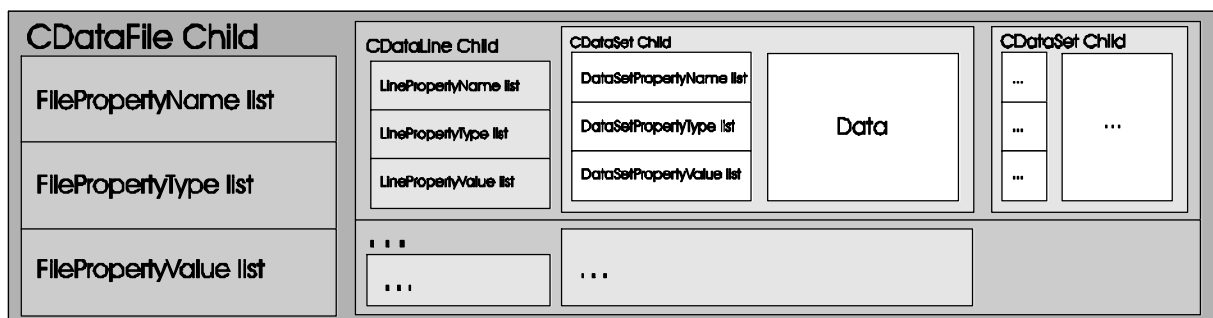


Fig. 19: Sketch of the object nesting in a realization of a child class.

file, a superclass for 'lines' and a superclass for 'data sets' were implemented. Again, all methods non-specific to a certain data format were implemented in the superclass and all specific methods were implemented as virtual methods to force implementation after inheritance. Fig. 16 shows the entire object nesting of derived classes for a certain data format, together with the information the objects and sub-objects hold. Each data file object contains information about the data file and several line objects. Each line object contains information about the line together with several data set objects. The data set objects ultimately contain information about the particular data set as well as the actual data.

The mechanisms for the storage, retrieval and search of information are all implemented within the superclasses and thus no further programming effort is required to derive classes for a new data format. The most frequently used function, which is very helpful for any analysis, is conditional data set retrieval. This allows all data sets with certain properties to be returned. Either, for example, data sets of channels with a particular substring in the channel name or all data sets of channels 1, 4 and 9 which have the condition label  $x$  and a gamma content higher than  $y$  may thereby be returned.

### 4.3 Spike Extraction

After cleaning the band-pass filtered MUA signal with the PCA cleaning algorithm, the action potentials have to be extracted from the digitized analog signal. In order to automate this process in a reproducible and sound manner, a new algorithm was used. Usually, a threshold for spike detection is estimated either manually or by setting it to a fixed multiple of the signal's standard deviation. The first approach is time consuming and the latter approach has the disadvantage of being activity dependent, since the spikes alter the standard deviation. Here, the signal standard deviation was calculated for each channel. Subsequently, action potentials (and artifacts) were detected by a threshold of five times the standard deviation. Wherever the signal crossed the threshold from small to large values, a region starting at the intersection minus two milliseconds and ending at recross plus two milliseconds was deleted from the original data, leaving a residual signal that no longer contained large action potentials. This procedure can be executed recursively in order to detect smaller action potentials. Theoretically, the estimate of the residual signal's standard deviation should improve with each run, but in practice the estimate changes very little after the first run. Thus, no repetitive execution was performed on the data. The final threshold was then set to the

empirically determined value of 4.5 times the standard deviation of the residual signal. Wherever the original signal crossed the threshold and recrossed it within a time window of two milliseconds, the crossing was accepted to be caused by an action potential and was dismissed as an artifact otherwise. The time of the first threshold crossing was stored for each action potential as the time of spike occurrence and the bins within a time window starting one millisecond before and ending two milliseconds after that point in time were stored as the respective spike waveform.

#### 4.4 Spike Sorting

Based on the idea that different cells exhibit action potentials that can be distinguished either by form or by amplitude, the extracted spikes are often further processed to isolate the spikes belonging to one cell. In order to accomplish this, it is desirable to have an exact representation of the waveform, which, at first sight, demands the use of very high sampling rates. On the other hand, when recording from multiple electrodes a low sampling frequency is advantageous as it requires less storage resources. If the sampling points of the waveforms are directly taken as their representation, the following problem occurs for low sampling frequencies. As illustrated in Fig. 20, the offset of the sampling points is arbitrary and results in different representations of the action potential. In order to classify all recorded spikes with respect to their waveform, they must somehow be made comparable. To this end, all the action potentials are aligned with respect to their maximum. This is the most prominent feature of an action potential, since it is caused by the fastest channel kinetics involved in spike generation: the fast activating and fast deactivating voltage-dependent sodium channels.

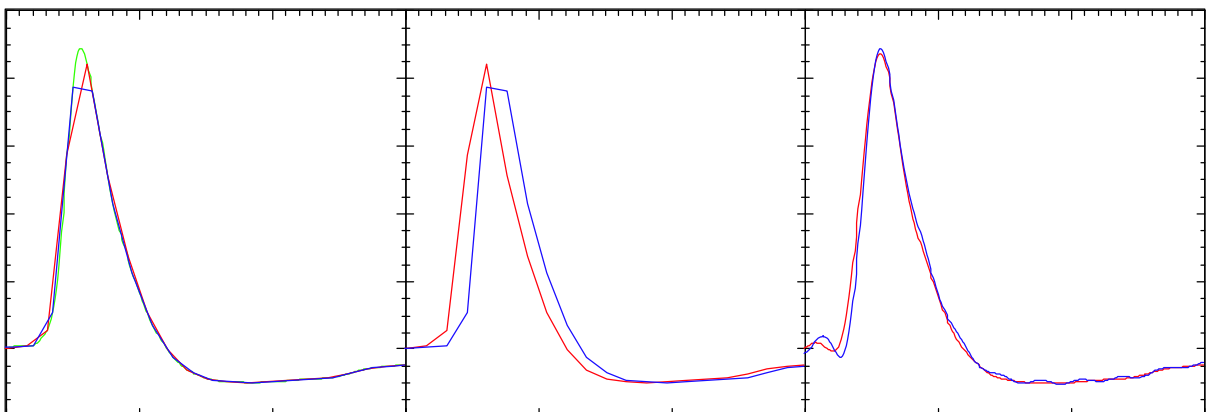


**Fig. 20:** Illustration of the effect a low sampling rate representation can have on the alignment of the waveforms. **Left:** a waveform (green) sampled with different time offsets (blue and red). **Centre:** when the sampled waveforms are aligned to their maximum they are shifted relative to each other although they represent exactly the same waveform. **Right:** the same waveforms aligned after up-sampling to 100 Hz. Apart from a residual ripple due to the finite time window the original waveform is represented sufficiently well in order to avoid errors in the alignment.

If the sampling rate is too low, the waveforms align themselves differently, depending on the arbitrary sampling offset, as shown in the middle inset of Fig. 20. In the worst case the two action potentials would be classified as belonging to different neurons. In order to avoid such sampling artifacts, the resolution of the waveforms must be increased for at least the process of aligning them with respect to their maximum (Fig. 20, right inset).

Here, the mathematical propositions and their application to the signal theory of sampling have been employed in order to record using the lowest sampling frequency possible, without losing any information about the original signal. During analysis, the action potential waveforms were temporally reconstructed and re-sampled with a high frequency in order to chart the waveforms precisely. Once the waveforms were assigned to a certain neuron, the shape was no longer of interest and the high precision waveforms could be released. In this way, the required resources were restricted to a minimum, without discarding any information and therefore without losing precision. The theory and specific proceeding is outlined in the following.

Starting out with the sampled signal  $s_s(t)$  in the time domain which can be formalized as

$$s_s(t) = s(t) \frac{1}{T} \text{III}\left(\frac{t}{T}\right) \quad (6)$$

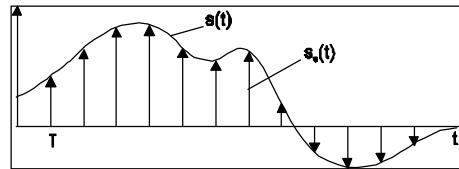


**Fig. 21: Schematic drawing of the sampling process of signal  $s_s(t)$  as formalized by Eq. (6) on the left. Arrows indicate the Dirac-pulses of the comb-function times the signal  $s_s(t)$  (solid line).**

where  $s(t)$  is the continuous (analog) band-passed MUA signal and  $\text{III}(t)$  the comb-function

$$\text{III}(t) = \sum_{n=-\infty}^{\infty} d(t-n) \quad (7)$$

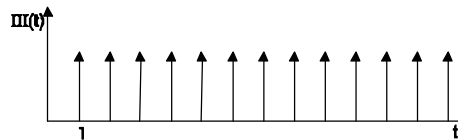


**Fig. 22: The comb function consist of an infinite number of equally spaced Dirac-pulses as indicated by the arrows.**

with Dirac-pulse  $d(t)$  at  $t=0$ .

Since the Fourier transformation of a product is equal to the convolution of the Fourier transforms of the multipliers, (6) transforms to

$$\begin{aligned}
 s_s(t) &= s(t) \cdot \frac{1}{T} \text{III}\left(\frac{t}{T}\right) \\
 \vdots & \quad \quad \quad \vdots \\
 S_s(f) &= S(f) * \text{III}(Tf)
 \end{aligned}
 \tag{8}$$

**Fig. 23:** The graphs depict the equations on the left and how the sampled signal (upper equation) transforms into frequency space (lower equation).

Due to the convolution of the spectrum with the Dirac-Pulses repeating with the period  $1/T$  the spectrum of a periodically sampled signal consists of the continuous spectrum repeating every  $1/T$  Hz in the frequency domain. If the left and right face of the continuous spectrum together are broader than  $1/T$ , then the repeating spectra overlap and the information on what the original continuous spectrum looked like in the area of overlap is lost. Thus, in order to avoid losing information about the original signal, the spectrum of that signal must not contain any frequencies higher than  $1/(2T)$ , i.e. half of the sampling frequency. This is known as the famous sampling-theorem. The minimum sampling frequency for which no information about a given signal is lost (two times the highest frequency contained in the signal) is called the Nyquist rate.

The spectrum of the original continuous signal can be extracted by multiplying the periodical spectrum of the sampled signal with an ideal low-pass filter with a cut-off frequency of  $1/(2T)$ . By transforming the low-pass filtered spectrum back into the time domain it is shown that the original signal can be reconstructed by the sum of isochronously spaced si-functions

$$\text{si}(x) = \frac{\sin(x)}{x}$$

each having an amplitude equal to the corresponding sampling value:

$$S(f) = S_s(f) \cdot T \operatorname{rect}\left(\frac{f}{2f_n}\right)$$

$$s(t) = s_s(t) * [2f_g T \operatorname{si}(pf_g t)]$$
(9)

**Fig. 24:** The graphs depict the equations on the left and how the upper equation transforms into the time domain (lower equation). This shows that a signal which was sampled with at least the Nyquist sampling rate can be reconstructed by convoluting the sampled time series with the si-function.

Since the spectra of the data discussed here were band-pass filtered with cut-off frequencies of 800 Hz and 5 kHz respectively, the frequency content of the filtered signal virtually vanished at 10 kHz and a sampling frequency of about 21 kHz was sufficient in order to obey the sampling-theorem. After spike extraction, the waveforms were reconstructed and re-sampled at a frequency of 100 kHz. The spikes were then aligned to their (now well-defined) maxima and down-sampled to 20 kHz again.

The action potentials were then classified using a custom made spike sorting program, which offers standard techniques for manual spike sorting as principal components, amplitude measures, derivative measures and template matching (for a review on those techniques see Lewicki, 1998).

#### 4.5 Cross-Correlation Analysis

Cross-correlation has long been established as a quantitative measure for the temporal relatedness of neuronal activity (for criticism on this approach, see Brody, 1999). There are several ways in which to derive the cross correlation function that lead to a pluralistic interpretation of its values. Here, the normalized cross-correlation function for signals of finite energy (i.e. of finite amplitude and finite length) was employed. For such signals, the energy of the difference of the two signals  $f(t)$  and  $g(t)$  can be taken as a similarity measure

$$E_{\Delta} = \int_{-\infty}^{\infty} (f(t) - g(t))^2 dt$$

In order to render  $E_{\Delta}$  invariant to the absolute energy of either signal,  $f(t)$  and  $g(t)$  are substituted by their identity normalized to have the energy of one

$$\begin{aligned} E_{\Delta N} &= \int_{-\infty}^{\infty} \left( \frac{f(t)}{\sqrt{E_f}} - \frac{g(t)}{\sqrt{E_g}} \right)^2 dt \\ &= \frac{\int_{-\infty}^{\infty} f(t)^2 dt}{E_f} + \frac{\int_{-\infty}^{\infty} g(t)^2 dt}{E_g} - 2 \frac{\int_{-\infty}^{\infty} f(t)g(t) dt}{\sqrt{E_f E_g}} \\ &= 2 - 2 \frac{\int_{-\infty}^{\infty} f(t)g(t) dt}{\sqrt{E_f E_g}} \end{aligned}$$

For perfectly co-varying  $f(t)$  and  $g(t)$ ,  $E_{\Delta N}$  takes a value of zero. For perfectly anti-correlated signals it will take a value of two. Hence, a similarity measure ranging from -1 for anti-correlation to +1 for correlation is defined by

$$\Phi_{fg} = 1 - \frac{E_{\Delta N}}{2} = \frac{\int_{-\infty}^{\infty} f(t)g(t) dt}{\sqrt{E_f E_g}}$$

In order to detect similarities shifted in time the same measure was taken, but with functions shifted in time relatively to each other by an amount of  $t$ :

$$\mathbf{j}_{fg}(\mathbf{t}_i) = \frac{\int_{-\infty}^{\infty} f(t)g(t+\mathbf{t}) dt}{\sqrt{E_f E_g}} \hat{=} \frac{\sum_k f(t_k)g(t_k + \mathbf{t}_i)}{\sqrt{E_f E_g}} \quad (\text{for discrete signals})$$

which is called the normalized cross-correlation function for energy signals (nCCF). However, when applied to signals of stochastic nature, such as neuronal spike trains are

thought to be, several CCFs must be averaged in order to obtain a reliable estimate of the underlying process. Furthermore, it is desirable to estimate the amount of correlation between the signals that is due to the co-stimulation of the receptive fields by the visual stimulus. The need for such an estimate arises, because the activity of the neurons follows the time course of the stimulus, e.g. if the stimulus shows up, the neurons become active, but after a while, they adopt and their activity fades. A cross-correlation between the signals of two neurons would show this gross time structure we are not interested in. The stimulus-evoked correlation can be estimated by calculating the so called shift predictor (Brody, 1999). The shift predictor estimates the correlation which is due to the stimulus by cross-correlating neuronal activity of different stimulus presentations. This estimate is subtracted from the correlations within one stimulus presentation. After that, the stimulus locked correlation should be gone and the intrinsic neuronal correlation should be visible in the cross-correlation diagram. If  $f_{ik}$  denotes the time series  $f(t)$  of the  $k$ 'th trial with stimulus condition  $i$ , and the same denotation is chosen for  $g(t)$ , then the shift predictor  $S^{ik}$  for that trial is estimated as being

$$S_{fg} = \frac{1}{N} \sum_{k=1}^N f_{ik} g_{ik+1}$$

where  $N$  is the number of shuffles taken to estimate the stimulus-evoked correlation of the spike trains.  $N$  has been empirically chosen from the data to be  $N=15$ , since no significant changes were observed when further increasing  $N$ . After calculation of the CCF of a certain trial, the shift predictor was calculated and subtracted in order to remain with the stimulus induced correlation generated by the network itself. Subsequently, the thereby corrected CCFs were averaged across all valid trials of the same stimulus condition as outlined above.

All CCFs were calculated with a time resolution of one millisecond. This precision in synchronization is still too narrow to display the physiologically relevant time window. Since postsynaptic integration sums up action potentials occurring within a time window of several milliseconds, all CCF values lying within a time window around a certain bin are physiologically relevant in driving a postsynaptic cell. Thus each bin of the CCFs was substituted by the average of all bins within a time window of  $\pm 10$  ms around it. Finally, the synchronization strength was evaluated as the maximum correlation value of the centre peak.

The evaluation of synchrony via the cross-correlation function can only be performed

pairwise for two neurons or channels, respectively. Hypothesis can be tested by comparing the degree of synchronization for each pair under those conditions in which synchronization is expected to those in which it is not expected. In multi electrode studies, many pairs of cells can be evaluated in light of a certain hypothesis in question. In order to summarize the results of the pairwise correlations into a single result, a correlation index  $I_{CC}$  was calculated. For each pair of channels, the mean of the synchronization strength under the condition the pair should not synchronize was subtracted from the average of the condition where it should synchronize. This difference was then averaged over all pairs for which the hypothesis in question predicts (de-)synchronization. The resulting value thus shows the average excess in synchronization strength of all cases in which synchronization is anticipated by the hypothesis.

## B Computer Simulation

### 1 The Simulation Environment

The computational simulation of a piece of cortex containing thousands of interconnected neurons requires a highly flexible yet comfortable and stable simulation environment, even more so, when prosecuting the claim to comprise all essential constituents which are physiologically relevant. Models for the investigation of neuronal network dynamics may recruit constituents which cover anything between the single gate of an ion channel and the gross connectivity between entire cortical areas. There are several simulation environments available, which already provide generic prototypes (or templates) of frequently used components. Among these environments, the concept of GENESIS (**GE**neral **N**eural **SI**mulation **S**ystem) (Bower and Beeman, 1998) best fits the need for building a large scale, yet biologically plausible, neuronal network. It is the only environment which provides all of the following:

- The ability to program and compile new objects that have not been implemented in GENESIS. This option is very important, since any solution other than compiled objects would drastically slow down the simulation of any large-scale network.
- Object-oriented techniques for a modular construction of neurons from their base parts.
- Building neuronal templates from readily constructed neurons.

- Building neuronal networks by creating and copying neuronal templates.
- Extensive scripting capabilities, allowing complex connectivity patterns to be set up and parameter values of the model neurons to be changed in order to produce a variety of values which fit to the experimentally determined means and distributions.
- Device independency allows GENESIS to run on any computer with a UNIX and X-window system (In principle, it also runs on other operation systems, but there are problems with the graphical user interface).
- Support for distributed processing allows multiple processors and/or computers running to be incorporated in the simulation as the network grows.

All simulations were carried out using GENESIS (v.2.2 or v.2.2.1 compiled with gcc 2.4.5 and 2.7.1) on an Intel platform (dual Pentium 3, 800 MHz or Pentium 4, 2.8 GHz, respectively) using SuSe Linux (v. 7.2 or v. 9.0).

The high non-linearity of neuronal signaling excludes the analytical treatment of neurons or even networks of neurons. Thus, the simulations must be conducted numerically, i.e. discrete in time and value. Most of the differential equations which must be solved for a network of neurons of just a few compartments (i.e. of simple morphology) are of the form:

$$\frac{df(t)}{dt} = \mathbf{a} - \mathbf{b} \cdot f(t) \quad (10)$$

which has an exact solution for constant  $\mathbf{a}$  and  $\mathbf{b}$ :

$$f(t_2) = f(t_1)e^{-\mathbf{b}(t_2-t_1)} + \frac{\mathbf{a}}{\mathbf{b}}(1 - e^{-\mathbf{b}(t_2-t_1)}) \quad (11)$$

Although  $\mathbf{a}$  and  $\mathbf{b}$  will depend on  $f(t)$  and  $t$  in very complicated ways, they can be assumed constant for time differences  $t_2 - t_1$ , for which  $\mathbf{a}$  and  $\mathbf{b}$  do not change significantly. It is this time difference that determines the maximum time step in which the simulation should proceed when using the numerical integration method (11). This so called “Exponential Euler Method” is the best compromise between accuracy and execution speed for such a network (,

1998; Gray et al., 1989). All simulations were, therefore, carried out using the “Exponential Euler Method” and a simulation time step of 100  $\mu$ s. Further reducing the simulation time step did not lead to any significant changes in the results.

## 2 The Model Neurons

### 2.1 Morphology and Electrotonic Properties

The primary neuron used for the network simulation was a reconstructed layer 5 pyramidal neuron (Koch et al., 1990). The neuron was reduced from originally 400 compartments to nine compartments using a method that preserves the electrotonic properties especially of the branching dendritic tree (Bush and Sejnowski, 1993). Inhibitory basket neurons were modeled as seven compartment cells (not based on a reconstructed cell). The compartment dimensions of both cell types are listed in Table 1.

	<i>Pvramid</i>		<i>Basket</i>	
	Length ( $\mu$ m)	Diameter ( $\mu$ m)	Length ( $\mu$ m)	Diameter ( $\mu$ m)
Soma	23	17	21	15.3
Apical trunk	60	6	35	2.5
Obliques	150	3	200	2.3
Apical no. 1	400	4.4	180	2.4
Apical no. 2	400	2.9	-	-
Apical tuft	250	2	-	-
Basal trunk	50	4	50	2.5
<i>Basals (2)</i>	<i>150</i>	<i>5</i>	<i>150</i>	<i>1.6</i>

**Table 1: Morphology of model basket and pyramidal cells.**

The passive cell properties  $R_m$  : specific membrane resistance,  $C_m$  : specific membrane capacitance,  $R_a$  : axial resistivity and the resulting values for the membrane time constant  $t_m$  and the input resistance  $R_{in}$  are listed in Table 2. The resting membrane potential was -55 mV for both cell types, where ‘resting’ assumes a background synaptic activity leading to a steady depolarization.

	<i>Pvramid</i>	<i>Basket</i>
$R_m / \text{Ocm}^2$	7042	6800
$C_m / \mu\text{F}/\text{cm}^2$	2.84	2.21
$R_a / \text{Ocm}$	200	200
$t_m / \text{ms}$	20	15
$R_{in} / \text{MO}$	45	164

**Table 2: Passive cell properties of the two model neuron types.**

## 2.2 Ion Currents and Channel Kinetics

The model neurons had fast voltage dependent sodium and potassium conductances ( $g_{Na}$ ,  $g_{Kd}$ ) at the soma only in order to generate action potentials. Additionally, the pyramidal cells had a fast high-threshold calcium conductance ( $g_{Ca}$ ) and a calcium concentration dependent potassium conductance. The calcium conductance introduced calcium into the cell during each action potential. The concentration of calcium then decayed exponentially with a time constant between 10 to 50 ms, which was randomly assigned to each cell. The potassium conductance produced a hyperpolarization as the calcium concentration raised and thus terminated bursts of action potentials. A detailed description of the implementation of the conductances is given below.

The active conductances were implemented in the commonly accepted framework developed by Hodgkin and Huxley in their original study of the ionic conductances underlying the action potential (Hodgkin, Huxley and Katz 1952; Hodgkin and Huxley, 1952). In this framework, each single ion channel is thought to consist of several gates, each of which can be in one of two states: permissive or non-permissive. The ion channel is open if all its gates are in a permissive state and closed if one or more gates are in a non-permissive state. The voltage-dependent rates of the gate state transitions are described in a Markov model by the voltage dependent kinetic variables  $a(V)$  from permissive toward non-permissive and  $\beta(V)$  vice versa, given in units of inverse time.

Originally, Hudkin and Huxley assigned different functions  $a(V)$  and  $\beta(V)$  to each unique channel type. Here, a generalization of these functions developed by (Borg-Graham, 1987; Borg-Graham, 1991) was used. This modification provides one single definition of  $a(V)$  and  $\beta(V)$  which can be utilized for all channel types. These are defined as

$$\mathbf{a}(V) = \mathbf{a}_0 e^{\frac{[zg(V-V_{1/2})F]}{RT}} \quad \mathbf{b}(V) = \mathbf{b}_0 e^{\frac{[-z(1-g)(V-V_{1/2})F]}{RT}} \quad (12)$$

where  $F$  is the Faraday constant,  $R$  the gas constant and  $T$  the absolute temperature. The other parameters determine the gate's kinetics. Further advantages of this parameterized formulation are its close relation to the Boltzmann function description used in voltage-clamp experiments and the specific effect of each parameter on the  $p_s$  and  $t_m$ -curves (see below). The parameters can thus be directly assessed by and/or fitted to experimental results.

Once  $a$  and  $\beta$  are defined, the probability of a gate being in a permissive state can be calculated and evolves in a time and voltage-dependent manner described by the differential equation:

$$\frac{dp}{dt} = \mathbf{a}(V) (1 - p) - \mathbf{b}(V) p \quad (13)$$

It can be shown that, for a constant voltage  $V$ , the probability approaches

$$p_{\infty} = \frac{\mathbf{a}(V)}{\mathbf{a}(V) + \mathbf{b}(V)} \quad (14)$$

exponentially with a time constant

$$\mathbf{t}(V) = \frac{1}{\mathbf{a}(V) + \mathbf{b}(V)} \quad (15)$$

So far, a single gate has been readily described. In order to implement a channel consisting of several gates, the gate state probabilities must be set off against each other. If we assume, that a certain channel type consists of three gates of type  $m$  and one gate of type  $h$ , then the probability for the channel to be open is the joint probability of all gates to be permissive:  $p = p_m^3 p_h$ . Thus, the average conductance this channel type contributes to a whole cell compartment is the maximum conductance  $\bar{g}$  if all the channels were open, multiplied by the probability that they actually are open:  $G_{ion} = \bar{g} p_m^3 p_h$ .

In order to calculate the trans-membrane current caused by a certain conductance, the “ionic driving force” has to be considered. Each ion type has an equilibrium potential  $E_{ion}$ , for which the net flux of ions through the membrane vanishes. The net electro chemical-driving force for a certain ion type is therefore proportional to the deflection of the membrane potential from the equilibrium potential:  $I_{ion} = \bar{g} p_m^3 p_h (V_m - E_{ion})$

Finally, all conductance and capacitance-based currents contributing to the dynamics of the membrane potential must be evaluated. In order to derive the differential equation for the membrane potential, it is assumed that the electrical properties of a cell segment can be described by an equivalent circuit as shown in Fig. 25. The behavior of the circuit is then

determined by the differential equation

$$C_m \frac{dV_m}{dt} + I_{Na} + I_K = I_{Ext} \quad (16)$$

where  $C_m$  is the membrane capacitance,  $V_m$  is the membrane potential,  $I_{Na}$  is the sodium,  $I_K$  the potassium and  $I_{Ext}$  any otherwise applied external current (e.g. synaptic currents, currents from a neighboring compartment, etc.).

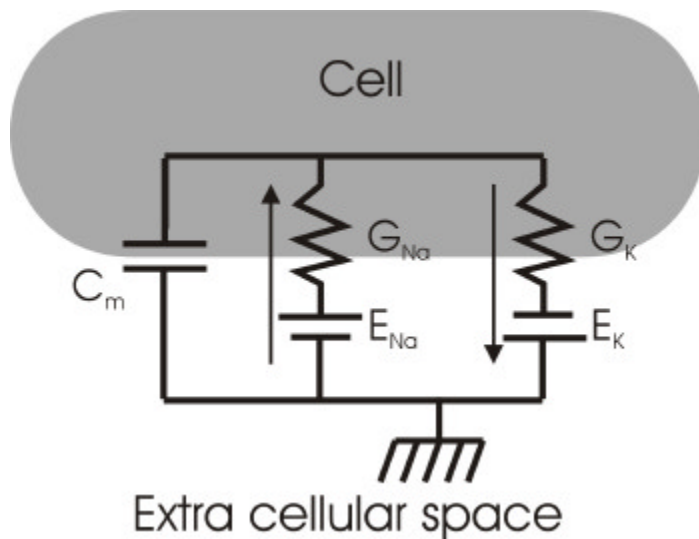


**Fig. 25: Equivalent circuit for action potential generating sodium and potassium channels.**

### 2.3 Synapses

Synaptic conductance changes were triggered by the presynaptic neuron each time the membrane potential exceeded a threshold at 0 mV. The wide range of synaptic delays found experimentally (Mason et al., 1991; Nicoll et al., 1990) was implemented as a Gaussian delay distribution with a mean of 1.6 ms, a standard deviation of 0.6 ms and a fixed minimum of 0.5 ms. The delays were randomly assigned to the network synapses. Wherever another mean is stated for the synaptic delay distribution, the standard deviation was set to half its mean. After the delay, each presynaptic event induced a postsynaptic alpha function based conduction change (one ms to peak conductance) (Bernander et al., 1991). Peak conductance amplitudes were distributed as well as a randomly assigned value out of a Gaussian distribution with a standard deviation equal to half of its mean. The mean amplitude was 2 nS, except for synapses from basket cells onto pyramidal cells which had been found to introduce larger conductance changes (Komatsu et al., 1988). These were implemented with a mean of 8 nS.

Reversal potentials were set to 0mV for excitatory and to -65 mV for inhibitory synapses (Connors et al., 1988).

### 3 The Network Architecture

#### 3.1 Intra-Columnar Architecture

Cortical columns were modeled with 100 neurons per column, 80% of which were pyramidal and 20% were basket cells (Douglas and Martin, 1990). The neurons had a synaptic connectivity of 10% (Komatsu et al., 1988; Mason et al., 1991) without any topographic preferences. Thus, each model neuron received synaptic input from eight pyramidal neurons and two basket cells, randomly chosen (but no self-connections were allowed). This scaling of the connectivity and of the number of neurons per column has been found to produce the most realistic behavior (Bush and Sejnowski, 1996) as opposed to columns modeled with more neurons, but a scaling factor of ten had to be applied to the synaptic strengths in order to maintain the activity statistics.

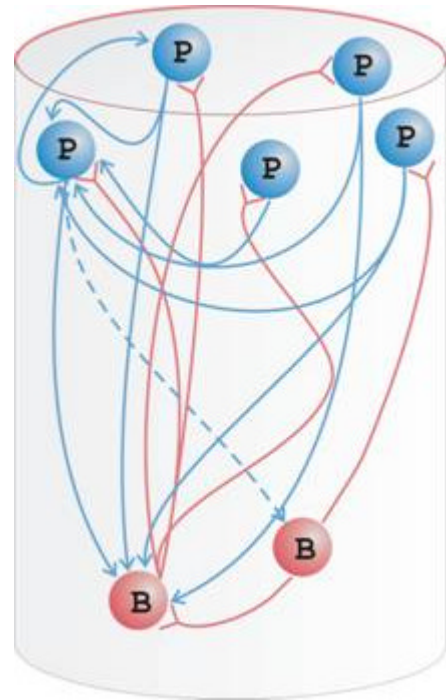


**Fig. 26: Sketch of the connectivity pattern of a model column. The connectivity of 10 % is reproduced for the leftmost pyramidal (P) and basket (B) cell.**

#### 3.2 Inter-Columnar Architecture

The reciprocal connection patterns between cortical columns depend on their relative position in stimulus feature space (Kisvarday et al., 1997; Gilbert and Wiesel, 1989; Schmidt et al., 1997; Löwel and Singer, 1992). Two types of long range connections between columns of the same specificity have been described, one as sparse pyramid-pyramid connections (Gilbert and Wiesel, 1989; Kisvarday and Eysel, 1992), the other as sparse pyramid-basket cell connections (Douglas, Martin, 1990; White 1989). The pyramid-pyramid connections were modeled by connecting neighboring columns at a density of 4% and the pyramid-basket cell connections by a density of 5%. Here, the connectivity patterns between columns of different specificity were not considered. All simulations were performed by setting up ten columns and connecting neighboring columns reciprocally as described above. Fig. 27 shows

schematically the projections between the columns.

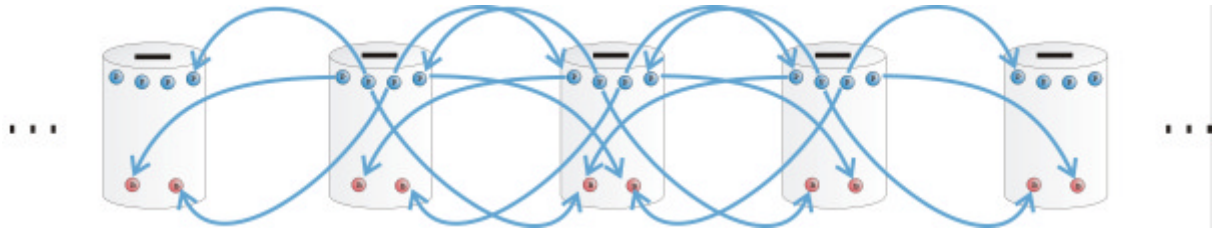


**Fig. 27: Scheme of the inter-columnar connectivity. Pyramidal neurons reciprocally project to both layers of adjacent columns. For simplicity, the randomness and the number of connections per cell were not reproduced in the figure.**

## 4 The Network Input

Synaptic background activity was simulated without affecting  $R_{in}$  and  $t_m$ . To this end, all neurons received a noisy input current injected into the cell soma. The noise was uniformly distributed around 0 nA with a maximum current of  $\pm 1$  nA for pyramidal neurons and  $\pm 0.3$  nA for basket cells. This produced a fluctuation about the resting membrane potential, as seen *in vivo*.

Stimulus evoked input from the thalamic afferents to the network was simulated by uncorrelated Poisson spike trains, with a mean rate of 200 Hz. All pyramidal neurons received four 20 nS excitatory synapses which were randomly connected to any compartment of the cell and activated by one of the Poisson spike trains.

## 5 Data Analysis

In addition to visually inspecting traces of neuronal membrane potentials, simulation data were analyzed by summarizing the behavior of all pyramidal neurons belonging to one column by building the average of their membrane potentials. In the following, this measure is denoted as the LAP (Local Average Potential), which captures sub-threshold variations as well as spiking activity. When related to electrophysiological measures as MUA or LFP, the LAP seems to overrate spiking activity, because action potentials cause much higher deflections of the membrane potential than the relatively small range of sub-threshold variations contribute. However, by averaging the membrane potentials of all pyramidal cells within one column the LAP rather gives a statistical estimation for the probability of the noisy membrane potentials to exceed the spike threshold, thereby yielding a measure for the

probability of the cells to discharge synchronously.

The detection of synchronization was performed as described in chapter IIA4.5 on page 52, but without subtracting a shift predictor, since this was not applicable here. In contrast to the experimental *in vivo* data, the correlation analysis of model data does not depend on two spike trains averaged over several repetitions under the same condition. Hence, the synchronization of the model columns was calculated by cross-correlating their LAPs, which already denote an average over a representative population.

The LAPs, usually of oscillatory nature, were also analyzed with respect to the major frequency components and their phases evolving over time. To this end, the Hilbert transformation was applied to the LAPs, resulting in a time series  $H(t)$  that has all periodic terms phase-shifted by 90 degrees. The original LAP and the real part of its complex valued Hilbert transform  $R(H(LAP(t)))$  were used to build the so-called “analytical signal” by  $A(t) = LAP(t) - i R(H(t))$ . Fig. 28 shows  $A(t)$  for a pure quadratic accelerated sinusoidal  $LAP(t)$  in the complex plane. For this signal, the length of the time dependent vectors -indicated in plot A of Fig. 28- stays equal to one, but its angle rotates ever faster as the signal frequency accelerates. By plotting the angle against time, a cumulative phase graph (CPG) was created for each LAP. In CPGs, phase shifts become visible by deflections from a straight line and the frequency of the oscillation is reflected by the slope of the graph. For instance, in the case of the quadratic accelerated sinusoidal of Fig. 28A, the plot would be a quadratic function of time, as shown by the solid line in plot B. A sinusoidal with a constant frequency of 1 Hz would result in a straight line of slope one cycle per second, as shown by the dotted line in Fig. 28B. If, however, the frequency remains constant but a transient phase shift occurs, the CPG would show two straight lines of the same slope before and after the phase shift, but at the time of the phase shift the line would transiently jump upwards or downwards, depending on whether the phase increases or decreases. The CPG thus allows for an analysis of the phase and frequency time courses of the LAPs.

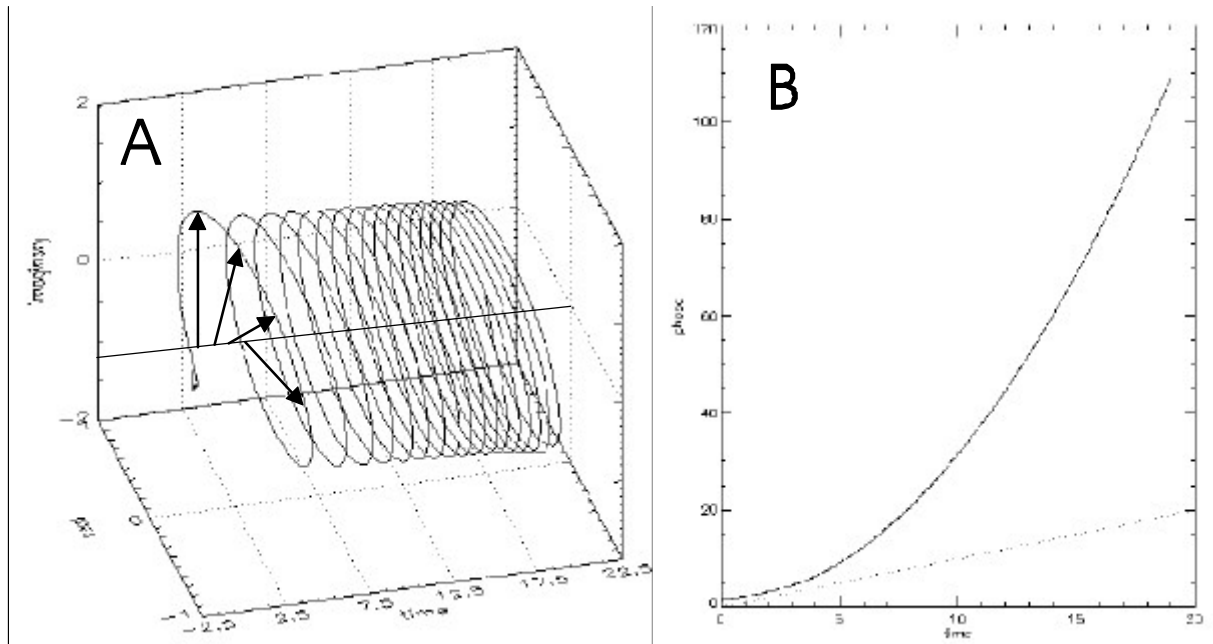


**Fig. 28:** Calculation steps for obtaining the cumulative phase graph (CPG). **A)** The analytical signal of an accelerated sinusoidal with constant amplitude. The projection on the real-time plane yields the original signal and the projection on the imaginary-time plane yields its Hilbert transform. The arrows indicate the corresponding polar vectors in the complex plane and how they evolve over time. For each point in time the vector length and the vector angle can be determined. The time course of the angle is then plotted against time, yielding the CPG as shown in plot **B** (solid line). The dotted line shows the CPG of a sinusoidal of a constant frequency of 1 Hz, which results in a straight line of slope 1 cycle per second.

### III Results

#### A Animal Experiment

##### 1 A New Technique for Targeted Cell Recordings

###### 1.1 System Precision

The spatial precision with which the system guides electrodes to the selected channel targets on the feature map was determined *ex-vivo*, as described above. The procedure for determining the system's spatial precision was carried out seven times using several electrodes inserted into different channels in each experiment. As shown in Fig. 29, the electrodes approached the target points as close as 64  $\mu\text{m}$  on average, with a maximum error of 130  $\mu\text{m}$ . No systematic error in electrode placement could be detected from the directions of displacement over all repetitions and electrode insertions. Comparison of the standard deviation of the distances to the

intended target points ( $s = 30 \mu\text{m}$ ) to the standard deviation of the same data after vector subtraction of the centre of mass within each experiment ( $s = 17 \mu\text{m}$ ) suggests that a major part of the deviation could be attributed to imprecise projection of the coordinates, since this error influences all electrode positions within one experiment in a common manner. The electrodes' angular play in the channels apparently did not contribute substantially to the deviations. Fig. 30 shows two holes in the plasticine. The lower one resulted from a single insertion of a blunt electrode wire through a channel, whereas the upper one resulted from ten

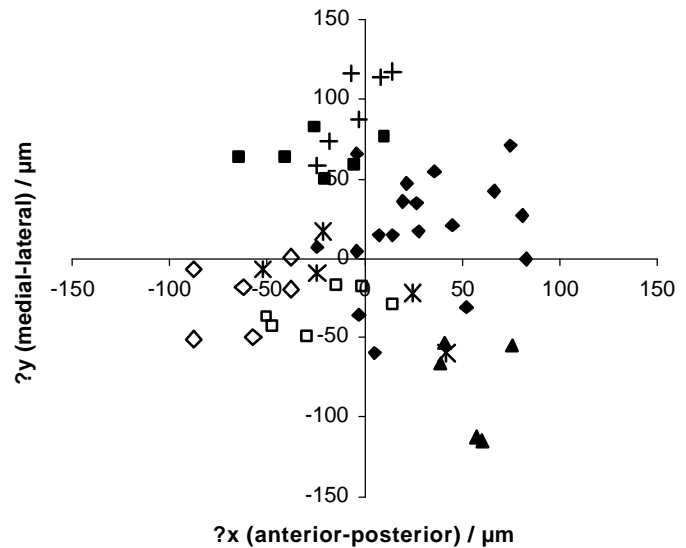


**Fig. 29: Deviation of holes in the plasticine from the intended target point. Points marked with the same symbol belong to electrode wire insertions during the same experiment, but into different channels, i.e. each symbol represents one experiment. The channels chosen for insertion differ between the experiments in order to cover a large sample of channels throughout the entire tube grid.**

insertions into another channel whilst inclining the wire into a different direction each time in order to fully exploit the whole range of angular play. The radius of the upper hole, as measured with a calibrated microscope reticule, is at most 20  $\mu\text{m}$  greater than that of the lower one. Assuming the blunt end of the wire would widen the hole by the amount of its displacement; this indicates that the precision is of the same order of magnitude as calculated (Eq. (1)).

## 1.2 Animal Experiment

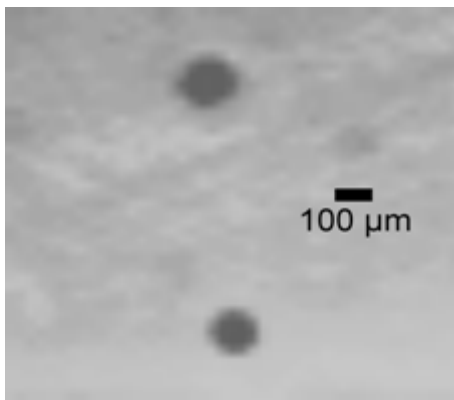


**Fig. 30:** Image of the plasticine surface taken by the optical imaging camera. The lower dark spot resulted from dipping an electrode once into the plasticine, the upper one resulted from several insertions through one channel of the tube grid whilst bending the end of the electrode into a different direction each time.

To test whether any unpredictable effects may render the above results invalid when the system is implemented in animal experiments, this method was used for positioning several electrodes according to orientation maps in area 18 of the cat visual cortex. The time course of such an experiment is as follows: implantation of recording chamber and adjustment of optical imaging setup, six hours; recording of optical data, two hours; adjusting and imaging of the projected coordinates, two hours. The time required for the selection of recording sites and the preparation of the electrode manipulator system is highly dependent on the number of electrodes to be used. Therefore, about three to six additional hours are required until the recording setup is ready for advancing the electrodes into the cortex.

Since it is difficult to determine from histological reconstructions and superimposed functional maps the precise locations at which the electrodes had entered the cortex, the direction preferences of the electrophysiological recordings were compared to the selected target points in the feature map. Fig. 31 shows the orientation map and the direction preferences for all electrodes from which visually evoked activity was recorded. All measurements of selectivity are congruent with the expectations from the functional maps.

The best correspondence was found to exist for electrodes 2, 4 and 5, whose direction tunings agree exactly with what one would expect from the target sites of the feature map.

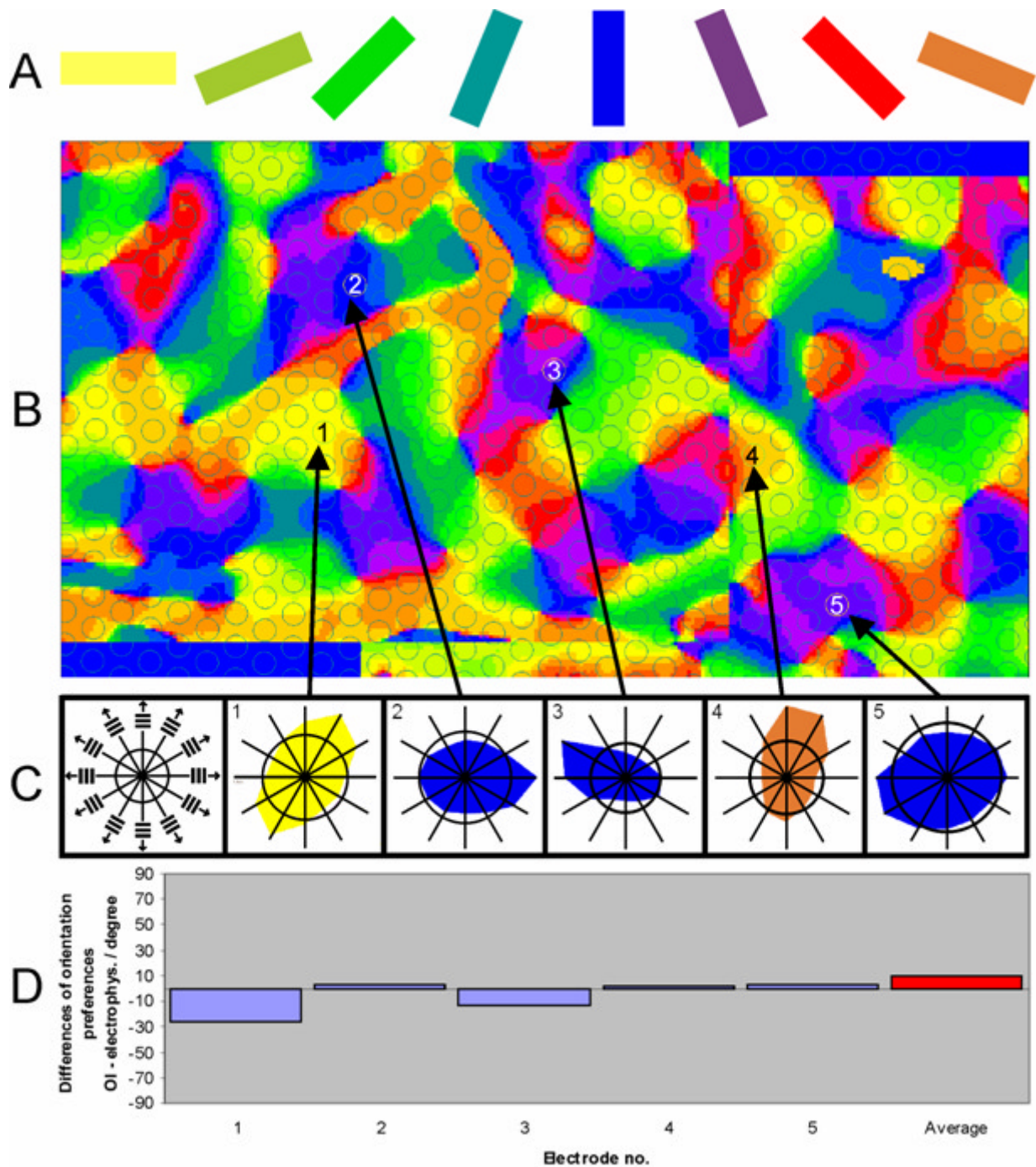


**Fig. 31:** Comparison of orientation preferences as determined by OI and electrophysiological recordings. (A) The colored bars relate the preferred grating orientation to the color code in the orientation map. (B) Two overlapping orientation maps aligned such that the corresponding images of the epicortical vessels would optimally fit if aligned in the same manner. (C) The polar plots labeled from 1 to 5 show the direction tunings of the multi unit activity as recorded with the respective electrodes. In the leftmost box, gratings and their drifting directions are sketched at the elongation of the corresponding polar plot axis as used for the tuning curves. Arrows point from the tuning curves in (C) to the intended recording sites in (B). (D) Differences in preferred orientation between optical and electrophysiological recordings. The rightmost beam shows the average absolute difference of all five electrodes.

Electrodes 1 and 3 differ slightly from the feature map such that they hit the feature map

about a hundred micrometers right below the intended target point. In order to quantify the match, the preferred orientation at an intended recording site was determined by vectorial summation of all pixel orientations within a radius of  $75\ \mu\text{m}$  around the desired target point in the orientation map. This corresponds to the area under the respective guide tube, as shown by the circles in Fig. 31B. For the electrophysiological recordings, that orientation was classified as the preferred one that corresponded to the longest vector in the tuning curve. For electrodes 2, 4 and 5 the preferred orientation differed by only two to three degrees from that of the orientation map. For electrode 3 the difference amounted to thirteen and for electrode one to twenty six degrees.

These values agree with the spatial deviations anticipated from the ex-vivo experiments and indicate that the targeting method successfully placed the electrodes into the desired sites of the feature map. With up to 16 electrodes, some of them as close to each other as  $660\ \mu\text{m}$ , neither visible cortical damage, nor any loss of cell response without deliberately changing the electrode depths by the respective electrode drives could be observed. Although dimpling effects were not observed directly, due to the Agar above the cortex, the missing cross-influence between the individually adjustable electrodes suggests that no severe dimpling effects had occurred. Moreover, figure 31 compares two examples of the PSTHs and orientation tunings of two recording sessions separated by more than 3 hours time. The similarity of these two data sets illustrates the stability of the recording conditions which allowed for recording unchanged neuronal responses over several hours throughout the experiment's duration of up to five days.

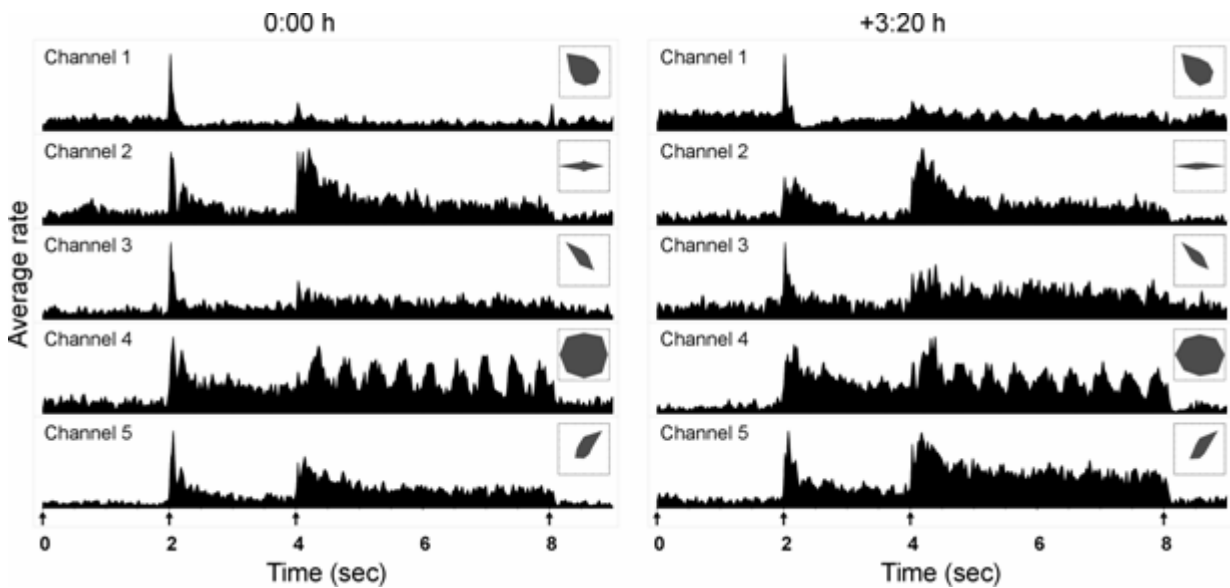


Fig. 32: PSTHs and tuning profiles (insets) of multiple unit responses recorded from five electrodes. For the PSTHs the responses were averaged over all 8 different conditions of a whole field grating stimulus and smoothed with a Gaussian Kernel of 50 ms width at half height. The data in the right column were recorded 3 hours 20 minutes later than the data of the left column. The onsets of the distinct phases of the stimulus protocol are indicated by arrows at the time axis. In the first two seconds an iso-luminant gray screen was presented. After two seconds a static oriented grating appeared and started to drift after another two seconds. The grating disappeared at time 8 seconds and the initial gray screen was shown for the last second of the protocol. The insets in the upper right corner of each PSTH show the orientation tuning of the respective channel as calculated from the same data sets.

## 2 Data Analysis

### 2.1 A New Method for Removal of Correlated Noise

The PCA de-noising algorithm was applied to the simulated data as described in *Materials and Methods*. Fig. 33 shows one original signal sharing no common noise with the other channels, the same signal after contaminating all channels and applying the cleaning algorithm and the noise remaining after the cleaning (determined by subtracting the first two signals from each other). As one would expect from a good cleaning technique, the residual signal amplitude is just slightly higher than the level of uncorrelated noise. From the flatness

of the residual signal it is visible that the signals of interest, the spikes, were successfully restored. Otherwise, the errors to these transients would show up as prominent events in the residual.

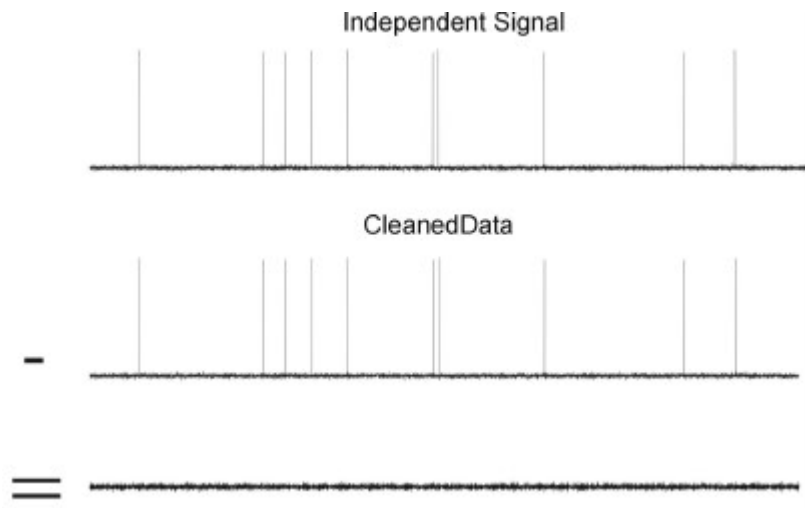


**Fig. 33: The residual signal as determined by subtracting the cleaned contaminated data from the original uncontaminated signal.**

In order to assess the dependence of the cleaning quality on experimentally relevant parameters, the number of simulated channels, the variance of common noise amplitude among the channels and the signal to noise ratio were varied. In practice, values of  $Q$  below 0.1 result in a good improvement of the signal to noise ratio. The standard set of signals consisted of 16 channels of independent Gaussian noise ( $s = 1$ ) and an independent Poisson process of amplitude 10. The common noise added to these channels consisted of a rounded sine wave of amplitude 2 and a Gaussian noise with  $s = 1$ . All relative values stated in the following refer to this reference signal.

Fig. 34A shows the cleaning quality  $Q$  for 3 to 32 channels. The minimum of three channels is inherent to the method, since the cleaning of one channel requires a minimum of two remaining channels for the calculation of the covariance matrix.  $Q$  rapidly degrades with the number of channels reaching satisfying values for seven or more electrodes.

The quality dependence on the amplitude variation of the common noise among the different channels is shown in Fig. 34B. Since 16 channels were simulated, the value at 0% amplitude variation is the same as in plot A at the abscissa value of 16 electrodes.  $Q$  increases with increasing amplitude variance and reaches the 0.1 value when the amplitude is varied by 480%. The decreasing smoothness of the curve is a result of randomly assigning noise levels

between 0% and the abscissa value to the channels. With increasing mean noise levels the effect of stochastically twisted amplitude distributions on the cleaning quality increases, thereby producing outliers that differ each time the simulation is repeated.

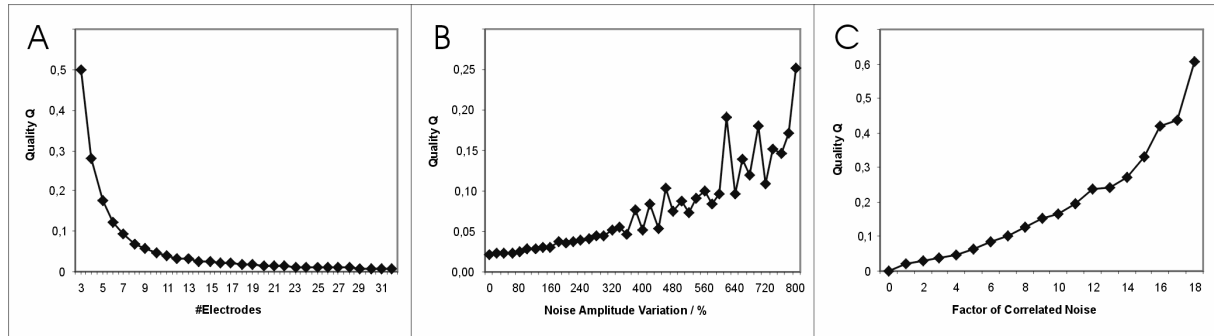


**Fig. 34: The dependency of the cleaning quality on experimentally relevant parameter. Lower values of  $Q$  denote better cleaning results. A) The dependency on the number of electrodes. The cleaning results improve rapidly with increasing quantities of electrodes. B)  $Q$  as a function of the amplitude range of the correlated noise among the channels. C) The dependency of  $Q$  on the amplitude of the correlated noise. Here, the amplitude is the same for all channels.**

Overall, these tests reveal a parameter range of applicability for the PCA cleaning process as described in the materials and methods chapter. Since the influences of these parameters are most likely interdependent in a non-linear fashion, the boundary conditions estimated here will be an overestimation. In practice, when varying the parameters together, satisfying results were obtained throughout the parameter space if only i) the number of electrodes added to at least 10, ii) the amplitude variation did not exceed 400 % and iii) the fraction of common noise bore an amplitude about or less the size of the signal to restore.

As demonstrated in Fig. 35, the PCA cleaning technique was applied to electrophysiological extra-cellular recordings. The spectrum shows massive disturbances in the shape of needle-like deflections at 50 Hz harmonics. This disturbance originated from a malfunctioning CRT monitor. As indicated below, these disturbances could not totally be removed but their amplitude and, thus, their contribution to the actual signal to be analyzed could be reduced significantly to about one third of its original amplitude.

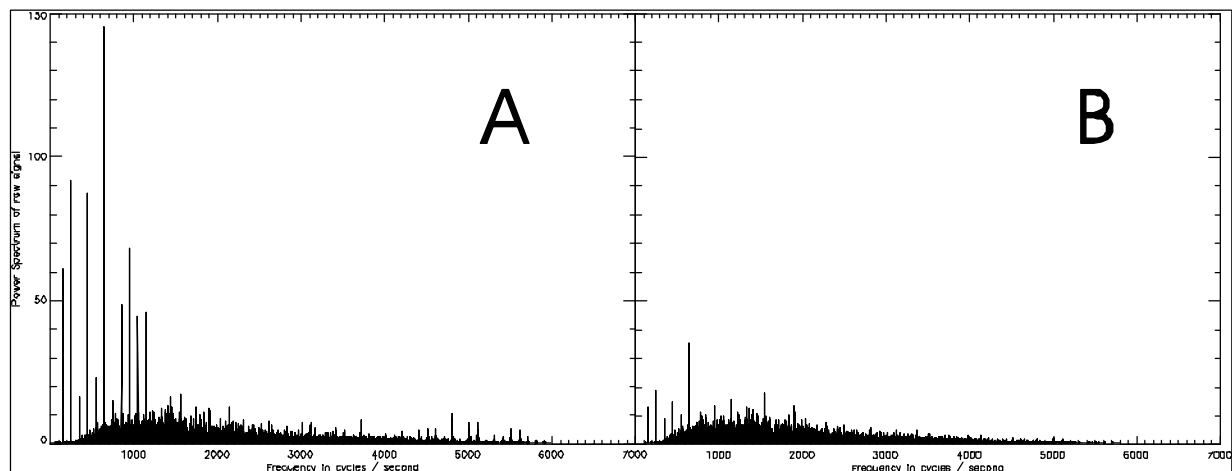


**Fig. 35: Power spectra of A) a disturbed electrophysiologically recorded signal and B) the same signal but with perturbations drastically reduced by the PCA cleaning technique.**

## 2.2 A New Software Design for Flexible Data Organization and Data Access

The software concept presented in the materials and methods section has so far been implemented for four data types: Spike2 format of Cambridge Electronic Design company, the commercial Nex-format of Plexon Inc., the Nev-format of Bionic Technologies and for a custom designed data format for intermediate results. Deriving the superclasses and implementing the virtual methods typically required one to two days of programming work. Subsequently, the whole functionality of managing and retrieving data was provided automatically by the methods inherited from the superclass. This analysis and programming framework was used throughout the data analysis and proved to be very practical since it i) reduced medium term programming effort, ii) unified the syntax for all data formats, iii) simplified data organization by means of the implemented data base and iv) ran stably during several months of data processing.

## 2.3 Spike Sorting

Spike extraction and spike sorting was performed on all data of the five experiments as described in the chapter *Materials and Methods*. However, various sources of noise blurred the spike waveforms to an amount that the waveform characteristics of different cells became indistinguishable. Although several sources of noise were identified and eliminated during and between the experiments, none of the recorded data yield distinct action potential waveforms. For this reason, all MUA (**m**ultiple **u**nit **a**ctivity) data were cleaned with the PCA denoising algorithm as described in *Materials and Methods*. Furthermore, the spikes were

extracted, reconstructed and re-sampled at a frequency of 100 kHz, aligned to their maxima and down-sampled again to 20 kHz in order to optimize the comparison of the spike waveforms. Although this procedure of cleaning and aligning rendered some channels suitable for spike sorting, none of the recordings could be processed such that a sufficient number of parallel channels could be sorted and their separated neurons still bore spike rates high enough for further analysis. Thus, all of the following results are based on multiple unit activity spike trains extracted from the cleaned data.

## 2.4 Foreground/Background Gratings

The data of the foreground/background gratings (FBG) were processed as described in section 2.3. Cross-correlation functions (CCF) were calculated for all possible pairs of MUA as described in *Materials and Methods*. The tuning characteristics, RF positions, CCFs and the correlation indices were inspected manually for the 15 sets of cells obtained during the five experiments. The outcome of these analyses will be outlined in the following by means of a representative case.

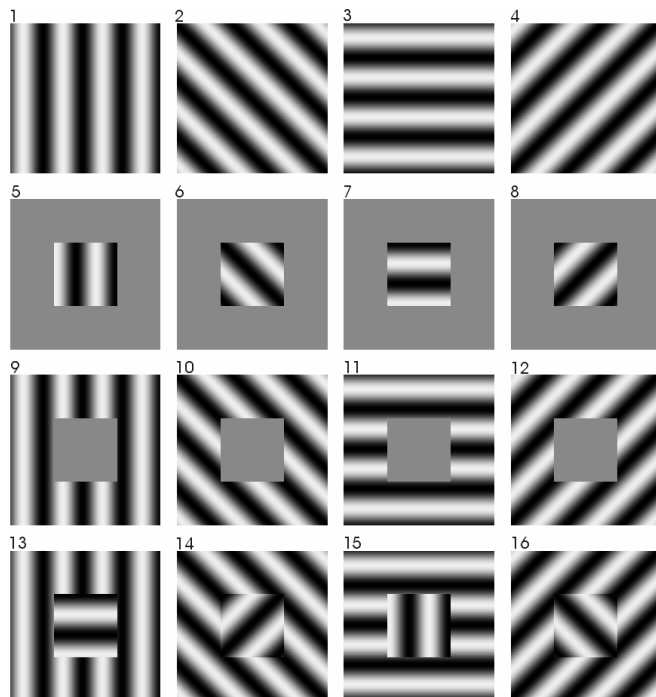


**Fig. 36: The conditions of the FBG stimulus. The receptive field positions are indicated conditions 13-16.**

Although RF positions were determined during the experiment in order to design the FBG stimuli, the first step of the analysis was to assure that the RFs were selectively stimulated by one of the two regions. To this end, the PSTHs for the stimulus conditions 5-8 and 9-11 (Fig. 36) were calculated and visually inspected to be driven by only one of the two condition sets. Those RFs that passed this inspection were further analyzed for their direction preferences. As shown in Fig. 37, most of the MUA was highly direction selective. The quantitative superiority of highly selective MUAs had severe consequences

for the cross-correlation analysis. For instance, assuming two RFs of vertical orientation preference, one inside the inner rectangle and one outside, then for testing the binding hypothesis, synchronization strengths must be compared between condition one and 13 or one and 15, respectively. For either condition, 13 and 15, one of the two MUA signals would drop its activity rate drastically since it would be stimulated orthogonally to its preferred orientation. From this follows, that the time series of MUA events would have only a few entries, thus yielding a weak estimate of synchronization strength. For the experiments discussed here, this phenomenon resulted in random CCFs with no clear dependency on the stimulus condition. All 15 sets of cells recorded under FBG stimulation had thus to be classified as not producing valid results.

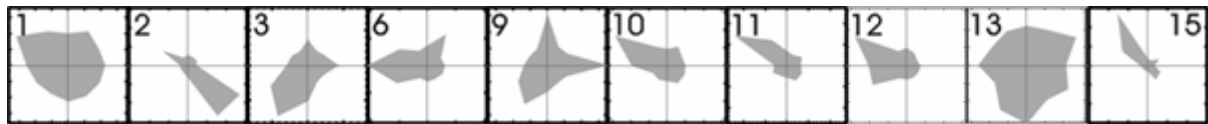


**Fig. 37: Polar plots of direction selectivity for all ten channels which showed MUA.**

## 2.5 Gabor Patches

Due to the disadvantages of the foreground/background gratings, the Gabor patches (GP) were applied to the last three experiments. These stimuli are superior to the FBG since the visual percept can be manipulated while the stimulation of most of the RFs is maintained. By virtue of this property, the spike rates of the MUAs of interest should stay the same and thus CCF should be smooth and meaningful throughout all conditions.

The three stimuli of GPs, a), b) and c), introduced in the chapter *Materials and Methods* are discussed further below. The other five configurations were dismissed for one of the following reasons:

- i) The response characteristics of the RFs were not dominated by the correct GPs but by adjacent ones. This may have happened due to eye shifts, a tolerance in measuring RF properties or a too large overlap of the RFs.
- ii) The orientation preference was determined incorrectly during the experiment and the stimulus was thus designed improperly
- iii) Changes in the excitability of the neurons rendered the CCF meaningless. For a discussion of such influences on CCFs see Brody, 1999.

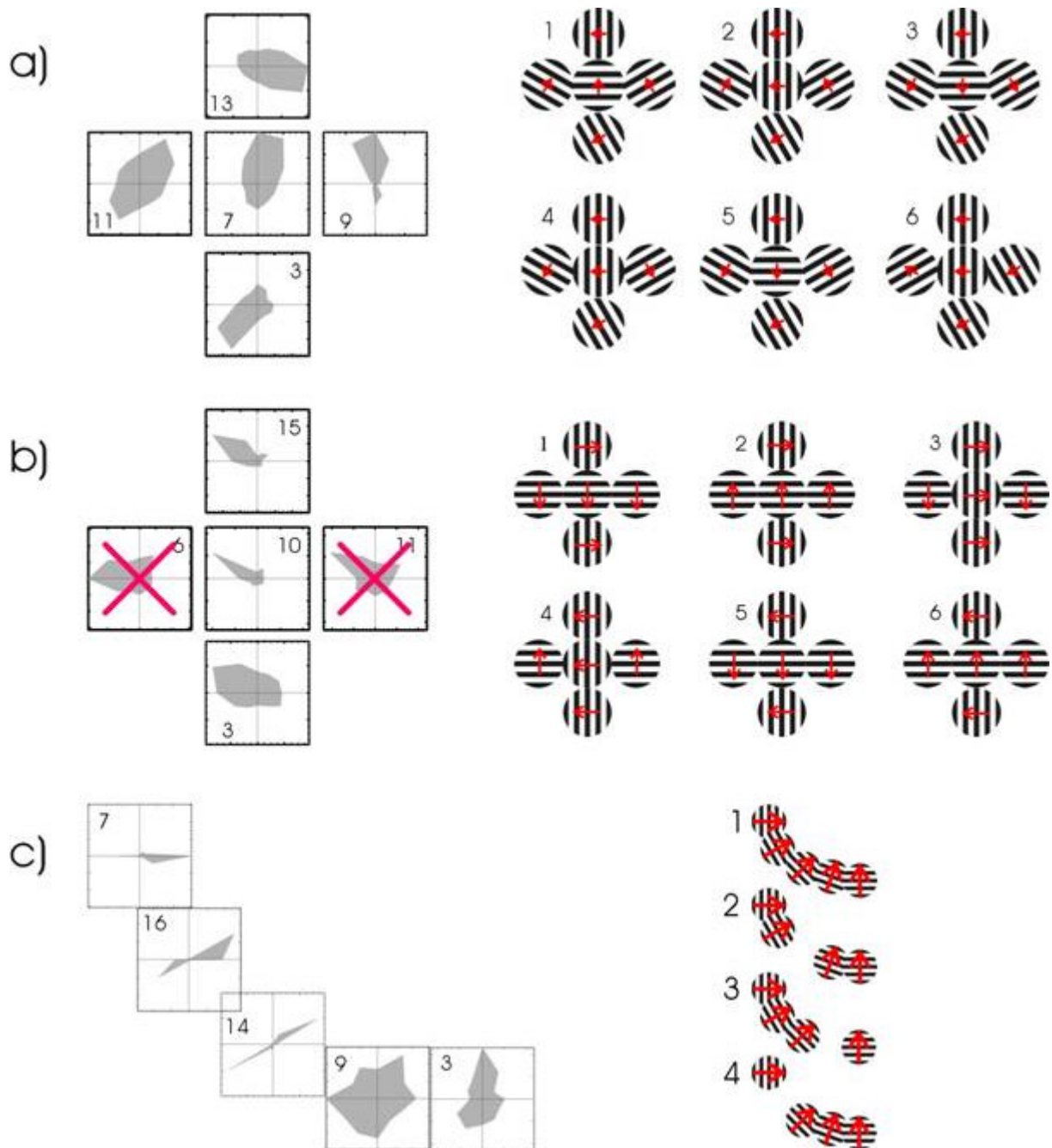


**Fig. 38: Summary of the RF properties (left) as determined offline after the experiments and the stimulus conditions (right) for all three Gabor patch stimuli a), b) and c). The numbers within the polar plots of the direction tunings denote the recording channel, and the numbers next to the stimuli indicate the condition number.**

Fig. 38 summarizes the results of the direction specificity next to the stimulus conditions for all three Gabor patch recordings that were not disturbed by one of the effects i) to iii). The polar plots of the direction tunings show for all stimuli a preference to be higher selective for one certain direction than for the opposite direction. However, since spike rates were high

enough and a sufficient number of repetitions were available in order to average the CCF, the conditions and MUA pairs sub-optimally stimulated in the non-preferred direction could be included into the analysis. For stimulus b) channels 6 and 11, the offline analysis yielded almost an orthogonal direction specificity to that determined during the experiment. Thus, the Gabor patches for these RFs were set up with the wrong orientation and direction of movement during the experiment. For this reason, these channels, marked by red crosses in Fig. 38, were not included into the analysis. Stimulus b) was thus left with only three channels resulting in three possible channel pairs to set up hypotheses for. The outer channels, three and 15, for instance should have synchronized for condition 4 only. The CCFs of this channel pair and the rate responses of all three channels are displayed in Fig. 39.

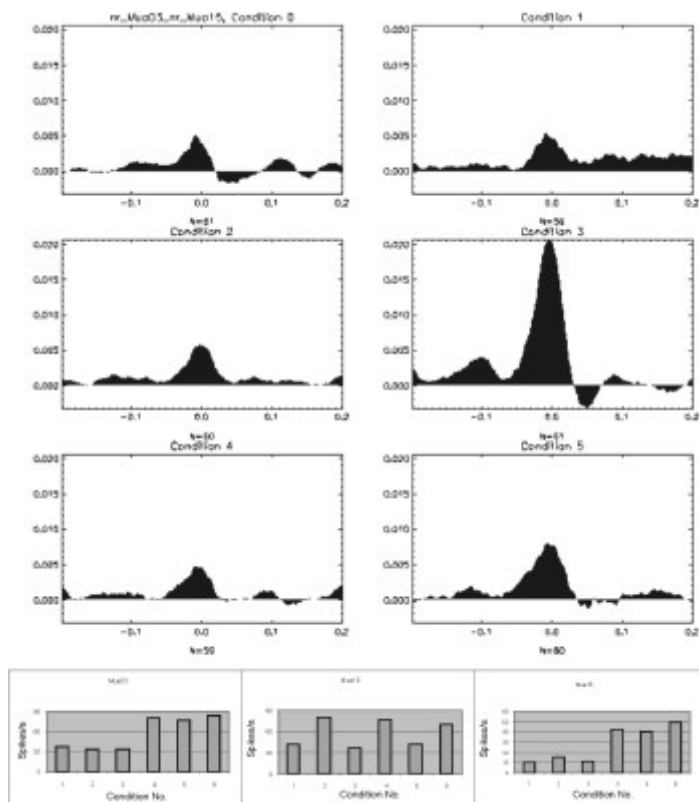
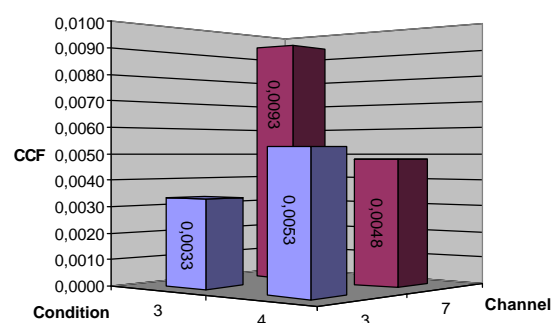


**Fig. 39: Cross-correlation functions of one pair of MUA signals for all conditions. This pair synchronized strongest for the one condition (3) the binding hypothesis predicts synchronization for.**

As can be seen in the figure, the CCFs show the highest centre peak for condition four, as expected. The rates reflect the gross behavior of the direction tunings of Fig. 38, although the direction selectivity seems to be weaker. Channel ten, for instance, had a very strict directional selectivity in the direction tuning, whereas it maintained rates of almost half the peak values when stimulated suboptimal with Gabor patches. Since the tunings were obtained

under stimulation with large gratings across the whole screen but the Gabor patches only covered the individual RF, this may reflect the classical notion that lateral inhibition sharpens orientation or direction selectivity. However, since the comparison of synchronization strengths between conditions which also alter the rates is often distrusted, one interesting feature of this example should be mentioned. The important point is, that channels three and 15 changed their rates only little among the last three conditions whilst changing the degree of synchronization tremendously.

Another case of interest is channel 14 of stimulus c). It had a RF with the unique property of once belonging to one visual object, the left line segment in condition three, and once belonging to another visual object, the right line segment in condition four, without a change in the stimulation of that RF. Since the stimulation of the RF did not change, it is very likely that the population of neurons recorded from did not change either. Thus, a change in synchronization strength would suggest that at least some of the recorded neurons switched the ensemble they participated in. Indeed, as shown in Fig. 40, the synchronization with channel seven was stronger for condition three, where both channels belonged to the same line segment, as compared to condition four, where they belonged to different line segments. *Vice versa*, the synchronization with channel three was higher for condition four compared to condition three. It thus seems, that either some of the channel 14 neurons have switched the ensemble or that the neurons participated in a statistical way more often in one of the two ensembles. Generally, this result is the strongest indicator for neurons switching ensembles one can get without spike sorting, i.e. without identifying and labeling single cells and tracking their participation in ensembles.



So far, examples and special cases were considered. To finally summarize the results of all stimulus and channel pair combinations, the correlation index was calculated for each stimulus a) to c) as

**Fig. 40: Correlation strengths of channel 14 to channels three and seven under stimulation with conditions three and four of stimulus c). The RF of channel seven belonged to the same line segment in condition three and to a different line segment in condition four. Correspondingly, the correlation strength (hind bars) was higher for condition three. The same holds true *vice versa* for channel three (front bars).**

described in *Materials and Methods*. This index summarizes the outcome of all possible channel combination under the different conditions. For instance, stimulus c) had ten possible channel pairs and four conditions resulting in a maximum of 40 combinatorial possibilities. The results are shown in Fig. 41. The index was positive for all three stimuli reflecting a “mean excess” of synchronization strengths for all cases where synchronization should take place according to the hypothesis. The values of the three indices were tested to be significantly higher than zero ( $p < 0.05$ ,  $p < 0.0005$  and  $p < 0.005$ , respectively, student’s t-test).

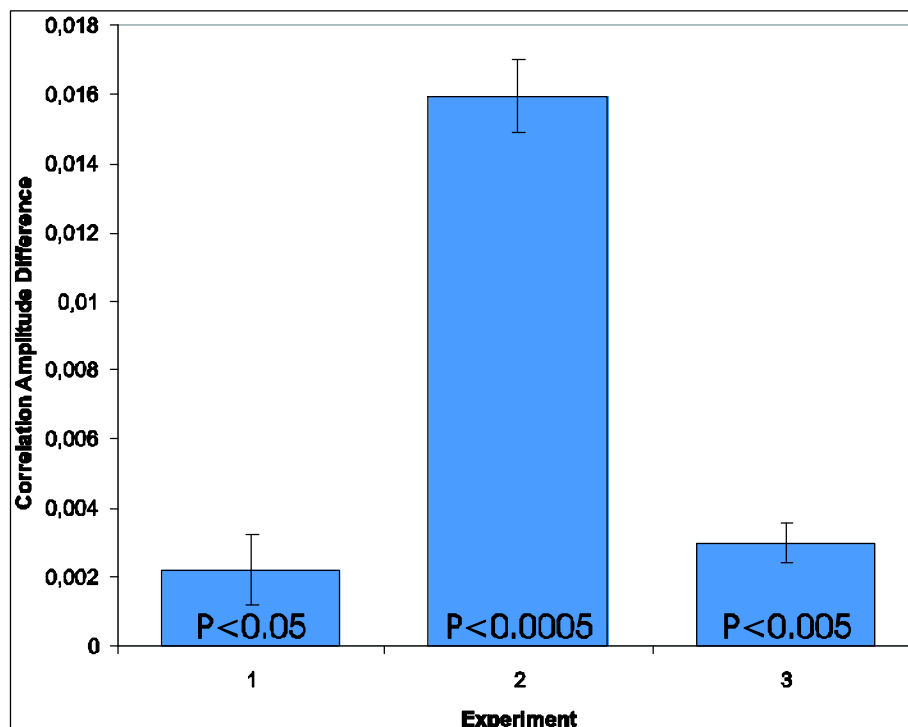
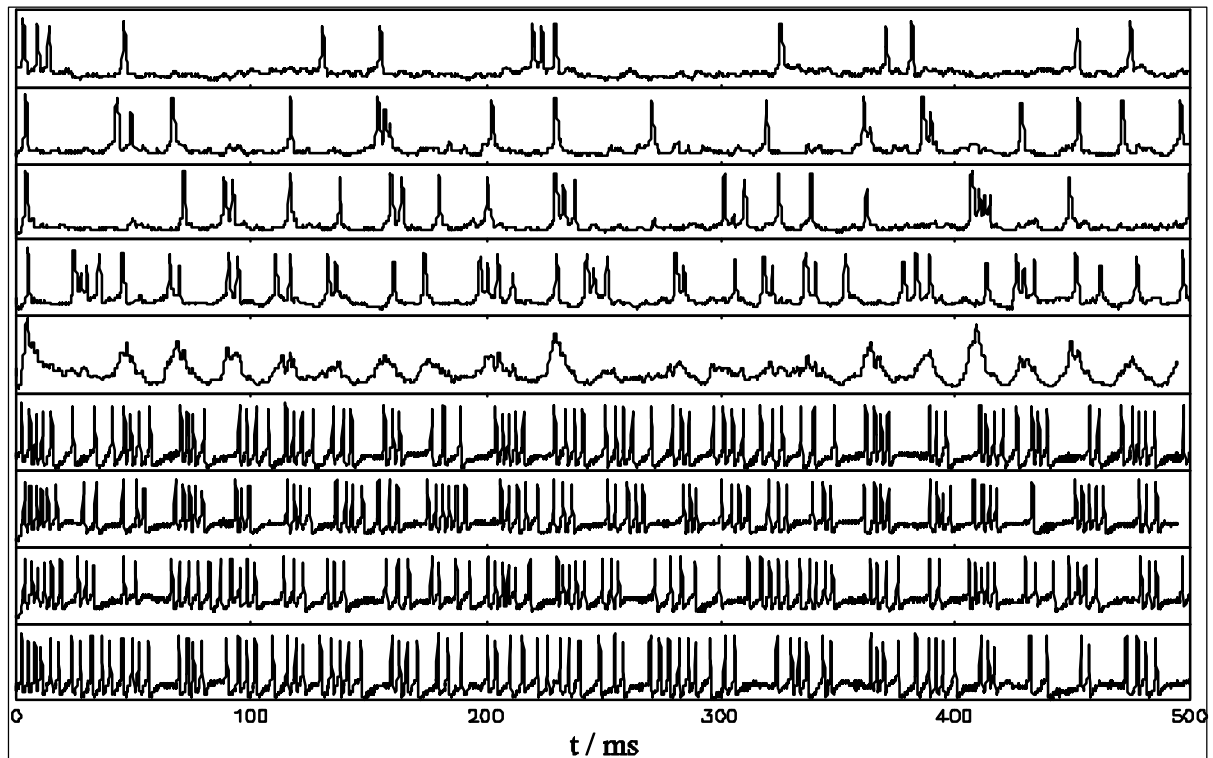


Fig. 41: Correlation index for the three experiments. Error bars indicate the standard deviation of the mean from which the significance levels P were calculated by means of the t-statistics.

## B Computer Simulations

The behavior of the isolated model neurons, of a single model column and of two interconnected model columns were assured to reproduce the results of the original study (Bush & Sejnowski 1996 332 /id) the model parameter were adapted from: Fig. 42 shows the membrane potential of four pyramidal neurons in the top four traces, of four basket cells in the lowermost traces and the LAP (**L**ocal **A**verage **P**otential) of all pyramidal cells within one column) in the centre trace.



**Fig. 42:** Membrane potentials of the cells in a single column not connected to any other column. The first four traces show the membrane potentials of four pyramidal cells showing various spiking behavior. The average of all pyramidal cell potentials, the LAP, was of oscillatory nature which is shown in the centre trace. The last four traces display samples of basket cells, firing vigorously thereby terminating each cycle of the LAP oscillations.

As in the original simulation by Bush et. al., the pyramidal neurons fired with different frequencies and bursting behavior, whilst synchronizing in a statistical sense. Synchronization was terminated by the firing of the reciprocally connected basket cells. The basket cells also showed various spike patterns, but nevertheless caused the LAP to oscillate for 250 ms at about 44 Hz before the oscillation broke down and reappeared at 350 ms. The length and phase of the oscillations varied randomly among columns not connected to each other. In contrast, the main oscillation frequency stayed reliably at about 44 Hz (not shown). When adding the connections between the columns, as outlined in "materials and methods" the two columns synchronized their oscillations in a cooperative manner, i.e. oscillations emerged and faded away again simultaneously in both columns, with no phase lag between their oscillations.

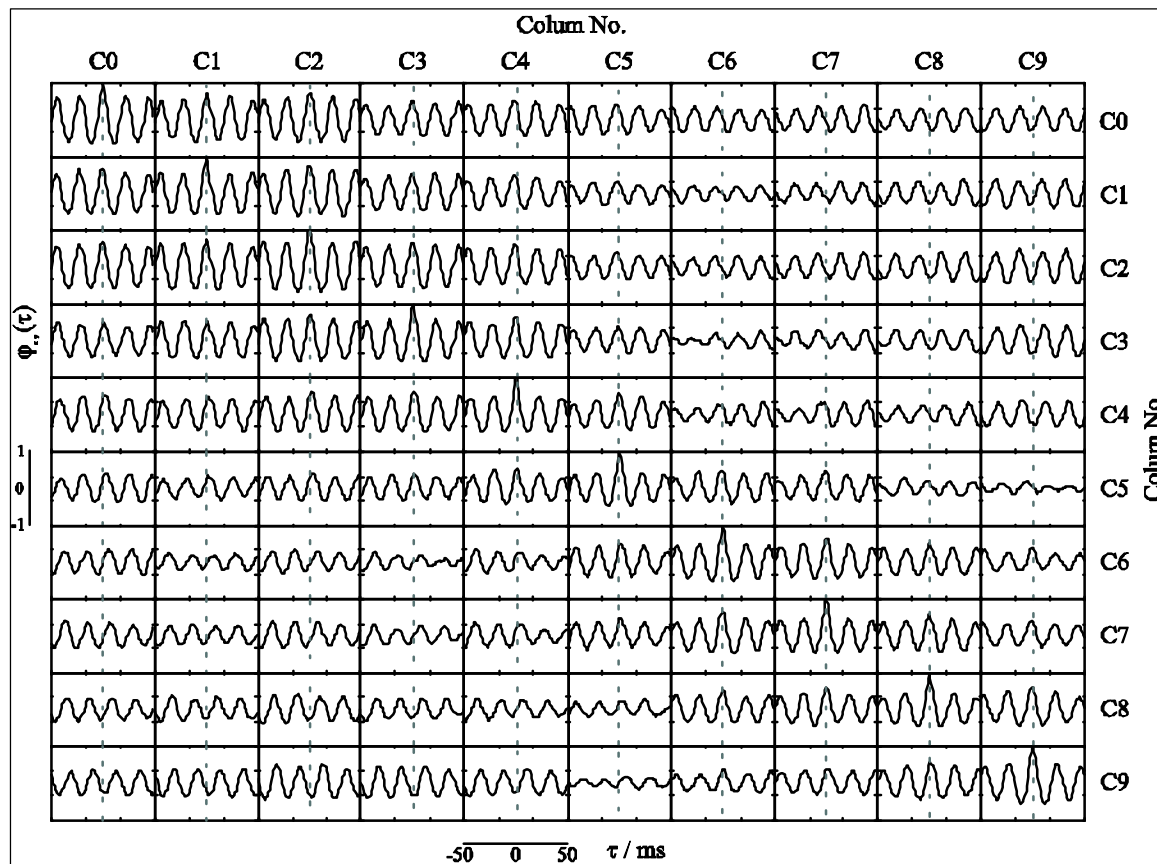


**Fig. 43: Cross-correlation functions between the LAPs of the fully connected ten column system. The order of the columns C0-C9 reflects the topology of the network, i.e. adjacent column numbers were neighboring columns in the simulation.**

However, Bush & Sejnowski studied a system of two columns only, presumably for reasons of computational expense. In the present study, the two-columnar system was extended to ten columns “in a row”, using the same patterns and values of connectivity as applied to the two-columnar model. 500 ms of real time were simulated, the LAP of each column and all pair wise cross-correlations between the LAPs were calculated. Fig. 43 shows these cross-correlations, with the auto-correlations on the diagonal. Correlation strengths were highest within two groups of adjacent columns: from column C0 to C4 and from column C5 or C6 to C9. Generally, when starting at any column’s auto-correlation on the diagonal and inspecting successively the cross-correlations with the adjacent and the more distant columns, some tendencies can be read: i) there is a local tendency to synchronize oscillations with the nearest one to three columns with no phase shift, ii) the synchronization strength first decreases with columnar distance, then iii) a transient phase shift occurs and iv) the amplitude increases again maintaining a  $90^\circ$  phase shift. In order to further investigate the observations about the phase shift, the time lag of the correlation centre peaks were plotted as a function of columnar distance (Fig. 44). The black line indicates the average time shift, which shows a sigmoid

form with its deepest slope occurring between columns three and four. Hence, the columns synchronize their oscillations very well locally, but desynchronize rapidly as the columnar distance increases. This notion is further supported by considering the average of the maximum slope of the curves in Fig. 44 which amounts to 6 ms per column (a quarter of a period). Hence, the phase shift occurs much more transiently than indicated by the average phase shift, but it does not always occur at the same columnar distance.

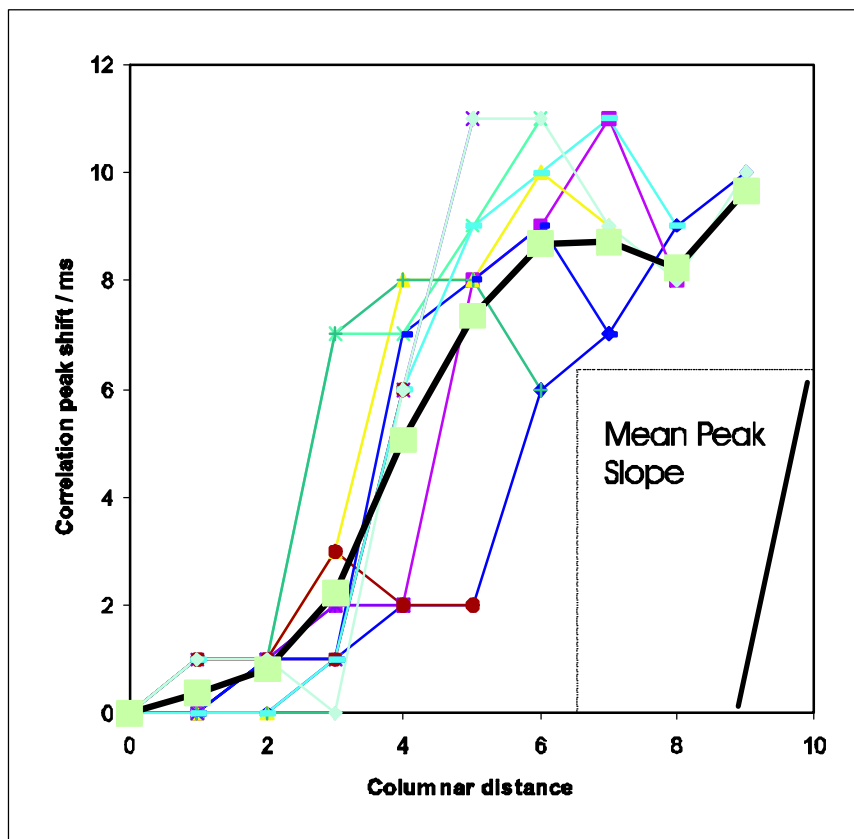


**Fig. 44:** Oscillation phase lags as a function of columnar distance whereby each graph represents one column. The phase lags were determined by measuring the positions of the centre peak of the cross-correlations. The black line shows the average over all columns, bearing the form of a sigmoid function. The line in the inset has a slope equal to the average of the maximum slope of all the other curves, which shows that the sigmoid shape of the average results from steeper phase shifts occurring at distances between two and six columns.

The cross-correlation functions give an estimate of the relatedness of two signals as a temporal average. In order to see how the oscillations dynamically evolve, the original LAP traces are displayed in Fig. 45. The first coherent oscillations appeared between columns C1 to C3 right from the start, being followed by adjacent columns C0, C4, C5, C6 (and even C7 a little bit) at about 100 ms. Another oscillatory regime built up between 250 and 350 ms, successively joined by the columns C9 to C6. The emergence of the second group of

coherently oscillating columns led to severe disturbance of the oscillations in the intermediate columns C4 and C5.

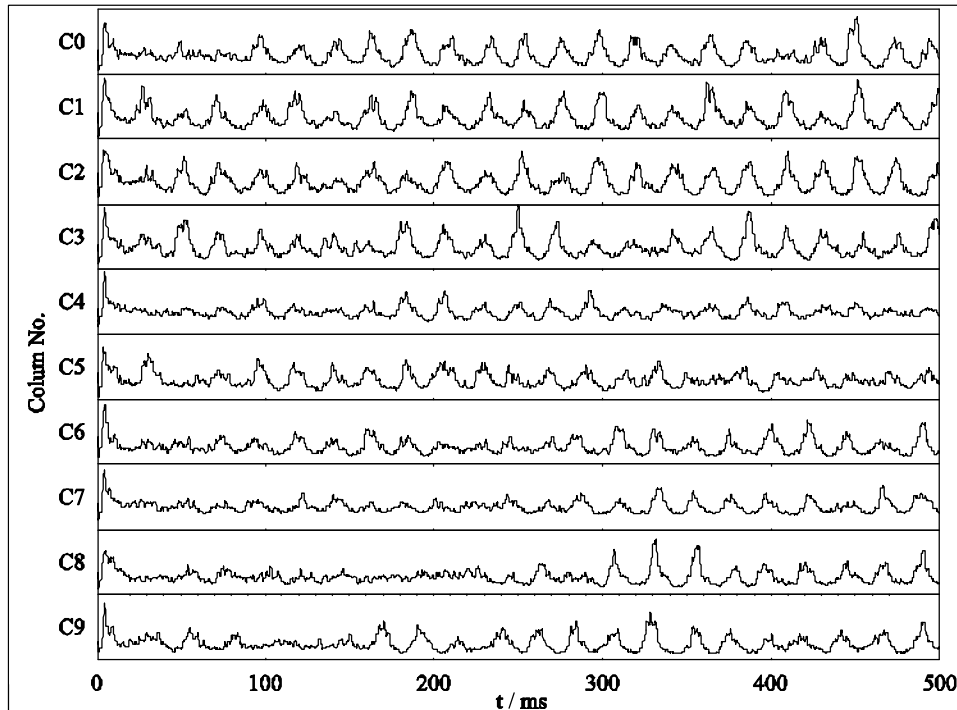


**Fig. 45:** The local average potentials (LAP) of columns C0 to C9 of the fully connected ten column system.

The dynamics of the oscillations were further investigated by means of the cumulative phase graph (CPG). Fig. 46 shows the CPGs of the LAPS. On average, the monotonically raising graphs run through a phase range of 148 rad within 500 ms corresponding to  $148 / (2\pi \cdot 0.5 \text{ s}) \sim 47 \text{ Hz}$ . This is slightly higher than the frequency determined for a single column not connected to any other column. The rise in oscillation frequency was probably due to an enhanced input to the pyramidal cells through the lateral connections, since the intrinsic oscillation frequency of a column was found to also depend on the input strength. Most of the CPGs are close to a straight line and if a small deflection occurs the graph usually returns to that straight line it followed before, indicating that the columns influenced each other only weakly. However, among the clearest peculiarities are the two phase shifts indicated by the arrows a) and b) in Fig. 46. Phase shift a) occurred after 75 ms in column C7, not obviously related to any network behavior, whereas the phase shift b) at 410 ms was caused by a cycle in the LAP which was replaced by two cycles of smaller amplitude, as can be seen in the LAP trace C0 in Fig. 45. Column C8 had the most irregular CPG for the first 292 ms, failing to build up coherent oscillations with one of its neighbors and thereby failing to mediate

coherency between the columns C9 and C7. Once, column C8 achieved to lock its phase into the oscillations of C9 (arrow c), Fig. 46 at 292 ms), the whole group of columns C9 to C6 was able to build up a coherent oscillatory behavior and 60 ms later, column C5 started to deviate its CPG from the adjacent columns, indicating that this column defined the border between the two groups of coherently oscillating columns.

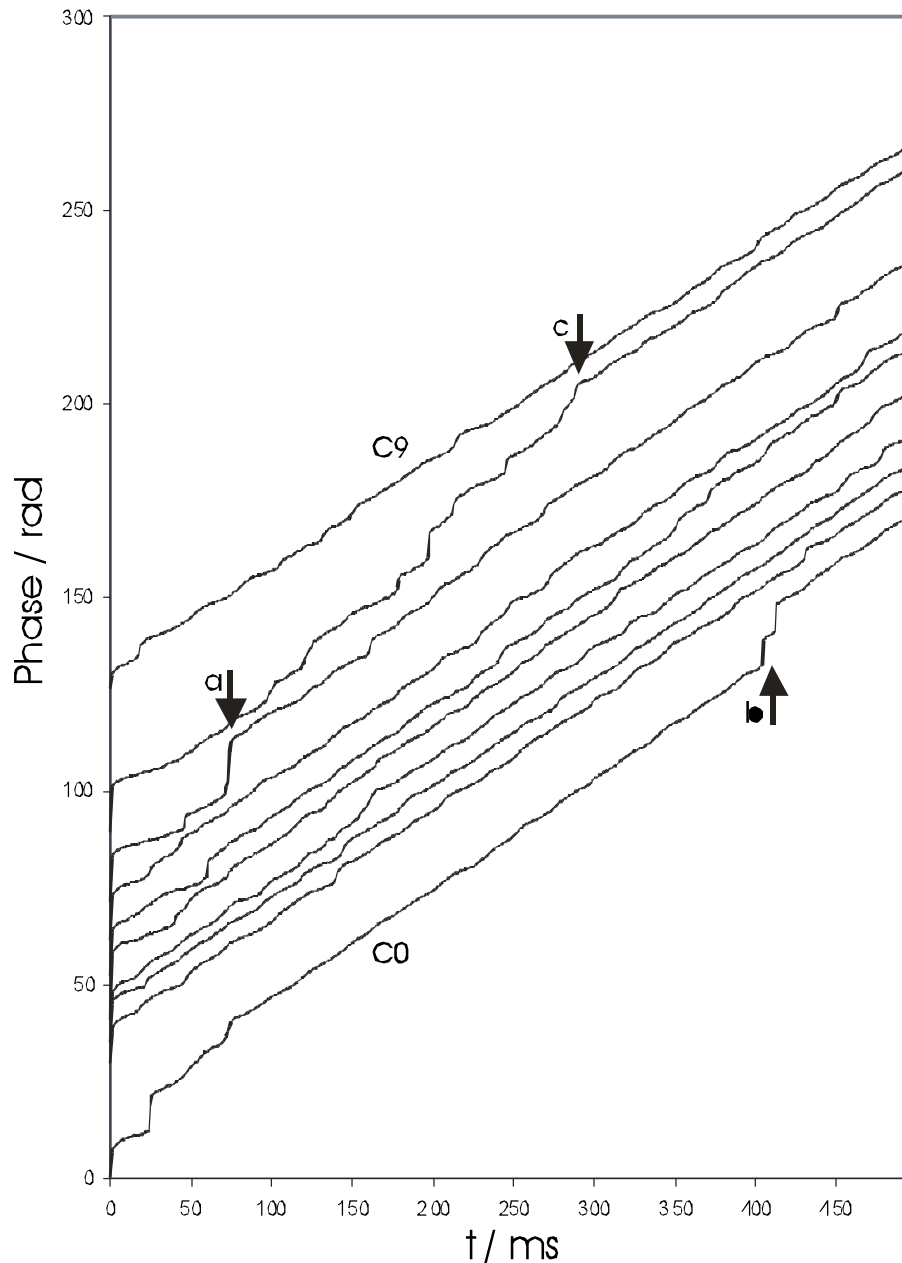


**Fig. 46:** Cumulative phase graphs of the LAPs of the fully connected ten column system. A phase offset was added to each CPG as to put them into the right order from the bottommost (C0) to the uppermost (C9) column. The mean slope corresponds to a frequency of 47 Hz. Arrows a) and b) indicate transient phase shifts at times 75 and 292 ms, respectively. The moment of C8 locking its phase into its neighboring column's oscillation is indicated by arrow c).





## **IV Discussion**

### **A Animal Experiment**

#### **1 A New Technique for Targeted Cell Recording**

##### **1.1 Summary**

A device has been developed which allows for the targeted electrophysiological recording from single neurons at multiple preselected cortical sites in parallel. As discussed below, this method allows for free selection of quantized recording sites from overlapping functional OI maps, covering a cortical region of about 4x8 mm and for subsequent precise positioning of the electrodes to the corresponding cortical sites. Additionally, the depth of penetration remains individually adjustable for each electrode. The method is applicable to virtually all cortical areas where OI can be performed and is not restricted to the use of tungsten microelectrodes only.

##### **1.2 Fabrication of the Tube Grid**

The tube grid is an integral and crucial part of this new recording approach. Ideally, it should allow for recording with infinitesimal thin electrodes and individual guide tubes should have likewise infinitesimal thin walls to allow for optimal resolution in targeting the locations within the feature maps. Practically, however, its geometry and, therefore, its resolution is to great extent dictated by technical constraints such as the required diameter of an electrode to remain stable when advancing and thickness of channel walls to ensure stability of the material. Moreover, the aspect ratio of the channels should be as high as possible in order to minimize the angular play of the electrodes and, by this, optimize the system precision; the spacing between the channels should be as small as possible to result in the highest possible system resolution. In addition, the material should be elastic, for the thin walls between the channels must not break or damage the electrode's insulation. Finally, the material must be inert under exposure to a humid environment and cerebrospinal fluid because this would alter

the channel positions and could immobilize the electrodes within the channels. Conventional product engineering approaches such as drilling or etching proved to be unsuitable. Our solution was to develop such a tube grid in cooperation with a company (microTEC, Duisburg, Germany) mastering the RMPD<sup>®</sup> technology. With this technology it is possible to build up the tube grid by binding a liquid monomer layer after layer by masked light rays. By just altering the light mask other geometries can easily be produced.

The final product, the tube grid, possesses the requirements stated above: the material is insulating, elastic and it did not swell when sunk into pure water over two weeks time; the channels have an extremely high aspect ratio of 15.0 : 0.15, being crucial to the system precision by leaving very little angular play to the electrodes; the precision of RMPD<sup>®</sup> and the elastic material made it possible to produce channels of a diameter just above the electrode's diameter and walls between the channels as thin as 0.07 mm resulting in a high system resolution. Further improvements of the system's resolution by optimizing electrode diameter and channel wall thickness may well be possible and the final limitation of this approach in terms of practical resolution has not yet been reached.

Furthermore, the flexibility, rapidity and low cost of RMPD<sup>®</sup> production allows for the fast construction of similar tube grids permitting other new approaches, inventions or techniques than the targeting method presented here.

### **1.3 System Precision & Handling**

The results of ex-vivo and in-vivo measurements of the system's precision demonstrate that it is possible to simultaneously record from multiple pre-selected sites whose location is constrained only by the spacing of the tube grid channels. They further show that the system reproducibly places the electrodes with a spatial precision in the order of one hundred micrometers relative to the determined channel position. The close spacing of the channels renders the system resolution to suffice for most applications, i.e. the available recording sites permit to record neurons exhibiting virtually all conceivable feature constellations. Restrictions emerge only if parallel recordings are desired from structures which are smaller than the channel spacing and, therefore, smaller than the system's resolution. The number of electrodes which can be inserted with this method is only restricted by the layout of the manipulator used to advance the electrodes and, of course, by the number of channels in the

tube grid ( $\sim 3000$ ).

The most critical issues of the procedure are the matching of the channel positions with the feature map and the projection of the coordinate system onto the cortex. The preparation time of 14 to 16 hours allows the performance of classical electrophysiological experiments with the added benefit of being able to implement the targeting technique. Although the system was not tested in a semi-chronical preparation, this should be feasible because feature maps in visual cortex are stable over time (Shtoyerman et al., 2000). Once the base ring is implanted and all necessary images are taken, the respective electrode constellations can be designated beforehand and different combinations of recording sites can be selected in different recording sessions without the need to repeat the mapping of the channel positions onto the OI map. However, the spatial relationship between base ring and cortex must not be corrupted, for instance, by actions of the behaving animal or growth of the skull.

As the ex-vivo results show, the establishment of relations between the cortical maps and the coordinate system is the most critical step with respect to the system precision. The analysis of the inter-experimental variability indicates that errors in the position of the coordinate grid affect the mapping of all channel positions onto the functional map in a common manner and thus introduces a systematic error in the resulting electrode positions (which can lead to unsystematic errors in neuronal feature response due to the inhomogeneous organization of the feature map). This variability is greater among the experiments than within one experiment. The match between maps and electrode positions was realized by projecting the coordinate system directly onto the cortical surface. This is superior to the use of a coordinate system which is positioned, e.g. on a glass plate, above the cortex because the distance of the plate to parts of the curved cortical surface is never constant and hence errors due to parallax distortions are unavoidable. Errors associated with the direct projection of the coordinate grid onto the cortical surface could arise from inhomogeneous refraction and reflection due to the curved moist surface of the cortex. These problems have been overcome by projecting the coordinate grid through the liquid filled optical imaging chamber that was closed with a glass plate and provided a plane transition from air to the fluid.

Another potential problem is dimpling: the electrodes, although very thin and sharp, depress the cortical tissue. This dimpling effect increases with the number of electrodes used and can influence neuronal activity or even damage the cortex. Dimpling also affects the stability of the recording, since the elastic cortical tissue will slowly return to its initial position, which

virtually has the same effect as advancing the electrodes deeper into the cortex. Even though the method does not avoid these problems, the targeted positioning of the electrodes reduces the number of electrodes required to record cells with the desired properties and, thus, minimizes dimpling and potential cortical damage.

#### **1.4 Alternative Approaches**

Some approaches for the placement of multiple electrodes according to functional maps have been published. However, these lack several of the advantages of the method discussed here, such as individual electrode adjustability or the freedom of targeting multiple cortical sites independently as outlined in greater detail below. Other approaches like a recently described device Arieli and Grinvald, 2002 are optimized for different purposes such as the simultaneous recording of OI data together with electrophysiological data from one or a few electrodes and are thus not comparable to the technique developed here.

One of the most common techniques for advancing multiple electrodes into a relatively confined cortical region uses arrays of guide tubes. The guide tubes are mounted onto a holder which allows them to be arranged in a fixed geometric constellation. The electrodes are guided through the tubes to their target points, which in turn can only be altered collectively by moving the holder of the guide tubes. In principle, it should be possible to enhance the chance of recording a desired combination of neuronal response properties with the different electrodes by fitting the design of the guide tube holder to typical columnar distances. After the OI feature maps have been obtained, this module could be positioned by using the pattern of epicortical blood vessels on the cortical surface as a spatial reference. The success of this approach, however, depends on the regularity of the functional organization, which, in turn, is highly dependent on the feature to be mapped by OI Hübener et al., 1997, the species Rao et al., 1997, the individual animal Horton and Hocking, 1996, the cortical area compare Bonhoeffer and Grinvald, 1991 Rao et al., 1997 and the spatial extent of the electrode insertion sites. Therefore, the limited regularity of cortical domains will not allow for an optimal positioning of the electrodes when separated by up to several millimeters.

Another technique of recording from previously characterized regions is to use thin wires that are chronically implanted into the cortex as described by Mioche and Singer, 1988. This method has the advantage of allowing for the unconstrained placement of several electrodes.

As for the fixed guide tube design, the positioning of the electrodes is accomplished by visual orientation along the pattern of epicortical blood vessels. This method has proven to be sufficiently accurate to target selected orientation domains in cat primary visual cortex Galuske et al., 1997 Schmidt et al., 2002. It is suited for parallel optical and electrophysiological recordings and for recordings in behaving animals. However, it lacks the possibility of manipulating the penetration depth of electrodes after they have been implanted into the cortex. Furthermore, the electrode density is restricted due to the glue around each electrode which is needed to fix the electrodes after insertion.

In summary, the techniques available for the precise placement of multiple electrodes according to functional maps constrain either the possibility to independently select many different recording sites or to advance the electrodes once they are positioned. An ideal solution would consist e.g. of an array of extremely small and maybe even implantable micro-drives put together to a device which renders both possible, the precise placement of electrodes and the possibility to advance them. For the time being these drives and devices are not available. Therefore, the new method presented here combines the advantages of the available methods. By using the tube grid the idea of guide tubes with a fixed geometry is maintained but the necessity of moving electrodes or guide tubes to a certain site above the cortex is avoided. The main improvement over common guide tubes is the extremely high aspect ratio of the channels which has two advantages: first, the electrodes are guided very precisely to their target points and second, the channels are thin enough to be clustered together forming a matrix of densely packed guide tubes. These improvements allow for new possibilities, as the absolute and the relative electrode positions can be defined ad hoc without building a new guide tube holder. Furthermore, the precise parallel guidance of the electrodes allows for accurate definition of electrode spacing as well as for high density arrangements. Adding the possibility of mapping the channels positions onto a functional OI map as outlined in Materials and Methods allows for a choice from hundreds of possible recording sites with defined functional properties as determined by optical imaging of intrinsic signals. The method presented here should thus be considered to be a good compromise between technical complexity and the experimental need of unrestricted, independent and precise placement of several electrodes according to functional OI maps.

## **1.5 Conclusion**

Given the precision with which the system is able to guide the electrodes to target points

segregated by distances in the centimeter range, a large variety of applications in brain research could be envisaged: investigation of interactions between local peculiarities in feature representations (e.g. singularities and fractures in visual cortex) and identified domains within areas as well as between topographically corresponding regions in different areas or hemispheres. Moreover, the device is not restricted to a certain geometry of the applied probes except for their diameter. Thus, incorporating a tool for front-loading the tube grid with probes, combined recording, stimulation and pharmacological application at predefined sites using single electrodes, tetrodes or pipettes is conceivable. In summary, this novel method is ideally suited for studying complex interactions between multiple functionally defined sites using multi electrode recordings, multi site stimulation or pharmacological modulations.

## **2 Data Analysis**

### **2.1 Summary**

The recording and analysis of highly parallel electrophysiological recordings is indispensable for current and future investigations on the computational strategies of the brain. Since cortical operation is likely to use different orthogonal information channels like activity rates, synchronization, oscillations, phase coupling or even synfire chains, the detection, separation and computational interpretation of these information channels inherently requires massive parallel recordings of single neuron activity. The data of such recordings easily amount to an explosion of combinatorial numbers of analyses which will only be coped with by the aid of automated computer processing. Hence, methods were developed in the course of this thesis to improve the data quality of the sensitive recordings, to cope with the informational flood of parameters and intermediate results, to extract action potential waveforms and to improve the means of assigning them to single units. These developments are not restricted to the processing of data obtained with the technique for targeted recordings, but are applicable and helpful for the analysis of any highly parallel recorded data. Furthermore, experiments were performed using paradigms suitable for the investigation of the role of neuronal synchronization as a correlate of gestalt laws. To this end, the recorded data were successfully processed using the above mentioned developments and analyzed by their cross-correlation functions. Most recordings had to be excluded from the analysis for several reasons leading to

insights for the design of new stimuli. The other cases, however, produced highly significant correlation indices, thereby confirming that synchronization is a neuronal correlate of perceptual object definition.

## **2.2 A New Method for the Removal of Correlated Noise**

The PCA cleaning procedure was tested for its general applicability to parallel electrophysiological recordings. The first parameter tested was the number of channels that suffice for a sound removal of correlated noise. The derived minimum of ten electrodes lies well below the standards of parallel recordings since commercially available electrode arrays and manipulators offer the use of 16 to 64 electrodes. Since the thoroughness of the PCA cleaning procedure increases with the number of electrodes and the trend in electrophysiology points towards an even higher number of recording sites (Buzsaki, 2004), this cleaning technique will provide valuable help for the removal of common noise and artifacts in the future.

The second parameter relevant for the application of the PCA cleaner was the amplitude variation of the common noise among the channels. It was found that the noise should vary no more than 400 % (for 10 channels). In real electrophysiological recordings, the main source of noise amplitude variations is most likely the allowance of electrode impedances. For commercially available electrodes this allowance is small enough that it should not be a limiting factor, for custom made electrodes, however, impedances may easily vary sufficiently to deteriorate the cleaning quality. However, the noise amplitude variation will no longer be a matter of concern when the number of electrodes reaches high values such like 64.

The results for the dependency of the PCA cleaner on the signal to noise ratio show that the cleaning is satisfying as soon as the common noise amplitude is of the order of the wanted signal. In praxis, this just means that the noise must not dominate the signal to an extent that it is eye-catching. Thus, the signal to noise ratio is clearly not a limiting factor for the applicability of the PCA cleaner.

Another potentially limiting factor is the duration of the cleaning process. For example, ten minutes of 16 recorded MUA channels, sampled at 20 kHz, required six hours of processing on an dual Pentium 600 MHz computer. This time scales linearly with the recording length but if more channels are added, the number of PCs and the size of the covariation matrix increases, resulting in an exponential relationship between calculation time and number of

channels. On the other hand, the whole cleaning processed runs completely unsupervised and commercially available computers run much faster than the one used here. Keeping in mind that reasonable cleaning results were obtained for ten or more channels the applicability of the PCA cleaner is clearly restricted to offline analyses and there, it is a matter of computational power and time how many channels and how long recording times can be processed.

It is noteworthy that the PCA cleaner has a prospect for nearby MUA recordings as is increasingly performed with stereotrodes or tetrodes. These probes capture the neuronal signals with several very closely spaced recording sites in order to target cell positions by the amplitude ratios of the APs at the different recording sites. Thus, common waveforms are inherent to the channels of such a probe. Principal components can be computed for the channels either within or among several probes. In the first case, the result indicates when a neuron has fired because such an event would result in a common waveform at all recording sites of a single probe. In the second case the result can be used to clean the data because probes at different recording sites should not detect the same neurons and any common waveform is therefore not likely to be of neuronal origin and has to be eliminated.

Overall, the PCA cleaning method provides good means to remove artificial contributions to the sensitive electrophysiological recordings of parallel MUA signals. Restrictions result mainly from the number of channels and the computational expense of the procedure. However, the increasing need of massively parallel recordings and the dependence of the cleaning quality on the number of channels mutually benefit from each other, such, that the PCA cleaning method provides excellent means for improving the quality of contemporary and future experiments.

### **2.3 Spike Extraction**

The process of spike extraction and reconstructions was automated as far as possible since for the high number of recording channels, which would at least double after spike sorting, each automated step saves a lot of manual routine work. Usually, the detection of APs is accomplished by setting a threshold manually to a certain value above the noise level. A common method for the automation of this procedure calculates the standard deviation of the signal and sets the threshold to a fixed manifold. This approach clearly has the disadvantage of yielding rate dependent thresholds, because APs are the signal component with the largest

amplitude and therefore contribute significantly to the standard deviation. Depending on whether the threshold is calculated on a trial to trial basis or not this may lead to a stimulus dependent inclusion or exclusion of small APs. However, in any case it is desirable to estimate the threshold in a rate independent fashion. One step into that direction would be to calculate the standard deviation from a pre-stimulus interval where the rate is independent of the stimulus, but the results would still depend on the spontaneous activity. Therefore, another approach was taken here by detecting and removing APs and calculating the standard deviation from the residual signal. In this way, the resulting threshold was rendered to be independent of either, stimulus response and spontaneous activity.

After spike extraction the AP waveforms were reconstructed as described in *Materials and Methods*. The goal of this reconstruction was to determine the exact position of the initial peak, the best defined part of an AP, in order to align the waveform with respect to the peak and thereby to minimize errors when comparing the waveforms. To this end the si-interpolation was applied, the waveforms were up-sampled with 100 kHz, were aligned and down-sampled to 20 kHz again. It should be stressed that the si-interpolation actually reconstructs the original signal whereas other interpolation methods like the cubic spline interpolation are only methods to make the data “look smooth” and would therefore not reproduce the original peak position. It is the term si-interpolation that frequently leads to confusion in that aspect.

The importance of a precise alignment becomes directly evident when calculating the error for the data discussed in this work: The data were sampled at 20 kHz, thus the misalignment can be up to the time difference between two subsequent bins, 50  $\mu$ s. The steepest part of an AP is the initial voltage raise due to the opening of the voltage dependent sodium channels with very fast kinetics. The velocity of the voltage raise reaches some thousand Volts per second. If we only take a velocity of one thousand V/s then the discrepancy in the waveform voltage of the misaligned waveform would be  $1000 \text{ V/s} * 50 \mu\text{s} = 50 \text{ mV}$ , about the size of an AP. Although this value represents the maximum error along the entire waveform, the effect of this error on the sorting quality depends very much on the method used to actually distinguish the waveforms. However, the most sever effects have to be expected for modern sorting techniques like the principle components of the waveforms. These techniques are superior to classical ones, but they are extremely sensitive to shifts of the waveform in the time domain.

## 2.4 Foreground/Background Gratings

The inspection of the foreground/background grating paradigm (FBG) rendered the respective results unsuitable for testing the hypothesis of binding by synchrony, as described under *Results*. Although the reasons for excluding single repetitions, certain conditions or entire recording sessions were manifold, the one encountered most frequently was the huge variation of neuronal activity among the conditions to compare. It should thus be stressed that the absence of systematic changes in correlation strengths did neither prove nor disprove a functional role of neuronal synchronization.

However, the problems encountered with the FBG gave a cue for the design of new stimuli. Since the neurons in area 18 of cat visual cortex are detectors of exactly that parameter that was varied in order to establish perceptual object borders, the populations that became activated changed from condition to condition. Hence, for the design of stimuli the conclusion must be drawn, that object borders must be established by varying stimulus parameters the recorded neurons are explicitly invariant to. That means for area 18 that in any case the spatial frequency and velocity, the mean luminance and the contrast presented to the RFs must not change. Parameters that can be varied are phase offsets and contextual changes outside the classical RF's spatial extend. These boundary conditions led to the design of the Gabor patch stimuli discussed in the following section.

## 2.5 Gabor Patches

Results were obtained for three spatial configurations of Gabor patches. Two configurations, a) and b), had a cross shaped design which enabled a switching of the perceived line segments by turning single Gabor patches and thereby aligning the orientation and direction of movement of a subset of patches. The results of the cross-correlation analyses showed significant raise of the synchronization strength between MUA pairs when belonging to the same perceptual object as opposed to conditions where they belonged to different objects. They also reveal that the correlation changes can occur independently of rate changes, which has been shown in other contexts (Fries et al., 2001; Samonds et al., 2004) and could here be shown to exist for the segregation of visual objects.

The third configuration of Gabor patches, c), built up a curved line and was split into several objects by removing single patches. For this configuration, the differences of the

synchronization strengths were significant too and followed the predictions of the binding by synchrony hypothesis. In contrast to stimuli a) and b), one RF and its corresponding Gabor patch were once members of the left and once members of the right line segment. Since the stimulation of the RF did not change between those two conditions, the MUA signal should have resulted from the same neurons irrespective of the line segment they represented. These neurons always synchronized better with the ones of the same line segment than with the ones of the other line segment. This provides evidence that the neurons have switched their participation between the two ensembles by synchronizing their discharges.

However, the mechanisms underlying the changes in synchronization still need to be resolved. Functional long range synchronization has been shown to occur preferentially under network gamma oscillations (König et al., 1995). It is not yet clear whether the statistical synchronization as shown by correlating MUA signals is due to an oscillatory phase shifting of the activity of single neurons or whether the neurons participate in different cycles of the oscillations. Since the concept of creating visual objects out of Gabor patches produced changes of synchronization strength without a change in spike rates, the MUA signals were most likely composed of the same neuronal populations under all conditions. This feature renders the stimulation concept ideally suited in order to record from the same neurons under different conditions. As soon as single neurons can be identified, either by their waveforms or by different recording techniques such as tetrode recordings, the mechanisms of the recruitment of single neurons for different ensembles can be tracked down with this paradigm.

Finally, the difficulties in applying the Gabor patch stimulation shall be discussed. The drawbacks of the FBG have been successfully bypassed with the Gabor patches. However, when designing visual objects by placing and sizing the patches, care must be taken that the patches overlap sufficiently in order to be perceived as belonging to one visual object. On the other hand, a stimulation of neighbouring RFs must be avoided, at least for stimulus designs that rely on the turning of patch orientations. Hence, the most frequent reason for rejecting a recording under Gabor patch stimulation was that, especially for the “cross design” of stimuli a) and b), some or all RFs were influenced if not dominated by another Gabor patch. The conclusion must be drawn that for future experiments precise mapping techniques are required that allow the determination of the specificity, location and particularly the spatial extent of RFs more precisely than it is possible with manual measurements (Eckhorn et al., 1993; Ringach, 2004).

## B Computer Simulation

The neuronal mechanisms underlying perceptual grouping are still a matter of debate, but recent studies provided evidence for a role of network oscillations as a means to synchronize the activity of neurons over macroscopic cortical distances or even between areas (Eckhorn et al., 1988, Engel et al., 1991, Nelson et al., 1992). In order to assess the hidden parameters that can not be controlled experimentally, a biologically plausible network model has been created on the basis of an existing model that already reproduced many of the experimentally found oscillation phenomena. The model was extended to cover a larger cortical region and the oscillatory behavior of columns with similar orientation preferences was analyzed. When activated by uncorrelated Poissonian spike trains, the columns oscillated in the gamma frequency range. The oscillations of the columns synchronized locally over a distance of two to four neighboring columns. At a columnar distance of about four, synchronization broke down rapidly by means of a rapid phase shift which was maintained for columns even further apart. This local synchronization of the columns suggests, that for the same network parameters that reproduced cortical behavior best in the underlying study, columnar oscillatory synchronization is a local phenomenon, merely due to the inter columnar circuitry. However, the desynchronization for larger columnar distances suggest either, that the physiological and anatomical data on which the network is based are not correct or that other processes such as top-down influences (Salin and Bullier 1995, Engel et al 2001) or projections from the brain stem (Munk et al 1996, Herculano-Houzel 1999, Verschure and König 1999) must modulate the long range interactions between columns in order to synchronize their oscillations.

The results of the network model require some consolidation in terms of the stability of the results under variation of network parameters. The network oscillations emerged as an intrinsic property of the columns, each having a different intrinsic oscillation frequency. The columns synchronized their oscillations only if pyramidal-pyramidal and pyramidal-basket connections between the columns were introduced. Hence, both kinds of lateral connections were vital for the synchronization of the columns and are thus the most influential parameters for the spatial range of columnar synchronization. Therefore, most importantly, the effect of varying the strength of the lateral connections on the synchronization range between columns will be addressed to the model. To this end, a sample grid within the two dimensional

parameter space of pyramid-pyramid and pyramid-basket connection strengths will be simulated. It can be expected that the parameter plane yields regions of no synchronization and an elongated region traversing the plane diagonally, along which local synchronization emerges at first and builds up to larger synchronization distances as connection strengths increase. The diagonal region is expected because synchronization did build up neither when pyramid-pyramid connections were absent nor when pyramid-basket connections were too strong. This suggests a region of operation to exist for the synchronization of columns. The width of this region would provide a range for the ratio of the connection strengths for which synchronization can take place and the length of the region together with the columnar synchronization range would provide an estimate on how far processes that modulate effective coupling strengths (Munk et al., 1996; Herculano-Houzel et al., 1999; Salin and Bullier, 1995) can influence cortical long range synchronization.

After all basic modules like channel kinetics, neuronal morphology, intra-columnar connection patterns and the connectivity of lateral long range connection between columns of the same specificity are established, further questions can easily be addressed to the model. One issue that can be studied is the network behavior after extending the model by columns of different specificity with the distinct connection patterns recently found *in vitro* (Kisvarday and Eysel, 1993; Kisvarday et al., 1994; Kisvarday et al., 1996). Competing stimuli could be mimicked by simulating geniculate input by uncorrelated spike trains that differ in intensity and latency. The phase relationships between the columns would be analyzed in order to confirm or reject, for a biologically plausible model, recent theoretical suggestions after which competition plays a fundamental role in dynamically modulating synchronization (Tiesinga and Sejnowski 2004). Another question that can be addressed to the model is concerned with the theory of synfire chains (Abeles, 1991; Diesmann et al., 1999; Abeles et al., 1993), which recently experienced evidence to actually exist (Abeles et al., 1993; Mao et al., 2001; Ikegaya et al., 2004). Still, the existence and possible functional role of synfire chains are still a matter of debate. However, even if synfire chains exist it is not clear whether they participate in information processing or whether they emerge by chance as an epiphenomenon of the network complexity. This issue will be addressed by scaling the network model to a realistic size of neurons per column. Since the connectivity within a column is much higher than between the columns, synfire chains are most likely to build up within the pyramidal layer of a column and the network can be reduced to one column of realistic size at first stage. Even though the intra-columnar connections are random, in a

computer model all connections, APs and membrane potentials can be pursued and all synfire chains will be detected. Another scenario could be that Hebbian learning is required for the synfire chains to build up (Bienenstock, 1995). In this case, a functional role for the information processing could not be denied and their coexistence with the intrinsic network oscillations as possibly two orthogonal information channels could be studied by virtue of the model.

## V Reference List

Abeles M 1982 Role of the cortical neuron: integrator or coincidence detector? *Isr. J. Med. Sci.* 18, 83-92.

Abeles M 1982 Quantification, smoothing, and confidence limits for single-units' histograms. *J. Neurosci. Methods* 5, 317-325.

Abeles M 1983 The quantification and graphic display of correlations among three spike trains. *IEEE Trans. Biomed. Eng* 30, 235-239.

Abeles M and Gerstein G L 1988 Detecting spatiotemporal firing patterns among simultaneously recorded single neurons. *J Neurophysiol.* 60, 909-924.

Abeles M, Bergman H, Margalit E and Vaadia E 1993 Spatiotemporal firing patterns in the frontal cortex of behaving monkeys. *J Neurophysiol.* 70, 1629-1638.

Adelson E H and Movshon J A 1982 Phenomenal coherence of moving visual patterns. *Nature* 300, 523-525.

Aertsen A and Arndt M 1993 Response synchronization in the visual cortex. *Curr. Opin. Neurobiol.* 3, 586-594.

Agmon-Snir H and Segev I 1993 Signal delay and input synchronization in passive dendritic structures. *J. Neurophysiol.* 70, 2066-2085.

Agmon-Snir H, Carr C E and Rinzel J 1998 The role of dendrites in auditory coincidence detection. *Nature* 393, 268-272.

Alonso J M, Usrey W M and Reid R C 1996 Precisely correlated firing in cells of the lateral geniculate nucleus. *Nature* 383, 815-819.

Aoyagi T, Takekawa T and Fukai T 2003 Gamma rhythmic bursts: coherence control in networks of cortical pyramidal neurons. *Neural Comput.* 15, 1035-1061.

Arieli A and Grinvald A 2002 Optical imaging combined with targeted electrical recordings, microstimulation, or tracer injections. *J. Neurosci. Methods* 116, 15-28.

Azouz R and Gray CM 2000 Dynamic spike threshold reveals a mechanism for synaptic coincidence detection in cortical neurons in vivo. *Proc. Natl. Acad. Sci. U. S. A* 97, 8110-8115.

Baker S N and Lemon R N 2000 Precise spatiotemporal repeating patterns in monkey primary and supplementary motor areas occur at chance levels [In Process Citation]. *J. Neurophysiol.* 84, 1770-1780.

- Bar-Gad I, Ritov Y and Bergman H 2001 The neuronal refractory period causes a short-term peak in the autocorrelation function. *J. Neurosci. Methods* 104, 155-163.
- Bar-Gad I, Ritov Y, Vaadia E and Bergman H 2001 Failure in identification of overlapping spikes from multiple neuron activity causes artificial correlations. *J. Neurosci. Methods* 107, 1-13.
- Barbas H 1988 Anatomic organization of basoventral and mediodorsal visual recipient prefrontal regions in the rhesus monkey. *J. Comp Neurol.* 276, 313-342.
- Barlow HB 1953 Summation and inhibition in the frog's retina. *J. Physiol* 119, 69-88.
- Barlow HB 1972 Single units and sensation: a neuron doctrine for perceptual psychology? *Perception* 1, 371-394.
- Bedenbaugh P and Gerstein G L 1997 Multiunit normalized cross correlation differs from the average single-unit normalized correlation. *Neural Comput.* 9, 1265-1275.
- Bernander O, Douglas R J, Martin K A and Koch C 1991 Synaptic background activity influences spatiotemporal integration in single pyramidal cells. *Proc. Natl. Acad. Sci. U. S. A* 88, 11569-11573.
- Bialek W, Rieke F, de Ruyter van Steveninck RR and Warland D 1991 Reading a neural code. *Science* 252, 1854-1857.
- Bialek W and Rieke F 1992 Reliability and information transmission in spiking neurons. *Trends Neurosci.* 15, 428-434.
- Bienenstock E 1995 A model of neocortex. *Network.* 179-224.
- Bonhoeffer T and Grinvald A 1991 Iso-orientation domains in cat visual cortex are arranged in pinwheel-like patterns. *Nature* 353, 429-431.
- Bonhoeffer T and Grinvald A 1993 The layout of iso-orientation domains in area 18 of cat visual cortex: optical imaging reveals a pinwheel-like organization. *J Neurosci.* 13, 4157-4180.
- Bonhoeffer T and Grinvald A 1996 Optical Imaging Based on Intrinsic Signals. *In Brain Mapping: The Methods.* Eds. Toga A W and Mazziotta J C. pp 55-97. Academic Press Inc., San Diego.
- Borg-Graham L J, Monier C and Fregnac Y 1998 Visual input evokes transient and strong shunting inhibition in visual cortical neurons. *Nature* 393, 369-373.
- Brecht M, Singer W and Engel A K 1998 Correlation analysis of corticotectal interactions in the cat visual system. *J Neurophysiol.* 79, 2394-2407.
- Brecht M, Singer W and Engel A K 1999 Patterns of synchronization in the superior colliculus of

anesthetized cats. *J Neurosci.* 19, 3567-3579.

Brecht M, Goebel R, Singer W and Engel A K 2001 Synchronization of visual responses in the superior colliculus of awake cats. *Neuroreport* 12, 43-47.

Bressler S L, Coppola R and Nakamura R 1993 Episodic multiregional cortical coherence at multiple frequencies during visual task performance. *Nature* 366, 153-156.

Bressler S L 1996 Interareal synchronization in the visual cortex. *Behav. Brain Res.* 76, 37-49.

Bressloff P C, Cowan J D, Golubitsky M, Thomas P J and Wiener M C 2002 What geometric visual hallucinations tell us about the visual cortex. *Neural Comput.* 14, 473-491.

Bretzner F, Aitoubah J, Shumikhina S, Tan Y F and Molotchnikoff S 2000 Stimuli outside the classical receptive field modulate the synchronization of action potentials between cells in visual cortex of cats. *Neuroreport* 11, 1313-1317.

Brillinger D R 1978 A note on the estimation of evoked response. *Biol. Cybern.* 31, 141-144.

Bringuier V, Chavane F, Glaeser L and Fregnac Y 1999 Horizontal propagation of visual activity in the synaptic integration field of area 17 neurons. *Science* 283, 695-699.

Britten K H, Shadlen M N, Newsome W T and Movshon J A 1992 The analysis of visual motion: a comparison of neuronal and psychophysical performance. *J. Neurosci.* 12, 4745-4765.

Brody C D 1999 Correlations without synchrony. *Neural Comput.* 11, 1537-1551.

Brunel N 2000 Dynamics of sparsely connected networks of excitatory and inhibitory spiking neurons. *J. Comput. Neurosci.* 8, 183-208.

Bryant H L, Jr., Marcos A R and Segundo J P 1973 Correlations of neuronal spike discharges produced by monosynaptic connections and by common inputs. *J. Neurophysiol.* 36, 205-225.

Bullier J and Nowak L G 1995 Parallel versus serial processing: new vistas on the distributed organization of the visual system. *Curr. Opin. Neurobiol.* 5, 497-503.

Bullier J, Schall J D and Morel A 1996 Functional streams in occipito-frontal connections in the monkey. *Behav. Brain Res.* 76, 89-97.

Bush P and Sejnowski T 1996 Inhibition synchronizes sparsely connected cortical neurons within and between columns in realistic network models. *J Comput. Neurosci.* 3, 91-110.

Bush P C and Sejnowski T J 1993 Reduced compartmental models of neocortical pyramidal cells. *J Neurosci. Methods* 46, 159-166.

Bush P C and Sejnowski T J 1994 Effects of inhibition and dendritic saturation in simulated

- neocortical pyramidal cells. *J Neurophysiol.* 71, 2183-2193.
- Buzsaki G 1996 The hippocampo-neocortical dialogue. *Cereb. Cortex* 6, 81-92.
- Buzsaki G and Draguhn A 2004 Neuronal oscillations in cortical networks. *Science* 304, 1926-1929.
- Buzsaki G 2004 Large-scale recording of neuronal ensembles. *Nat. Neurosci.* 7, 446-451.
- Castelo-Branco M, Neuenschwander S and Singer W 1998 Synchronization of visual responses between the cortex, lateral geniculate nucleus, and retina in the anesthetized cat. *J Neurosci.* 18, 6395-6410.
- Castelo-Branco M, Goebel R, Neuenschwander S and Singer W 2000 Neural synchrony correlates with surface segregation rules. *Nature* 405, 685-689.
- Connors B W, Malenka R C and Silva L R 1988 Two inhibitory postsynaptic potentials, and GABAA and GABAB receptor-mediated responses in neocortex of rat and cat. *J. Physiol* 406, 443-468.
- Cooke D F, Taylor C S, Moore T and Graziano M S 2003 Complex movements evoked by microstimulation of the ventral intraparietal area. *Proc. Natl. Acad. Sci. U. S. A* 100, 6163-6168.
- Csibra G, Davis G, Spratling M W and Johnson M H 2000 Gamma oscillations and object processing in the infant brain. *Science* 290, 1582-1585.
- Dan Y, Alonso J M, Usrey W M and Reid R C 1998 Coding of visual information by precisely correlated spikes in the lateral geniculate nucleus. *Nat. Neurosci.* 1, 501-507.
- de Ruyter van Steveninck RR, Lewen G D, Strong S P, Koberle R and Bialek W 1997 Reproducibility and variability in neural spike trains. *Science* 275, 1805-1808.
- deCharms R C, Blake D T and Merzenich M M 1999 A multielectrode implant device for the cerebral cortex. *J Neurosci. Methods* 93, 27-35.
- Desimone R, Schein S J, Moran J and Ungerleider L G 1985 Contour, color and shape analysis beyond the striate cortex. *Vision Res.* 25, 441-452.
- Diesmann M, Gewaltig M O and Aertsen A 1999 Stable propagation of synchronous spiking in cortical neural networks. *Nature* 402, 529-533.
- Douglas R J and Martin K A 2004 Neuronal circuits of the neocortex. *Annu. Rev. Neurosci.* 27, 419-451.
- Eckhorn R, Bauer R, Jordan W, Brosch M, Kruse W, Munk M and Reitboeck H J 1988 Coherent oscillations: a mechanism of feature linking in the visual cortex? Multiple electrode and correlation

analyses in the cat. *Biol. Cybern.* 60, 121-130.

Eckhorn R, Krause F and Nelson J I 1993 The RF-cinematogram. A cross-correlation technique for mapping several visual receptive fields at once. *Biol. Cybern.* 69, 37-55.

Engel A K, Kreiter A K, Konig P and Singer W 1991 Synchronization of oscillatory neuronal responses between striate and extrastriate visual cortical areas of the cat. *Proc. Natl. Acad. Sci. U. S. A* 88, 6048-6052.

Engel A K, Konig P, Kreiter A K and Singer W 1991 Interhemispheric synchronization of oscillatory neuronal responses in cat visual cortex. *Science* 252, 1177-1179.

Engel A K, Fries P and Singer W 2001 Dynamic predictions: oscillations and synchrony in top-down processing. *Nat. Rev. Neurosci.* 2, 704-716.

Fee M S, Mitra P P and Kleinfeld D 1996 Automatic sorting of multiple unit neuronal signals in the presence of anisotropic and non-Gaussian variability [published erratum appears in *J Neurosci Methods* 1997 Feb;71(2):233]. *J. Neurosci. Methods* 69, 175-188.

Fee M S, Mitra P P and Kleinfeld D 1996 Automatic sorting of multiple unit neuronal signals in the presence of anisotropic and non-Gaussian variability. *J. Neurosci. Methods* 69, 175-188.

Fee M S, Mitra P P and Kleinfeld D 1996 Variability of extracellular spike waveforms of cortical neurons. *J. Neurophysiol.* 76, 3823-3833.

Felleman D J and Van Essen D C 1991 Distributed hierarchical processing in the primate cerebral cortex. *Cereb. Cortex* 1, 1-47.

Frien A, Eckhorn R, Bauer R, Woelbern T and Kehr H 1994 Stimulus-specific fast oscillations at zero phase between visual areas V1 and V2 of awake monkey. *Neuroreport* 5, 2273-2277.

Fries P, Roelfsema P R, Engel A K, Konig P and Singer W 1997 Synchronization of oscillatory responses in visual cortex correlates with perception in interocular rivalry. *Proc. Natl. Acad. Sci. U. S. A* 94, 12699-12704.

Fries P, Neuenschwander S, Engel A K, Goebel R and Singer W 2001 Rapid feature selective neuronal synchronization through correlated latency shifting. *Nat. Neurosci.* 4, 194-200.

Fries P, Reynolds J H, Rorie A E and Desimone R 2001 Modulation of Oscillatory Neuronal Synchronization by Selective Visual Attention 1. *Science* 291, 1560-1563.

Friston K J 1995 Neuronal transients. *Proc. R. Soc. Lond B Biol. Sci.* 261, 401-405.

Friston K J 1997 Another neural code? *Neuroimage.* 5, 213-220.

- Fukai T 1994 Synchronization of neural activity is a promising mechanism of memory information processing in networks of columns. *Biol. Cybern.* 71, 215-226.
- Gadicke R and Albus K 1995 Real-time separation of multineuron recordings with a DSP32C signal processor. *J. Neurosci. Methods* 57, 187-193.
- Gallant J L, Braun J and Van Essen D C 1993 Selectivity for polar, hyperbolic, and Cartesian gratings in macaque visual cortex. *Science* 259, 100-103.
- Garcia P, Suarez C P, Rodriguez J and Rodriguez M 1998 Unsupervised classification of neural spikes with a hybrid multilayer artificial neural network. *J. Neurosci. Methods* 82, 59-73.
- Gerstein G L and Perkel D H 1969 Simultaneously recorded trains of action potentials: analysis and functional interpretation. *Science* 164, 828-830.
- Gerstein G L, Perkel D H and Subramanian K N 1978 Identification of functionally related neural assemblies. *Brain Res.* 140, 43-62.
- Gerstein G L, Bedenbaugh P and Aertsen M H 1989 Neuronal assemblies. *IEEE Trans. Biomed. Eng* 36, 4-14.
- Gerstein G L 2000 Cross-correlation measures of unresolved multi-neuron recordings. *J. Neurosci. Methods* 100, 41-51.
- Gerstner W, Kempter R, van Hemmen J L and Wagner H 1996 A neuronal learning rule for sub-millisecond temporal coding. *Nature* 383, 76-81.
- Ghose G M, Ohzawa I and Freeman R D 1994 Receptive-field maps of correlated discharge between pairs of neurons in the cat's visual cortex. *J Neurophysiol.* 71, 330-346.
- Gilbert C D and Wiesel T N 1983 Clustered intrinsic connections in cat visual cortex. *J Neurosci.* 3, 1116-1133.
- Gilbert C D and Wiesel T N 1989 Columnar specificity of intrinsic horizontal and corticocortical connections in cat visual cortex. *J Neurosci.* 9, 2432-2442.
- Gilbert C D, Das A, Ito M, Kapadia M and Westheimer G 1996 Spatial integration and cortical dynamics. *Proc. Natl. Acad. Sci. U. S A* 93, 615-622.
- Gilbert C D 1998 Adult cortical dynamics. *Physiol Rev.* 78, 467-485.
- Gochin P M, Kaltenbach J A and Gerstein G L 1989 Coordinated activity of neuron pairs in anesthetized rat dorsal cochlear nucleus. *Brain Res.* 497, 1-11.

- Gochin P M, Miller E K, Gross C G and Gerstein G L 1991 Functional interactions among neurons in inferior temporal cortex of the awake macaque. *Exp. Brain Res.* 84, 505-516.
- Gochin P M, Colombo M, Dorfman G A, Gerstein G L and Gross C G 1994 Neural ensemble coding in inferior temporal cortex. *J. Neurophysiol.* 71, 2325-2337.
- Goldman-Rakic P S 1995 Cellular basis of working memory. *Neuron* 14, 477-485.
- Goodale M A, Milner A D, Jakobson L S and Carey D P 1991 A neurological dissociation between perceiving objects and grasping them. *Nature* 349, 154-156.
- Goodale M A and Milner A D 1992 Separate visual pathways for perception and action. *Trends Neurosci.* 15, 20-25.
- Gray C M and Singer W 1989 Stimulus-specific neuronal oscillations in orientation columns of cat visual cortex. *Proc. Natl. Acad. Sci. U. S A* 86, 1698-1702.
- Gray C M, Konig P, Engel A K and Singer W 1989 Oscillatory responses in cat visual cortex exhibit inter-columnar synchronization which reflects global stimulus properties. *Nature* 338, 334-337.
- Gray C M, Engel A K, Konig P and Singer W 1990 Stimulus-Dependent Neuronal Oscillations in Cat Visual Cortex: Receptive Field Properties and Feature Dependence. *Eur. J. Neurosci.* 2, 607-619.
- Gray C M, Engel A K, Konig P and Singer W 1992 Synchronization of oscillatory neuronal responses in cat striate cortex: temporal properties. *Vis. Neurosci.* 8, 337-347.
- Gray C M, Maldonado P E, Wilson M and McNaughton B 1995 Tetrodes markedly improve the reliability and yield of multiple single-unit isolation from multi-unit recordings in cat striate cortex. *J. Neurosci. Methods* 63, 43-54.
- Gray C M and McCormick D A 1996 Chattering cells: superficial pyramidal neurons contributing to the generation of synchronous oscillations in the visual cortex [see comments]. *Science* 274, 109-113.
- Gray C M 1999 The temporal correlation hypothesis of visual feature integration: still alive and well. *Neuron* 24, 31-25.
- Graziano M S, Patel K T and Taylor C S 2004 Mapping from motor cortex to biceps and triceps altered by elbow angle. *J. Neurophysiol.* 92, 395-407.
- Gross C G, Rocha-Miranda C E and Bender D B 1972 Visual properties of neurons in inferotemporal cortex of the Macaque. *J. Neurophysiol.* 35, 96-111.
- Grossberg S 1980 How does a brain build a cognitive code? *Psychol. Rev.* 87, 1-51.
- Hansel D and Sompolinsky H 1996 Chaos and synchrony in a model of a hypercolumn in visual

cortex. *J. Comput. Neurosci.* 3, 7-34.

Hansel D and Mato G 2003 Asynchronous states and the emergence of synchrony in large networks of interacting excitatory and inhibitory neurons. *Neural Comput.* 15, 1-56.

Harris K D, Henze D A, Csicsvari J, Hirase H and Buzsaki G 2000 Accuracy of tetrode spike separation as determined by simultaneous intracellular and extracellular measurements. *J. Neurophysiol.* 84, 401-414.

Hausser M and Mel B 2003 Dendrites: bug or feature? *Curr. Opin. Neurobiol.* 13, 372-383.

Herculano-Houzel S, Munk M H, Neuenschwander S and Singer W 1999 Precisely synchronized oscillatory firing patterns require electroencephalographic activation. *J Neurosci.* 19, 3992-4010.

Hilgetag C C, O'Neill M A and Young M P 1996 Indeterminate organization of the visual system. *Science* 271, 776-777.

Hubel D H and Wiesel T N 1959 Receptive fields of single neurones in the cat's striate cortex. *J. Physiol* 148, 574-591.

Hubel D H and Wiesel T N 1963 Shape and arrangement of columns in cat's striate cortex. *J. Physiol* 165, 559-568.

Hubel D H and Wiesel T N 1968 Receptive fields and functional architecture of monkey striate cortex. *J. Physiol* 195, 215-243.

Hubel D H and Wiesel T N 1969 Anatomical demonstration of columns in the monkey striate cortex. *Nature* 221, 747-750.

Humphreys G W, Cinel C, Wolfe J, Olson A and Klempen N 2000 Fractionating the binding process: neuropsychological evidence distinguishing binding of form from binding of surface features. *Vision Res.* 40, 1569-1596.

Hupe J M, James A C, Payne B R, Lomber S G, Girard P and Bullier J 1998 Cortical feedback improves discrimination between figure and background by V1, V2 and V3 neurons. *Nature* 394, 784-787.

Hübener M, Shoham D, Grinvald A and Bonhoeffer T 1997 Spatial relationships among three columnar systems in cat area 17. *J Neurosci.* 17, 9270-9284.

Ikegaya Y, Aaron G, Cossart R, Aronov D, Lampl I, Ferster D and Yuste R 2004 Synfire chains and cortical songs: temporal modules of cortical activity. *Science* 304, 559-564.

Johnson D H, Gruner C M, Baggerly K and Seshagiri C 2001 Information-theoretic analysis of neural

coding. *J. Comput Neurosci.* 10, 47-69.

Jones J P and Palmer L A 1987 The two-dimensional spatial structure of simple receptive fields in cat striate cortex. *J Neurophysiol.* 58, 1187-1211.

Kirkwood P A 1979 On the use and interpretation of cross-correlations measurements in the mammalian central nervous system. *J. Neurosci. Methods* 1, 107-132.

Kisvarday Z F, Martin K A, Freund T F, Magloczky Z, Whitteridge D and Somogyi P 1986 Synaptic targets of HRP-filled layer III pyramidal cells in the cat striate cortex. *Exp. Brain Res.* 64, 541-552.

Kisvarday Z F and Eysel U T 1992 Cellular organization of reciprocal patchy networks in layer III of cat visual cortex (area 17). *Neuroscience* 46, 275-286.

Kisvarday Z F and Eysel U T 1993 Functional and structural topography of horizontal inhibitory connections in cat visual cortex. *Eur. J. Neurosci.* 5, 1558-1572.

Kisvarday Z F, Beaulieu C and Eysel U T 1993 Network of GABAergic large basket cells in cat visual cortex (area 18): implication for lateral disinhibition. *J. Comp Neurol.* 327, 398-415.

Kisvarday Z F, Kim D S, Eysel U T and Bonhoeffer T 1994 Relationship between lateral inhibitory connections and the topography of the orientation map in cat visual cortex. *Eur. J. Neurosci.* 6, 1619-1632.

Kisvarday Z F, Bonhoeffer T, Kim D S and Eysel U T 1996 Functional topography of horizontal neuronal networks in cat visual cortex (Area 18). *In Brain Theory: Biological Basis and Computational Principles.* Eds. Aertsen A and Braitenberg V. pp 97-121. Elsevier Science, Amsterdam.

Kisvarday Z F, Toth E, Rausch M and Eysel U T 1997 Orientation-specific relationship between populations of excitatory and inhibitory lateral connections in the visual cortex of the cat. *Cereb. Cortex* 7, 605-618.

Klemm W R and Sherry C J 1981 Serial ordering in spike trains: what's it "trying to tell us"? *Int. J. Neurosci.* 14, 15-33.

Koch C, Douglas R and Wehmeier U 1990 Visibility of synaptically induced conductance changes: theory and simulations of anatomically characterized cortical pyramidal cells. *J. Neurosci.* 10, 1728-1744.

Koch C, Rapp M and Segev I 1996 A brief history of time (constants). *Cereb. Cortex* 6, 93-101.

Kohler E, Keysers C, Umiltà M A, Fogassi L, Gallese V and Rizzolatti G 2002 Hearing sounds, understanding actions: action representation in mirror neurons. *Science* 297, 846-848.

Komatsu Y, Nakajima S, Toyama K and Fetz E E 1988 Intracortical connectivity revealed by spike-

- triggered averaging in slice preparations of cat visual cortex. *Brain Res.* 442, 359-362.
- Konig P, Engel A K and Singer W 1995 Relation between oscillatory activity and long-range synchronization in cat visual cortex. *Proc. Natl. Acad. Sci. U. S A* 92, 290-294.
- Konig P, Engel A K, Roelfsema P R and Singer W 1995 How precise is neuronal synchronization? *Neural Comput.* 7, 469-485.
- Konig P, Engel A K and Singer W 1996 Integrator or coincidence detector? The role of the cortical neuron revisited. *Trends Neurosci.* 19, 130-137.
- Kopell N, Ermentrout G B, Whittington M A and Traub R D 2000 Gamma rhythms and beta rhythms have different synchronization properties. *Proc. Natl. Acad. Sci. U. S. A* 97, 1867-1872.
- Kreiter A K and Singer W 1992 Oscillatory Neuronal Responses in the Visual Cortex of the Awake Macaque Monkey. *Eur. J. Neurosci.* 4, 369-375.
- Kreiter A K and Singer W 1996 Stimulus-dependent synchronization of neuronal responses in the visual cortex of the awake macaque monkey. *J Neurosci.* 16, 2381-2396.
- Kruger J and Aiple F 1988 Multimicroelectrode investigation of monkey striate cortex: spike train correlations in the infragranular layers. *J. Neurophysiol.* 60, 798-828.
- KUFFLER S W 1953 Discharge patterns and functional organization of mammalian retina. *J. Neurophysiol.* 16, 37-68.
- Kuhn A, Aertsen A and Rotter S 2004 Neuronal integration of synaptic input in the fluctuation-driven regime. *J. Neurosci.* 24, 2345-2356.
- Lachaux J P, Rodriguez E, Martinerie J and Varela F J 1999 Measuring phase synchrony in brain signals. *Hum. Brain Mapp.* 8, 194-208.
- Le Van Quyen M, Foucher J, Lachaux J, Rodriguez E, Lutz A, Martinerie J and Varela F J 2001 Comparison of Hilbert transform and wavelet methods for the analysis of neuronal synchrony. *J. Neurosci. Methods* 111, 83-98.
- Letelier J C and Weber P P 2000 Spike sorting based on discrete wavelet transform coefficients. *J. Neurosci. Methods* 101, 93-106.
- Lewicki M S 1994 Bayesian Modeling and Classification of Neural Signals. *Neural Comput.* 6, 1005-1030.
- Lewicki M S 1998 A review of methods for spike sorting: the detection and classification of neural action potentials. *Network.* 9, R53-R78.

- Livingstone M and Hubel D 1988 Segregation of form, color, movement, and depth: anatomy, physiology, and perception. *Science* 240, 740-749.
- Livingstone M S and Hubel D H 1984 Anatomy and physiology of a color system in the primate visual cortex. *J. Neurosci.* 4, 309-356.
- Logothetis N K, Pauls J, Augath M, Trinath T and Oeltermann A 2001 Neurophysiological investigation of the basis of the fMRI signal. *Nature* 412, 150-157.
- Löwel S and Singer W 1992 Selection of intrinsic horizontal connections in the visual cortex by correlated neuronal activity. *Science* 255, 209-212.
- Löwel S, Schmidt K E, Kim D S, Wolf F, Hoffsummer F, Singer W and Bonhoeffer T 1998 The layout of orientation and ocular dominance domains in area 17 of strabismic cats. *Eur. J Neurosci.* 10, 2629-2643.
- Maass W, Natschlager T and Markram H 2002 Real-time computing without stable states: a new framework for neural computation based on perturbations. *Neural Comput.* 14, 2531-2560.
- MacLeod K, Backer A and Laurent G 1998 Who reads temporal information contained across synchronized and oscillatory spike trains? *Nature* 395, 693-698.
- Maex R and De Schutter E 2003 Resonant synchronization in heterogeneous networks of inhibitory neurons. *J. Neurosci.* 23, 10503-10514.
- Mainen Z F and Sejnowski T J 1995 Reliability of spike timing in neocortical neurons. *Science* 268, 1503-1506.
- Martignon L, Von Hasseln H, Grun S, Aertsen A and Palm G 1995 Detecting higher-order interactions among the spiking events in a group of neurons. *Biol. Cybern.* 73, 69-81.
- Martin K A 1994 A brief history of the "feature detector". *Cereb. Cortex* 4, 1-7.
- Mason A, Nicoll A and Stratford K 1991 Synaptic transmission between individual pyramidal neurons of the rat visual cortex in vitro. *J. Neurosci.* 11, 72-84.
- Maunsell J H and Newsome W T 1987 Visual processing in monkey extrastriate cortex. *Annu. Rev. Neurosci.* 10, 363-401.
- Mel B W 1993 Synaptic integration in an excitable dendritic tree. *J. Neurophysiol.* 70, 1086-1101.
- Melssen W J and Epping W J 1987 Detection and estimation of neural connectivity based on crosscorrelation analysis. *Biol. Cybern.* 57, 403-414.
- Michalski A, Gerstein G L, Czarkowska J and Tarnecki R 1983 Interactions between cat striate cortex

- neurons. *Exp. Brain Res.* 51, 97-107.
- MILLER W H, RATLIFF F and HARTLINE H K 1961 How cells receive stimuli. *Sci. Am.* 205, 222-238.
- Milner P M 1974 A model for visual shape recognition. *Psychol. Rev.* 81, 521-535.
- Miyashita Y 1993 Inferior temporal cortex: where visual perception meets memory. *Annu. Rev. Neurosci.* 16, 245-263.
- Moore G P, Segundo J P, Perkel D H and Levitan H 1970 Statistical signs of synaptic interaction in neurons. *Biophys. J.* 10, 876-900.
- Munk M H, Roelfsema P R, Konig P, Engel A K and Singer W 1996 Role of reticular activation in the modulation of intracortical synchronization [see comments]. *Science* 272, 271-274.
- Musial P G, Baker S N, Gerstein G L, King E A and Keating J G 2002 Signal-to-noise ratio improvement in multiple electrode recording. *J Neurosci. Methods* 115, 29-43.
- Nelson J I, Salin P A, Munk M H, Arzi M and Bullier J 1992 Spatial and temporal coherence in cortico-cortical connections: a cross-correlation study in areas 17 and 18 in the cat. *Vis. Neurosci.* 9, 21-37.
- Neuenschwander S and Singer W 1996 Long-range synchronization of oscillatory light responses in the cat retina and lateral geniculate nucleus. *Nature* 379, 728-732.
- Nguyen D P, Frank L M and Brown E.N. 2003 An application of reversible-jump Markov chain Monte Carlo to spike classification of multi-unit extracellular recordings. *Network:Comput Neural Syst* 61-82.
- Niessing M . Mikrosakkaden und ihre Auswirkungen auf Signale im primären Sehcortex. 1999. Philipps-Universität.  
Ref Type: Thesis/Dissertation
- Nowak L G, Munk M H, Nelson J I, James A C and Bullier J 1995 Structural basis of cortical synchronization. I. Three types of interhemispheric coupling. *J. Neurophysiol.* 74, 2379-2400.
- Pauluis Q, Baker S N and Olivier E 1999 Emergent oscillations in a realistic network: the role of inhibition and the effect of the spatiotemporal distribution of the input. *J. Comput. Neurosci.* 6, 27-48.
- Payne B R 1993 Evidence for visual cortical area homologs in cat and macaque monkey. *Cereb. Cortex* 3, 1-25.
- Perkel D H, Gerstein G L and Moore G P 1967 Neuronal spike trains and stochastic point processes. II. Simultaneous spike trains. *Biophys. J.* 7, 419-440.
- Perkel D H, Gerstein G L and Moore G P 1967 Neuronal spike trains and stochastic point processes.

I. The single spike train. *Biophys. J.* 7, 391-418.

Pesaran B, Pezaris J S, Sahani M, Mitra P P and Andersen R A 2002 Temporal structure in neuronal activity during working memory in macaque parietal cortex. *Nat. Neurosci.* 5, 805-811.

Peterhans E and von der H R 1989 Mechanisms of contour perception in monkey visual cortex. II. Contours bridging gaps. *J. Neurosci.* 9, 1749-1763.

Phillips W A and Singer W 1997 In search of common foundations for cortical computation. *Behav. Brain Sci.* 20, 657-683.

Pouzat C, Mazor O and Laurent G 2002 Using noise signature to optimize spike-sorting and to assess neuronal classification quality. *J. Neurosci. Methods* 122, 43-57.

Pouzat C, Delescluse M, Viot P and Diebolt J 2004 Improved spike-sorting by modeling firing statistics and burst-dependent spike amplitude attenuation: a Markov chain Monte Carlo approach. *J. Neurophysiol.* 91, 2910-2928.

Prut Y, Vaadia E, Bergman H, Haalman I, Slovin H and Abeles M 1998 Spatiotemporal structure of cortical activity: properties and behavioral relevance. *J Neurophysiol.* 79, 2857-2874.

Rapp P E, Zimmerman I D, Vining E P, Cohen N, Albano A M and Jimenez-Montano M A 1994 The algorithmic complexity of neural spike trains increases during focal seizures. *J. Neurosci.* 14, 4731-4739.

Reinoso-Suarez F 1961 *Topographischer Hirnatlas der Katze*. E. Merck AG, Darmstadt.

Reyes A D 2003 Synchrony-dependent propagation of firing rate in iteratively constructed networks in vitro. *Nat. Neurosci.* 6, 593-599.

Reyes A D 2003 Synchrony-dependent propagation of firing rate in iteratively constructed networks in vitro. *Nat. Neurosci.* 6, 593-599.

Reynolds J H and Desimone R 1999 The role of neural mechanisms of attention in solving the binding problem. *Neuron* 24, 19-25.

Riehle A, Grun S, Diesmann M and Aertsen A 1997 Spike synchronization and rate modulation differentially involved in motor cortical function [see comments]. *Science* 278, 1950-1953.

Rieke F, Bodnar D A and Bialek W 1995 Naturalistic stimuli increase the rate and efficiency of information transmission by primary auditory afferents. *Proc. R. Soc. Lond B Biol. Sci.* 262, 259-265.

Riesenhuber M and Poggio T 1999 Are cortical models really bound by the "binding problem"? *Neuron* 24, 87-25.

- Ringach D L 2004 Mapping receptive fields in primary visual cortex. *J. Physiol.*
- Rodriguez E, George N, Lachaux J P, Martinerie J, Renault B and Varela F J 1999 Perception's shadow: long-distance synchronization of human brain activity. *Nature* 397, 430-433.
- Roelfsema P R, Engel A K, Konig P and Singer W 1997 Visuomotor integration is associated with zero time-lag synchronization among cortical areas. *Nature* 385, 157-161.
- Rolls E T 1992 Neurophysiological mechanisms underlying face processing within and beyond the temporal cortical visual areas. *Philos. Trans. R. Soc. Lond B Biol. Sci.* 335, 11-20.
- Rosenberg J R, Amjad A M, Breeze P, Brillinger D R and Halliday D M 1989 The Fourier approach to the identification of functional coupling between neuronal spike trains. *Prog. Biophys. Mol. Biol.* 53, 1-31.
- Roskies A L 1999 The binding problem. *Neuron* 24, 7-25.
- Roy S A, Dear S P and Alloway K D 2001 Long-range cortical synchronization without concomitant oscillations in the somatosensory system of anesthetized cats. *J. Neurosci.* 21, 1795-1808.
- Rudolph M and Destexhe A 2003 Tuning neocortical pyramidal neurons between integrators and coincidence detectors. *J. Comput. Neurosci.* 14, 239-251.
- Salin P A and Bullier J 1995 Corticocortical connections in the visual system: structure and function. *Physiol Rev.* 75, 107-154.
- Salinas E and Sejnowski T J 2000 Impact of correlated synaptic input on output firing rate and variability in simple neuronal models. *J. Neurosci.* 20, 6193-6209.
- Salinas E and Sejnowski T J 2001 Correlated neuronal activity and the flow of neural information. *Nat. Rev. Neurosci.* 2, 539-550.
- Samonds J M, Allison J D, Brown H A and Bonds A B 2003 Cooperation between area 17 neuron pairs enhances fine discrimination of orientation. *J. Neurosci.* 23, 2416-2425.
- Samonds J M, Allison J D, Brown H A and Bonds A B 2004 Cooperative synchronized assemblies enhance orientation discrimination. *Proc. Natl. Acad. Sci. U. S. A* 101, 6722-6727.
- Scannell J W, Blakemore C and Young M P 1995 Analysis of connectivity in the cat cerebral cortex. *J. Neurosci.* 15, 1463-1483.
- Schmidt K E, Kim D S, Singer W, Bonhoeffer T and Lowel S 1997 Functional specificity of long-range intrinsic and interhemispheric connections in the visual cortex of strabismic cats. *J. Neurosci.* 17, 5480-5492.

- Schmidt K E, Galuske R A and Singer W 1999 Matching the modules: cortical maps and long-range intrinsic connections in visual cortex during development. *J Neurobiol.* 41, 10-17.
- Schmidt K E and Löwel S 2001 Long-Range Intrinsic Connections in Cat Primary Visual Cortex. *In* The Cat Primary Visual Cortex.pp 387-426.
- Schwarz C and Bolz J 1991 Functional specificity of a long-range horizontal connection in cat visual cortex: a cross-correlation study. *J. Neurosci.* 11, 2995-3007.
- Shadlen M N and Movshon J A 1999 Synchrony unbound: a critical evaluation of the temporal binding hypothesis. *Neuron* 24, 67-25.
- Sheinberg D L and Logothetis N K 2001 Noticing familiar objects in real world scenes: the role of temporal cortical neurons in natural vision. *J. Neurosci.* 21, 1340-1350.
- Sherrington C S 1941 *Man on His Nature*. Cambridge University Press, Cambridge.
- Shoham S, Fellows M R and Normann R A 2003 Robust, automatic spike sorting using mixtures of multivariate t-distributions. *J. Neurosci. Methods* 127, 111-122.
- Shtoyerman E, Arieli A, Slovin H, Vanzetta I and Grinvald A 2000 Long-term optical imaging and spectroscopy reveal mechanisms underlying the intrinsic signal and stability of cortical maps in V1 of behaving monkeys. *J Neurosci.* 20, 8111-8121.
- Singer W 1977 Control of thalamic transmission by corticofugal and ascending reticular pathways in the visual system. *Physiol Rev.* 57, 386-420.
- Singer W 1990 The formation of cooperative cell assemblies in the visual cortex. *J. Exp. Biol.* 153, 177-197.
- Singer W and Gray C M 1995 Visual feature integration and the temporal correlation hypothesis. *Annu. Rev. Neurosci.* 18, 555-586.
- Singer W 1999 Neuronal synchrony: a versatile code for the definition of relations? *Neuron* 24, 49-25.
- Skinner F K, Kopell N and Marder E 1994 Mechanisms for oscillation and frequency control in reciprocally inhibitory model neural networks. *J. Comput. Neurosci.* 1, 69-87.
- Softky W R 1994 Sub-millisecond coincidence detection in active dendritic trees. *Neuroscience* 58, 13-41.
- Softky W R 1995 Simple codes versus efficient codes. *Curr. Opin. Neurobiol.* 5, 239-247.
- Somogyi P, Kisvarday Z F, Martin K A and Whitteridge D 1983 Synaptic connections of morphologically identified and physiologically characterized large basket cells in the striate cortex of

cat. *Neuroscience* 10, 261-294.

Steinmetz P N, Roy A, Fitzgerald P J, Hsiao S S, Johnson K O and Niebur E 2000 Attention modulates synchronized neuronal firing in primate somatosensory cortex [see comments]. *Nature* 404, 187-190.

Stopfer M, Bhagavan S, Smith B H and Laurent G 1997 Impaired odour discrimination on desynchronization of odour-encoding neural assemblies. *Nature* 390, 70-74.

Svirskis G and Rinzel J 2000 Influence of temporal correlation of synaptic input on the rate and variability of firing in neurons. *Biophys. J.* 79, 629-637.

Tanaka K 1992 Inferotemporal cortex and higher visual functions. *Curr. Opin. Neurobiol.* 2, 502-505.

Tanaka K 1993 Neuronal mechanisms of object recognition. *Science* 262, 685-688.

Bower JM and Beeman D 1998 *The Book of Genesis*. Springer-Verlag New York

Tiesinga P H and Sejnowski T J 2004 Rapid temporal modulation of synchrony by competition in cortical interneuron networks. *Neural Comput.* 16, 251-275.

Toyama K, Kimura M and Tanaka K 1981 Organization of cat visual cortex as investigated by cross-correlation technique. *J. Neurophysiol.* 46, 202-214.

Traub R D, Whittington M A, Stanford I M and Jefferys J G 1996 A mechanism for generation of long-range synchronous fast oscillations in the cortex. *Nature* 383, 621-624.

Traub R D, Jefferys J G and Whittington M A 1997 Simulation of gamma rhythms in networks of interneurons and pyramidal cells. *J. Comput. Neurosci.* 4, 141-150.

Treisman A 1999 Solutions to the binding problem: progress through controversy and convergence. *Neuron* 24, 105-125.

Ts'o D Y and Gilbert C D 1988 The organization of chromatic and spatial interactions in the primate striate cortex. *J. Neurosci.* 8, 1712-1727.

Tusa R J, Palmer L A and Rosenquist A C 1978 The retinotopic organization of area 17 (striate cortex) in the cat. *J Comp Neurol.* 177, 213-235.

Tusa R J, Rosenquist A C and Palmer L A 1979 Retinotopic organization of areas 18 and 19 in the cat. *J Comp Neurol.* 185, 657-678.

Usrey W M and Reid R C 1999 Synchronous activity in the visual system. *Annu. Rev. Physiol* 61, 435-456.

- Van Essen D C, Anderson C H and Felleman D J 1992 Information processing in the primate visual system: an integrated systems perspective. *Science* 255, 419-423.
- Van Essen D C and Felleman D J 1996 On hierarchies: response to Hilgetag et al. *Science* 271, 777.
- van Vreeswijk C and Sompolinsky H 1996 Chaos in neuronal networks with balanced excitatory and inhibitory activity. *Science* 274, 1724-1726.
- Varela F, Lachaux J P, Rodriguez E and Martinerie J 2001 The brainweb: phase synchronization and large-scale integration. *Nat. Rev. Neurosci.* 2, 229-239.
- von der Malsburg C . The correlation theory of brain function. 1-40. 1981. *Int Rep MPI Biophys Chem.*
- Ref Type: Report
- von der Malsburg C 1999 The what and why of binding: the modeler's perspective. *Neuron* 24, 95-25.
- von der H R, Peterhans E and Baumgartner G 1984 Illusory contours and cortical neuron responses. *Science* 224, 1260-1262.
- von der Heydt R and Peterhans E 1989 Mechanisms of contour perception in monkey visual cortex. I. Lines of pattern discontinuity. *J. Neurosci.* 9, 1731-1748.
- von der Malsburg C and Schneider W 1986 A neural cocktail-party processor. *Biol. Cybern.* 54, 29-40.
- von Stein A, Chiang C and Konig P 2000 Top-down processing mediated by interareal synchronization. *Proc. Natl. Acad. Sci. U. S. A* 97, 14748-14753.
- Wachsmuth E, Oram M W and Perrett D 1994 Recognition of objects and their component parts: responses of single units in the temporal cortex of the macaque. *Cereb. Cortex* 4, 509-522.
- Wang G, Tanaka K and Tanifuji M 1996 Optical imaging of functional organization in the monkey inferotemporal cortex. *Science* 272, 1665-1668.
- Wessinger C M, VanMeter J, Tian B, Van Lare J, Pekar J and Rauschecker J P 2001 Hierarchical organization of the human auditory cortex revealed by functional magnetic resonance imaging. *J Cogn Neurosci.* 13, 1-7.
- Wolfe J M and Cave K R 1999 The psychophysical evidence for a binding problem in human vision. *Neuron* 24, 11-25.
- Yamane S, Kaji S and Kawano K 1988 What facial features activate face neurons in the inferotemporal cortex of the monkey? *Exp. Brain Res.* 73, 209-214.

Zeki S M 1974 Functional organization of a visual area in the posterior bank of the superior temporal sulcus of the rhesus monkey. *J. Physiol* 236, 549-573.

Zouridakis G and Tam D C 1997 Multi-unit spike discrimination using wavelet transforms. *Comput. Biol. Med.* 27, 9-18.

Zouridakis G and Tam D C 2000 Identification of reliable spike templates in multi-unit extracellular recordings using fuzzy clustering. *Comput. Methods Programs Biomed.* 61, 91-98.

## VI Summary

In order to investigate the role of neuronal synchronization in perceptual grouping, a new method was developed to record selectively from multiple cortical sites of known functional specificity as determined by optical imaging of intrinsic signals. To this end, a matrix of closely spaced guide tubes was developed in cooperation with a company providing the essential manufacturing technique RMPD<sup>®</sup> (Rapid Micro Product Development). The matrix was embedded into a framework of hard and software that allowed for the mapping of each guide tube onto the cortical site an electrode would be led to if inserted into that guide tube. With these developments, it was possible to determine the functional layout of the cortex by optical imaging and subsequently perform targeted recordings with multiple electrodes in parallel. The method was tested for its accuracy and found to target the electrodes with a precision of 100  $\mu\text{m}$  to the desired cortical locations.

Using the developed technique, neuronal activity was recorded from area 18 of anesthetized cats. For stimulation, Gabor-patches in different geometrical configurations were placed over the recorded receptive fields merging into visual objects appropriate for testing the hypothesis of feature binding by synchrony. Synchronization strength was measured by the height of the cross-correlation centre peaks. All pairwise synchronizations were summarized in a correlation index which determined the mean difference of the correlation strengths between conditions in which recording sites should or should not fire in synchrony according to the binding hypothesis. The correlation index deviated significantly from zero for several of these configurations, further supporting the hypothesis that synchronization plays an important role in the process of perceptual grouping. Furthermore, direct evidence was found for the independence of the synchronization strength from the neuronal firing rate and for neurons that change dynamically the ensemble they participate in.

In parallel to the experimental approach, mechanisms of oscillatory long range synchronization were studied by network simulations. To this end, a biologically plausible model was implemented using pyramidal and basket cells with Hodgkin-Huxley like conductances. Several columns were built from these cells and intra- and inter-columnar connections were mimicked from physiological data. When activated by independent Poisson spike trains, the columns showed oscillatory activity in the gamma frequency range. Correlation analysis revealed the tendency to locally synchronize the oscillations among the columns, but a rapid phase transition occurred with increasing cortical distance. This finding suggests that the present view of the inter-columnar connectivity does not fully explain oscillatory long range synchronization and predicts that other processes such as top-down influences are necessary for long range synchronization phenomena.



## VII Ausführliche Zusammenfassung

Die über den visuellen Kortex verteilte Repräsentation von Objektmerkmalen wirft die Frage auf, wie Merkmalsbezüge aufrecht erhalten werden. So muss z.B. in irgendeiner Weise kodiert werden ob zwei Liniensegmente, die von im Gesichtsfeld weit entfernten rezeptiven Feldern detektiert werden, zu einer oder zwei verschiedenen Linien gehören, d.h. ob die beiden Liniensegmente verbunden sind oder nicht. Eine Möglichkeit solche Bezüge zu kodieren liegt darin, sie in den zeitlichen Bezügen der neuronalen Entladungsmuster einzubetten und zwar derart, dass Neurone zusammengehöriger Merkmale ihre Entladungen synchronisieren. Dieser relationalen Kodierungsstrategie ist inhärent, dass sie nur durch gleichzeitige Messung mehrerer neuronaler Signale nachgewiesen werden kann. Ein weiteres Problem bei der Suche nach der vom Gehirn verwendeten Kodierung besteht in der anisotropen Verteilung der rezeptiven Feldeigenschaften über die Kortexoberfläche hinweg. Diese variiert von Individuum zu Individuum und macht es daher schwer, gezielt von mehreren Neuronen mit bestimmten rezeptiven Feldeigenschaften elektrophysiologische Daten zu erheben. Daher wurde im Rahmen der hier vorliegenden Arbeit eine Methode entwickelt, um die Techniken des *Optical Imagings* (OI) intrinsischer Signale und der Elektrophysiologie zu vereinen und so die simultane Aufnahme mehrerer neuronaler Signale von vorbestimmter Funktionalität zu ermöglichen. Die Entwicklung und die Methode selbst werden im Folgenden näher beschrieben.

Durch OI kann die funktionelle Architektur des Kortex über einen makroskopischen Bereich (ca. 5 x 10 mm) kartiert werden. Das Hauptproblem, das in dieser Dissertation gelöst werden sollte bestand darin, ein Platzierungssystem für Elektroden zu entwickeln, welches es ermöglicht, Punkte auf den OI-Karten auszuwählen und Elektroden an den korrespondierenden Stellen des Kortex' zu platzieren. Dazu wurden drei Ansätze verfolgt, von denen die ersten zwei verworfen werden mussten. Die Erfahrungen mit den ersten beiden Ansätzen, die benötigte Präzision von wenigstens 200 µm Platzierungsgenauigkeit und die gleichzeitige Anwendbarkeit auf viele Elektroden machten es notwendig, eine von Kanälen durchzogene Matrix mit einer Genauigkeit zu fertigen, die mit herkömmlichen Techniken wie Bohren, Ätzen

oder auch Laserbohrung nicht erreicht wird. Daher wurde in Kooperation mit einer Firma die das RMPD<sup>®</sup> (Rapid Micro Product Development) Fertigungsverfahren beherrscht eine Matrix entwickelt, die alle notwendigen, im Folgenden aufgezählten Eigenschaften besitzt:

- Hohe Dichte der Kanäle (>20 Kanäle pro mm<sup>2</sup>, 220 µm Gitterkonstante)
- Hohes Aspektverhältnis der Kanäle (15 mm Höhe : 0.15 mm Durchmesser) um Elektroden möglichst wenig Spiel zu geben
- Material quillt unter Einfluss von Feuchtigkeit nicht auf
- Material ist flexibel, sodass die dünnen Wände zwischen den Kanälen bei Einführung und Scherung der Elektroden nicht brechen
- Reproduzierbarkeit der Kanalpositionen bei erneuter Herstellung der Matrix (ca. 1 µm Fertigungsvarianz)

Weiterhin wurden Geräte und Software entwickelt, um die Positionen der Röhren auf die OI-Karten zu projizieren, die Elektroden in die ausgewählten Röhren einzufädeln und sie schließlich mittels Mikrotrieben kontrolliert in das kortikale Gewebe vorzufahren. Das Verfahren zeigte bei Tests, dass es Elektroden mit einer Genauigkeit von ca. 100 µm platziert.

Die entwickelte Methode zur Platzierung von Elektroden nach OI-Karten wurde in Tierexperimenten angewendet. In diesen Experimenten sollte die Abhängigkeit neuronaler Synchronisation von visueller Objektzugehörigkeit anhand des visuellen Areal 18 der anästhesierten Katze erörtert werden. Existierende Studien zu diesem Thema verwendeten zumeist paarweise elektrophysiologische Aufnahmen, weshalb hier mittels der neuen Aufnahmetechnik von mehreren kortikalen Stellen gleichzeitig Daten erhoben werden sollten. Eine Folge der Synchronisationstheorie ist, dass ein und dasselbe Neuron an verschiedenen Assemblies teilnehmen kann. Solch ein Wechsel zwischen zwei Assemblies ist noch nicht direkt nachgewiesen worden. Daher wurden in den Experimenten auch Stimuluskonfigurationen gewählt, die einen Wechsel der Teilnahme an einem von

zwei Assemblies provoziert. Erfolgreich verwendete Stimuli wurden in erster Linie aus mehreren so genannten Gabor-Patches (Kreisrunde Objekte mit einer räumlichen Gabor-Intensitätsverteilung) konstruiert. Die Objektzugehörigkeit von Neuronen konnte durch drehen oder entfernen eines Gabor-Patches geändert werden. Insgesamt wurden fünf Experimente von fünf bis sieben Tagen Dauer an anästhesierten Katzen durchgeführt.

Für die Analyse der in den Experimenten aufgenommenen *Multi Unit Activities* (MUAs) sollten ursprünglich die das MUA-Signal bildenden *Single Unit Activities* (SUAs) anhand der Form ihrer Aktionspotentiale (AP) extrahiert werden, um das Synchronizitätsverhalten auf Einzelzellebene untersuchen zu können. Um diese Sortierung durchführen zu können, dürfen die Signale keinerlei Störungen von einer den AP vergleichbaren Amplitude enthalten, da sonst die Charakteristik der Form verloren geht und eine Unterscheidung der verschiedenen Zellen unmöglich wird. Obwohl einige Störquellen vor und während der Experimente erkannt und eliminiert wurden verblieben einige Störungen im Signal aller Elektroden. Daher wurde ein Verfahren entwickelt um mittels *Principal Component Analysis* (PCA) zwischen den Kanälen korrelierte Störungen abzuschätzen und zu eliminieren. Obwohl sich das Verfahren in Simulationen als sehr effizient und nützlich herausstellte, konnte es die Störungen nicht hinreichend reduzieren, um eine Sortierung der AP zu ermöglichen. Da das PCA-Entstörungsverfahren um so besser wirkt, je mehr Kanäle zur Schätzung des Störanteils zur Verfügung stehen und mit fortschreitender Technik die Anzahl der verwendeten Kanäle weiter ansteigen wird, wird dieses Verfahren in Zukunft nützliche Dienste bei der nachträglichen Entfernung von Störungen leisten. Weiterhin wurde eine Methode entwickelt, um eine Rekonstruktion der mit ca. 20 kHz abgetasteten Signale und damit einen genauen Vergleich der AP zu erlauben. Die Aussicht von 16 Kanälen MUAs aufzunehmen, die sich durchschnittlich noch einmal in drei SUAs aufspalten und unter etwa acht verschiedenen Stimulusbedingungen erhoben wurden und damit an die 9000 Kreuzkorrelationsfunktionen entstünden, machte es notwendig ein Analysekonzept zu entwickeln, das weitgehende Automatisierungen zulässt. Ein solches Konzept wurde mittels objektorientierter Techniken in der Hochsprache IDL implementiert und erfolgreich zur Analyse eingesetzt.

Zur Analyse der in den Experimenten erhobenen Daten wurden alle paarweisen Kreuzkorrelationsfunktionen berechnet und die Höhe der zentralen Maxima als Grad der Synchronisierungsstärke gemessen. Für jedes paar wurden die Stimuluskonfigurationen bestimmt, in denen sie der Bindungshypothese zufolge stärker oder schwächer synchronisieren sollten und aus der Differenz der Synchronisierungsstärke für beide Fälle wurde ein Korrelationsindex erstellt. Dieser Index zeigte für alle Stimuli eine signifikante Erhöhung der Synchronisierungsstärke für die Fälle, für die nach der Bindungshypothese eine stärkere Synchronisierungsstärke vorausgesagt wird. Dieses Ergebnis bestätigt die Hypothese, dass die Synchronisierung neuronaler Aktivität eine wichtige Rolle bei der Kodierung von Zusammengehörigkeiten spielt. Weiterhin konnten mit den Gabor-Patches Stimuli erzeugt werden, die verschiedene visuelle Objekte bildeten, ohne die Raten der AP zu ändern. Damit konnte gezeigt werden, dass sich der Grad neuronaler Synchronisierung unabhängig von der Rate ändern und somit als unabhängigen Informationskanal neben den Raten genutzt werden kann. Als letzter wichtiger Befund konnte direkt gezeigt werden, wie sich eine Gruppe von Neuronen in Abhängigkeit vom Stimulus immer mit den Neuronen besser synchronisierten, deren receptive Felder auf dem gleichen visuellen Objekt positioniert waren. Da es sich dabei um zwei komplett verschiedene Gruppen von Neuronen handelte, ist das der direkte Nachweis für einen Wechsel der Teilnahme an verschiedenen Assemblies.

Der oben beschriebene experimentelle Ansatz kann prinzipiell die zugrunde liegende Hypothese lediglich falsifizieren, kann jedoch nicht die Mechanismen untersuchen, die zu den beobachteten Phänomenen führen. Die in dieser Arbeit untersuchten Synchronisierungsphänomene betreffen die Synchronisierung von Neuronengruppen über einen größeren Abstand hinweg, jedoch innerhalb eines Areal. Solche langreichweitigen Synchronisierungen sind in der Regel oszillatorischer Natur, wobei der die Oszillationen verursachende Mechanismus noch nicht gänzlich geklärt ist. Daher wurde parallel zu den experimentellen Ansätzen eine Computersimulation erstellt um der Frage nachzugehen, inwieweit das gegenwärtige Wissen über die intrinsische Konnektivität des Kortex die langreichweitige Synchronisierung neuronaler Gruppen erklären kann. Dazu

wurden anatomisch rekonstruierte und auf wenige Zylinder reduzierte Zellen mit Hodgkin-Huxley-Kinetiken zu Netzwerken verbunden, die einer kortikalen Kolumne entsprechen. Die Kolumnen wiederum wurden synaptisch verbunden, wie es in einschlägiger Literatur für Kolumnen gleicher Präferenz beschrieben wurde. Die Kolumnen wurden durch unabhängige Poisson-Prozesse aktiviert und zeigten darauf hin oszillatorische Aktivität im Gamma-Bereich. Eine Korrelationsanalyse zeigte die Tendenz, dass benachbarte Kolumnen ihre Oszillationen synchronisieren, aber einen rapiden Phasensprung um fast  $180^\circ$  zu Kolumnen von größerem kortikalen Abstand erfahren. Diese Ergebnisse legen nahe, dass die inter-kolumnären Verbindungen die Synchronisierung von Kolumnen über große kortikale Distanzen hinweg nicht erklären kann und legt den Schluss nahe, dass andere Prozesse wie z.B. Rückprojektionen von höheren Arealen für langreichweitige Synchronisierungen nötig sind.



## VIII Lebenslauf

### Michael Niessing

#### Persönliche Daten

Geburtsdatum 22. Oktober 1970  
Geburtsort Marburg  
Nationalität Deutsch  
Eltern Drs. Jürgen und Christa Lina Niessing, geb. Preis

#### Werdegang

2000-2004 Promotion: "Electrophysiological and computational studies on the mechanisms and functional impact of cortical synchronization", Abteilung für Neurophysiologie, Max-Planck-Institut für Hirnforschung, Frankfurt am Main, Betreuer: Prof. Dr. Wolf Singer

Dez. 1999 Diplom (Diplom-Physiker) Note: sehr gut  
Philipps-Universität Marburg  
Prüfungsfächer: Quantenmechanik, Experimentalphysik, Informatik, Neurophysik

Diplomarbeit: "Mikroaugenbewegungen und ihr Einfluß auf Signale Sehcortex"  
Abteilung Neurophysik, Philipps-Universität, Marburg, Betreuer: Prof. Dr. Reinhard Eckhorn

1993-1999 Studium der Physik (Philipps-Universität, Marburg und University of Kent at Canterbury, England)

1992-1993 Wehr-Ersatzdienst (Schule für Praktisch Bildbare, Marburg)

1991-1992 Studium der Physik (Philipps-Universität, Marburg)

1980-1991 Besuch des Elisabeth-Gymnasiums, Marburg

1976-1980 Besuch der Gebrüder Grimm Grundschule, Marburg